

Exploring the Potential Role of Transitional Elements to Understand the
Past and the Future of the Earth's Biosphere

March, 2024

RATNAYAKE MUDIYANSELAGE DILAN MADUSANKA RATNAYAKE

Graduate School of Natural Science and Technology

(Doctor's Course)

OKAYAMA UNIVERSITY

Acknowledgement

First and foremost, I would like to express my heartfelt gratitude to my supervisor professor Ryoji Tanaka, for guiding me in every possible way to make this program a success and most importantly for his patience, massive encouragement, and immense knowledge. I truly obliged to him for his overwhelming support given to me on and off the university.

I would also like to express my deep gratitude to professor Eizo Nakamura for his guidance and substantive discussions. Furthermore, I would like to acknowledge all the professors Katsura Kobayashi, Tak Kunihiro, Hiroshi Kitagawa, Christian Potiszil and staff members Chie Sakaguchi, Tsutomu Ota, Masahiro Yamanaka, Kayo Tanaka, Yukari Shimizu of the Pheasant Memorial Laboratory for the suggestions, guidance and help given on various occasions for successfully pursuing this study.

As a graduate student, completion of the doctorate program would not have been successful without the help and funding opportunity of both the Institute of Planetary Materials and Okayama University Science, Technology, and Innovation Creation Fellowship.

Special thanks and appreciation also go towards my family for their understanding and remarkable support during this very crucial period and encouraging me in this endeavor. Finally, I would like to convey my sincere gratitude to my colleagues and all the people who have willingly helped me out with their abilities. It is their kindness that have made my life in Japan wonderful.

Dedication

This thesis is dedicated to free education system that helped me to reach this goal ever since my childhood.

Abstract

Most living beings require transition elements as micronutrients. The essentiality of these metals varies from one species to another and their availability is critical to sustain certain metabolic functions. Therefore, variations in their availability in particular organism's habitat can determine its sustainability in that environment. Additionally, the metabolic processes of microbes can create significant isotope fractionation. These have the potential to help to reconstruct paleo-environmental conditions and can be a valuable tool in detecting life on exoplanets (under the broad assumption that extra-terrestrial life is similar to life on Earth). This study explored how the bio-availability of transition metals throughout the Earth's history has affected the evolution of life on Earth and the possibility of using the transition metal isotope signatures as bio-signatures. The **first chapter** provides an overview of the connection between the bio-availability of transition metals and the evolution of life, with a special focus on the evolution of biological nitrogen fixation.

The first part of this thesis explores the possibility of using transition metal isotope signatures as bio-signatures. However, many abiotic processes (such as authigenic minerals, post-depositional alteration, and weathering) can mask the signatures resulting from biological processes. Therefore, having precise techniques to isolate multiple transition metals from matrices would be useful in this regard. Thus, chapters 2 to 4 are dedicated to the development of ion chromatography techniques that were designed to isolate elements from geological samples to precisely measure isotope signatures. In **chapter 2**, a sequential ion chromatography method consisting of 10 steps is described for small sample volumes (sub-milligram) and it can achieve a separation of multiple transition elements including Ni, Cr, Fe, Ni, Cu, Zn, Cd, W, Mo \pm V, and several major elements (Ti, Mg, and Ca). Additionally, individual methods for Ni and Cr separation using minimal sample volumes were developed and evaluated by the measurement of corresponding isotopes in geological reference materials and these methods are presented in **chapter 3** and **chapter 4** respectively.

Despite having methods for precise isotope measurements, it is still important to differentiate between abiotic and biotic isotope fractionation processes. Therefore, following the method development, an experimental approach was used to evaluate the applicability of currently practiced sample preparation techniques for obtaining microbial enzyme-specific metal isotope fractionation and it is described in **Chapter 5**. The results indicate that current practices are not suitable to accurately differentiate enzyme-specific biotic signatures.

Therefore, determining biogenicity or assigning observed isotope variations in natural samples to biological processes should be carried out with extreme caution, and recommended procedures that should be followed are introduced. Furthermore, it is advised not to use or rely solely on isotope signatures for determining biogenicity in terrestrial as well as extra-terrestrial samples and use of in detail textural analysis followed by a combination of traditional and non-traditional stable isotope analysis is recommended.

One of the reasons for evolving complex life on Earth is the increase of oxygen in Earth's atmosphere. Oxygen also plays a major role in nutrient delivery to habitats by initiating oxidative weathering reactions. Therefore, to understand the transitional metal availability throughout the Earth's history it is necessary to understand the evolution of oxygen in Earth's atmosphere. Thus, in the second part of this thesis, the evolution of cyanobacteria, the only organism that was capable of producing oxygen in the primitive Earth was studied especially focusing on their nitrogen fulfilment, given the importance of transition metals such as Ni, Mo, V and Fe to the functioning of nitrogen metabolizing enzyme complexes. **Chapter 6** of the study analyzed the growth response of bacteria to urea, an alternative nitrogen source to N₂. Based on the results, an alternative view of the evolution of the biogeochemical nitrogen cycle and its connection to atmospheric oxygenation is proposed.

Table of Contents

Abstract	iv
List of Figures	x
List of Tables	xii
Chapter 1: Introduction	1
1.1. Overview	1
1.1.1. Outstanding questions	2
1.2. Objectives and thesis organization	5
1.3. Review of previous work	5
1.3.1. Evolution of the nitrogen cycle and cyanobacteria	5
1.3.2. Nitrogen acquisition by cyanobacteria	7
1.3.3. Nitrogen control and heterocyst formation	10
1.3.4. Urease, urea, and Ni	11
1.3.5. Occurrence of Urea	13
1.3.6. Importance of Ni for cyanobacterial growth and growth of cyanobacteria in urea rich media	14
1.3.7. Oceanic Ni biogeochemistry	16
1.4. References	17
Chapter 2: Development of a sequential ion exchange chromatography technique to separate transition metals	28
2.1. Abstract	28
2.2. Introduction	28
2.3. Materials and Methods	29
2.3.1. Reagents and materials	29
2.3.2. Sample Preparation	30
2.3.3. Determination of distribution coefficients	30
2.3.4. Chemical Separation	31
	vi

2.4.	Results	32
2.4.1.	Distribution coefficients (K_D)	32
2.4.2.	Element separation methods	35
2.5.	Discussion	47
2.6.	Conclusions	49
2.7.	References	49
Chapter 3: Novel nickel isolation procedure for a wide range of sample matrices without using dimethylglyoxime for isotope measurements using MC-ICP-MS		50
3.1.	Abstract	50
3.2.	Introduction	50
3.3.	Experimental	52
3.3.1.	Reagents and materials	52
3.3.2.	Sample preparation and digestion	53
3.3.3.	Chemical separation	53
3.3.4.	Mass spectrometry	55
3.3.5.	Double spike calibration	56
3.4.	Results and discussion	57
3.4.1.	Chemical separation	57
3.4.2.	Recovery yields and procedural blanks	60
3.4.3.	Evaluation of the procedure for the removal of interfering elements	61
3.4.4.	Ni isotope compositions of reference materials	64
3.5.	Conclusions	65
3.6.	References	65
Appendix A		70
A.1.	Ni Double-spike Calibration	70
A.3.	References	71
Appendix B : Ni Isotopic Composition of Geological Reference Materials		72

Chapter 4: Determination of mass-dependent chromium isotopic compositions in geological samples by double spike-total evaporation-thermal ionization mass spectrometry (DS-TE-TIMS)	74
4.1. Abstract	74
4.2. Introduction	74
4.3. Materials and Methods	76
4.3.1. Reagents and Materials	76
4.3.2. Sample Preparation	77
4.3.3. Chemical Separation	78
4.3.4. Mass Spectrometry	80
4.4. Results and Discussion	82
4.4.1. Chemical Separation	82
4.4.2. Recovery yields and procedural blanks	85
4.4.3. The analytical precision of Cr isotope measurements of an un-spiked standard	85
4.4.4. Double spike calibration	87
4.4.5. The effects of isobaric interferences and matrix elements on Cr isotope measurements	88
4.4.6. Blank contribution	93
4.4.7. Cr isotope variation in geological reference materials	93
4.5. Conclusions	97
4.6. References	97
Chapter 5: Obtaining accurate isotopic fractionation data from cells: the basics	104
5.1. Introduction	104
5.1.1. Removal of adsorbed elements from cell surfaces	105
5.2. Materials and Reagents	107
5.3. Methodology	108
5.3.1. Experiments for the removal of adsorbed elements on SiO ₂ particles	108

5.3.2.	Experiments for the removal of adsorbed elements on cyanobacterial cells	109
5.3.3.	Evaluation of the changes in isotopic composition of cyanobacterial cells upon different treatment procedures.	110
5.4.	Results	112
5.5.	Discussion	119
5.6.	Conclusions	121
5.7.	References	122
Chapter 6: Was the Great Oxidation Event controlled by the bioavailability of urea and Ni?		126
6.1.	Introduction	126
6.2.	Experimental Method	128
6.2.1.	Reagents and Materials	128
6.2.2.	Cell Growth Conditions	129
6.2.3.	Elemental and Stable isotope analysis	131
6.3.	Results	133
6.3.1.	Preliminary experiments	133
6.3.2.	Nitrogen and Ni isotope fractionation by <i>Synechococcus sp.</i> PCC 7002	135
6.4.	Discussion	138
6.4.1.	Urea as a potential nitrogen source	138
6.4.2.	Effect of Ni for the growth of cyanobacteria.	138
6.4.3.	Nitrogen and Ni isotope fractionation	139
6.4.4.	Hypothesis on the events that lead to the GOE	141
6.5.	Conclusions	146
6.6.	References	146
7.	Conclusions	152

List of Figures

Figure 1 - Evolution of oxygen through time	7
Figure 2 - Nitrogen assimilation pathways	8
Figure 3 - Late appearance of heterocysts in cyanobacterial evolution.....	11
Figure 4 - Maximum dissolved Ni in sea water through time	15
Figure 5 - Ni isotope variation in two regions of North Atlantic Ocean	16
Figure 6 - The GEOTRACES GA02 section in the West Atlantic Ocean.....	17
Figure 7 -Variation of Kd values with the HCl concentration on the AG1X8 resin	33
Figure 8 - Variation of Kd values with HCl and HNO3 concentration on the AG1X8 resin..	34
Figure 9 -Flow chart for the developed sequential element separation technique.....	35
Figure 10 - Elution profile for the separation of Ca and REE fraction in step 2.	42
Figure 11 - Elution profile for the steps 3 and 9 where separation of Cr from Al, V and Ti and the separation of Fe from Cu.	42
Figure 12 - Elution profile for the separation of V from Ti in step 4.	43
Figure 13 - Elution profile for Step 5 where Al and Ti was separated from each other.....	43
Figure 14 - Elution profile for Step 6 : separation of Cr from Ni and Mg.....	44
Figure 15 - Elution profile for the separation of Ni from Mg in step 7.	44
Figure 16 – Elution profile for the separation of Cu and Fe from Mo and W in step 8.	45
Figure 17 - Elution profile for Step 10 where Mo and W were separated.	45
Figure 18 - Elution profile for step 1: Separating Ni from Fe, V, Al, Ti, and Ca.....	58
Figure 19 - Elution profile for step 2: Separating Ni from Group 1 and Group 2 elements....	59
Figure 20 - Elution profile for step 3: Separating Ni from remaining transition metals	60
Figure 21 - $\delta^{60}\text{Ni}$ values for the geological samples analyzed in this study in comparison with literature data.	63
Figure 22 - Elution profile for Cr separation in step 1.....	83
Figure 23 - Elution profile for step 2	84
Figure 24 - Elution Profile for step 3.....	85
Figure 25 - Raw data of NIST SRM 979 measured by the normal-TIMS and TE-TIMS method.....	86
Figure 26 - The $\delta^{53}\text{Cr}$ of the DS – NIST 979 mixture with various ratios of DS and NIST 979.	88
Figure 27 - The proportion of ^{54}Fe in the $m/z=54$ during the measurement of the AGV-2....	90

Figure 28 - An example of the data profile against the filament temperature during the measurement of geological sample measured by the TE-TIMS method.	92
Figure 29 - The $\delta^{53}\text{Cr}$ values of the reference materials.	95
Figure 30 - Desorbed element fractions from SiO_2 and cell surfaces	114
Figure 31 - Yields of elements in treated cell fractions normalized to dry weight of cells ...	115
Figure 32 - Images of the filter unit after treating cells with - 0.5 mmol L^{-1} HCl and water	116
Figure 33 - SEM images of cells treated with HCl, SnCl_2 and water	117
Figure 34 - Zn isotopic variation in water and HCl treated cells and the HCl filtrate after treating cells.	118
Figure 35 - Absorbance values of cyanobacteria grown in 3 ml liquid media at different conditions on the 15th day after inoculation.....	134
Figure 36 - Growth curves of bacterial cultures grown.	137
Figure 37 - Urea and Ni controlled GOE.....	144

List of Tables

Table 1 - Key enzymes involved in nitrogen assimilation of cyanobacteria	8
Table 2 - Concentration of acids used for determining K_d and the corresponding resins used.	31
Table 3 - K_d values for AG1-X8 and nitrates of the transition elements	32
Table 4 - K_d values for AG1-X8 and chlorides of the transition elements	32
Table 5 - K_d values for AG50W-X8 and chlorides of the studied transition elements.....	33
Table 6 - K_d values for AG50W-X8 and nitrates of the transition elements	34
Table 7 - Sequential element separation procedure	36
Table 8 - Yields of the separated elements from the geological reference materials and the multi-element standard solution.....	46
Table 9 - Nickel separation procedure	54
Table 10 - Instrumental parameters and settings for the analysis of Ni isotopes on MC-ICP- MS.....	56
Table 11 - Ni isotope ratios for NIST SRM 986 and DS	58
Table 12 - Ni mass fraction and $\delta^{60}\text{Ni}$ value of reference materials	62
Table 13 - Chromium Separation Procedure	79
Table 14 - Impurities in the Cr fraction after column chromatography.....	88
Table 15 - The $\delta^{53}\text{Cr}$ values and mass fraction of Cr in reference materials	96
Table 16 - Techniques used for remove the adsorbed components from bacterial cells	106
Table 17 – Reagents used to treat cells and SiO_2 in the experiments carried out in this study	109
Table 18 - Instrument settings used for Zn isotope measurement	111
Table 19 - Removal of Fe and Zn from SiO_2 and Cells upon the use of different reagents to wash out adsorbed components.	113
Table 20 - Yield of elements in treated cell fractions normalized to dry weight of cells	115
Table 21 - Zn isotopic composition of the cells treated with different reagents and associated medium.	118
Table 22 - Composition of modified A+ medium	129
Table 23 - Growth Conditions	130
Table 24 - Absorbances (730nm) of 3 ml liquid cultures on the 15th day after inoculation.	134
Table 25 - Ni and nitrogen isotope fractionation by <i>Synechococcus</i> PCC 7002.....	135
Table 26 - Absorbance values of bacterial cultures grown in different growth media.....	135

Table 27 - Urea production yield in Archean oceans 146

Chapter 1: Introduction

1.1. Overview

One of the most fundamental questions about life on Earth is “Are we alone in the Universe?”. From time to time controversial news about alien life circulates in media around the world, but thus far there is no scientific confirmation that life exists beyond Earth. Despite the capability of space exploration by the advancement of technology, the origin and evolution of life on Earth itself is still not clearly understood and remains a mystery. The evolution of life on Earth is intertwined with its atmospheric evolution, and the advancement of knowledge about one will help the advancement of the other. Additionally, knowledge about the evolution of life on Earth may help to understand the conditions of Earth-like planets more in detail and will also help to define potential biosignatures to detect extant extra-terrestrial and paleo life.

During the Hadean eon (~4.6 to 4.0 billions of years ago) the Earth was completely different from today and hostile conditions such as continuous impacts, extreme temperatures etc. prevailed, making it uninhabitable. However, once primitive life evolved, it had to find a way to survive and evolve under these extreme conditions. The last big impact on Earth which could have vaporized the entire ocean is estimated to have happened 3.9~4.3 Ga (Abramov and Mojzsis 2009). Therefore, an upper age limit on the origin of life can be pinned to this event (Catling and Zahnle 2020; Marchi et al. 2014), which is also supported by phylogenetic inferences (Wolfe and Fournier 2018). The hypothetical late accretion of materials to Earth, named the Late Heavy Bombardment (LHB) is considered unlikely to have completely wiped out Earth’s early life (Abramov and Mojzsis 2009; Sleep et al. 1989). How life may have evolved in these extreme initial conditions mostly comes from theoretical work because of the lack of undisputed geochemical evidence and an extremely sparse geological record.

The earliest well-preserved sedimentary and volcanic rocks belong to the Archean eon (4.0 – 2.5 Ga), and this eon is characterized by negligible amount of oxygen in the atmosphere (<0.2 ppmv), which is constrained by numerous redox proxies (e.g. availability of pyrite and uraninite in detrital sediments) and mass-dependent and mass-independent isotope fractionation trends (e. g. Xe and S) (Catling and Zahnle 2020). The end of the Archean eon is characterized by the atmospheric oxygenation termed as “Great Oxidation Event” (GOE) where atmospheric oxygen rose to a level of ~10% of the Present Atmospheric Level (PAL) (see Lyons et al. 2014 for a review). Then oxygen levels in the atmosphere remained relatively constant until neo-Proterozoic oxygenation event (NOE) (Lyons et al. 2014).

The rise of atmospheric oxygen throughout Earth's history has significantly changed its biogeochemical cycles. Oxidative reactions altered the nutrient availability, especially redox sensitive metals, in the water column qualitatively as well as quantitatively, forcing the biosphere to adapt to new environmental conditions. Therefore, understanding the transition metal availability in the early Earth environment is entangled with the evolution of oxygen in the atmosphere. Therefore, understanding the root cause for the GOE is extremely important for evolutionary biologists as well as for planetary scientists. However, the exact timing, cause, and dynamics of this event are still under debate.

Abiotic and biotic causes have been proposed to explain what caused the rise of atmospheric O₂ and are debated (reviewed in (Kasting 2013)). Each of those explanations may have contributed to various degrees to the atmospheric oxidation and among these, understanding of the evolution of cyanobacteria is extremely important since they are single-handedly responsible for the generation of the most impactful waste gas, oxygen. The unquestionable fact is that if cyanobacteria were responsible for the GOE, there must have been favorable biogeochemical conditions prevailing throughout the Neoproterozoic period during which cyanobacteria are thought to have evolved.

Among many nutrients that are required to sustain cyanobacterial life, here in this work, nitrogen uptake and its isotopic fractionation were studied especially focusing the availability of transition metals including Mo, Ni, Fe and V. Nitrogen was specifically targeted because of its prominent role in biology especially in cyanobacteria as a macronutrient (Gladrow 2006, Kramer et al. 2022) and nickel was mainly focused among the transition metals involved in nitrogen acquisition due to its dominating role in relation to the success of methanogens that outcompeted the cyanobacteria before the GOE (Konhauser et al. 2009). Solving how cyanobacteria fulfilled its nitrogen requirement may shed light on the mechanisms underlying the GOE and evolution of Earth's atmosphere and hence the availability of transition metals in the habitats because supplementation of nitrogen, among other nutrients, is very important for the expansion of cyanobacteria (Kramer et al. 2022).

1.1.1. Outstanding questions

Using dinitrogen (N₂) gas as the nitrogen source for biological processes has both advantages and disadvantages. The main advantage is its higher abundance in present and past atmospheres (Catling and Zahnle 2020). On the other hand, the organism has to break up the strong bonds of the N₂ molecule to reduce it to the NH₄⁺ form to be utilized. This process is

called "nitrogen fixation" and requires a considerable amount of energy; and in fact, it is one of the most energetically expensive processes in biology (Raymond et al. 2004). However, the current understanding is that nitrogen fixation originated as far back as 3.2 Ga (Stüeken et al. 2015a). Was it possible for a primitive organisms to survive in the harsh environmental conditions to overcome this energy barrier and use N₂ as the nitrogen source? Or did they rely on an alternative nitrogen source?

To utilize N₂ as a nitrogen source, the earliest cyanobacteria should have possessed nitrogenase enzyme, the only enzyme that can catalyze the reduction of N₂ into bio-available forms. Among the three evolutionary-related nitrogenases, namely Mo-nitrogenase, V-nitrogenase, and Fe-only nitrogenase (Eady 1996), the former type, Mo-nitrogenase is most widely distributed among bacteria and is considered to be the one that was present in the primitive cyanobacteria (Leigh 2000; Raymond et al. 2004). It is also the isoform with the highest catalytic efficiency among the nitrogenases (Berman et al. 2003). However, depletion of Mo in oceans under anoxic conditions due to the insolubility of Mo sulfides (Anbar and Knoll 2002; Anbar et al. 2007; Scott et al. 2008) raises a question about the use of Mo for nitrogenase by Archean organisms and this has also been suggested as the reason for the low Proterozoic atmospheric O₂ concentration. Considering the presence of an anoxic ocean and abundance of reductants in the Archean, did cyanobacteria manage to overcome this nutrient limitation?

On the other hand, the nitrogenase enzyme is extremely oxygen-sensitive (Eady 1996) and it is irreversibly deactivated by molecular oxygen (Berman et al. 2003). Cyanobacteria have several protective mechanisms to overcome this deactivation such as having circadian (diurnal) expression (nitrogen fixation during the night when photosynthesis is on hold), diazocyte formation (multi-filament structures), and heterocyst formation (specialized nitrogen-fixing cells lacking the ability of photosynthesis). However, before the GOE, circadian expression was probably the only protective mechanism they had (reviewed in (Allen et al. 2019)). Therefore, if cyanobacteria had some kind of protective mechanism why the accumulation of oxygen in the atmosphere halt before reaching modern levels during/after the GOE in the Proterozoic eon (2.5 Ga ~ 0.5 Ga) (see figure 1) ?

To date, studies on the evolution of nitrogen fixation have been mainly done using nitrogen isotopic composition of organic matter preserved in sedimentary rocks. Using these data to interpret the nitrogen cycle without scrutiny is deceptive considering both the

uncertainties present in nitrogen isotope analysis, and given that the samples could have been modified by post-depositional geological processes (reviewed in (Ader et al., 2016). Experimental studies carried out with modern microbial cultures are extremely useful for the determination of nitrogen isotopic fractionation upon the utilization of various nitrogen sources. However, during these experimental studies ability of urea (H_2NCONH_2) and cyanide to be nitrogen sources has been neglected (Bauersachs et al. 2009; Hoch et al. 1992; Montoya and Mccarthy 1995; Nishizawa et al. 2014; Pennock et al. 1996; Waser et al. 1998; Zerkle et al. 2008; X. Zhang et al. 2014). It is important to consider these sources of nitrogen given that their abundance in primitive ocean (Salván et al. 2020; Tian et al. 2011). Experimental data for organic nitrogen species production from abiotic processes have shown that cyanide will be heavily fractionated from N_2 (Kuga et al. 2014). But it is important to consider and understand the nitrogen isotopic variation upon the use of these reduced nitrogen sources, especially when they were likely easily formed in the Precambrian atmosphere (Abelson 1966; Tian et al., 2011; Todd and Öberg 2020; Zahnle 1986).

Another issue regarding the evolution of primitive life on Earth is the question of how they managed to escape from the deleterious impacts of extreme UV irradiation before GOE which was penetrated to the Earth's surface due to the lack of ozone layer. Another explanation is the ability of living photosynthesizing multi-cellular cyanobacteria to move within microbial mats (Schirrmeister et al. 2015) to avoid the harmful irradiation. However, the technique they used survive extreme UV radiation while maintaining photosynthesis is problematic.

Finally, studying the evolution of primitive life from a geochemical perspective, especially from isotope studies is limited by the degree of technological and scientific advancement. It was proposed that isotope signatures can be used as biosignatures more than a decade ago (Anbar, 2001). However, the understanding of isotope fractionation associated with biogeochemical processes involving various metal isotope systems is still a daunting task because of the difficulty in resolving biotic from abiotic processes (Komárek et al. 2022). This assessment becomes especially difficult when working with ancient sedimentary rock samples where the environmental settings in which they have formed are unknown. The processes related to sorption, precipitation, evaporation, redox changes, and post depositional alterations are among many processes which can alter/overprint original isotopic signatures and these are not always addressed in the modern literature leaving a gap in understanding.

1.2. Objectives and thesis organization

Objectives of this study are twofold.

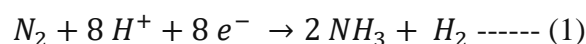
1. Determining the possibility of using transition metal isotope signatures to define biogenicity
2. Understanding how the availability of transition metals affected the evolution of life on Earth.

The first chapter discusses the current knowledge on the evolution of cyanobacteria and oxygen in the early Earth, and briefly introduces pitfalls that need to be addressed when using isotope signatures as biosignatures. Then a review of previous work on the evolution of cyanobacteria and oxygen is presented with a particular focus on the fulfilment of cyanobacterial nitrogen requirement. Chapters 2-4 describes methods for separating transition elements from geological matrices to precisely measure their isotope compositions. Chapter 5 evaluates the techniques that are available/followed for differentiating biotic and abiotic isotope fractionation caused by cellular metal assimilation and adsorption on cell surfaces respectively. In chapter 6 the evolution of biological N fixation is explored based on the availability of essential transition elements. Additionally, a conceptual model is presented to explain the occurrence of GOE and its relation to the expansion of cyanobacteria. Finally, the conclusions of this study are presented in chapter 7.

1.3. Review of previous work

1.3.1. Evolution of the nitrogen cycle and cyanobacteria

The main hypothesis of this work is that the growth of cyanobacteria, which played a major role in atmospheric oxygenation during the Archean, may have been hindered by the scarcity of nitrogen sources and Mo. This hypothesis stands on two factors. First, cyanobacteria may have faced difficulty in overcoming the energetic barrier to break the strong triple bonds of N_2 (eq 1), which is considered to have been the major source of nitrogen for their metabolic activities during Archaean (see below for a detailed explanation).



Secondly, cyanobacteria may have been challenged in synthesizing and protecting the nitrogenase enzyme responsible for biological nitrogen fixation (BNF). However, this hypothesis is counter to the current view of the evolution of BNF where it is accepted that BNF had already evolved by 3.2 Ga (Stüeken et al. 2015b), almost ~1 Ga before the GOE.

Nonetheless even in the existing scientific literature, there is no unified theory that explains the evolution of BNF and the planetary conditions that set the stage for its occurrence (Rucker and Kaçar 2023).

Nitrogen is essential for life because it is a principal constituent of nucleic acids and proteins (Zerkle et al. 2006). When considering bacterial cells, about 10% of their dry weight consists of nitrogen (Bradley and Nichols 1918a; Enrique Flores and Herrero 1994a). Furthermore, cyanobacteria need fixed nitrogen for the biosynthesis of photosynthetic pigments (Gruła 2005 and references therein). Depending on the nitrogen speciation of the source, various enzymes are necessary for the conversion of nitrogen into the bio-available NH_4^+ form. These enzymes require various transition metals for their proper functioning and the availability of these metals has changed throughout the Earth's history (Anbar and Knoll 2002; Moore et al. 2017). Therefore, transition metal availability may have controlled nitrogen availability. Additionally, the redox nature of early Earth may have also played a significant role in the biological nitrogen cycle because nitrogen is a highly redox-sensitive element. Since the evolution of cyanobacteria is entangled with the evolution of atmospheric composition, understanding their strategy for fulfilling their nitrogen requirement may shed light upon atmospheric oxygenation.

Cyanobacteria were the only organism that had the capability of producing oxygen as a waste product prior to 3.0 Ga, (Schirrmeister et al. 2015) and thus were solely responsible for early atmospheric oxygen production. Although there is no exact consensus on how or when the GOE occurred, it is generally believed that global atmospheric oxygenation increased to PAL (present atmospheric level) in three phases. Phase one consists of transient oxygen pulses called “whiffs” of oxygen until 2.5 Ga (Anbar et al. 2007), which is followed by an oxygen overshoot known as the great oxidation event (GOE), at around 2.4-2.1 Ga (Bekker and Holland 2012; Lyons et al. 2014). Phase 2 consists of a period during which atmospheric oxygen amount remained low for most of the Proterozoic period (Planavsky et al. 2014). Phase

3 began about 800 Ma during the Neoproterozoic, delineating an increase in atmospheric oxygen to modern levels.

However, the presence of more O₂ (3×10^{-4} PAL) around 3.0-3.2 Ga is argued by Cr, Fe, Mo, and C isotope data (Crowe et al. 2013; Lyons et al. 2014; Nisbet and Nisbet 2008; Planavsky et al. 2014) and phylogenomic analyses which suggest the presence of cyanobacteria prior to the GOE (reviewed in (Schirmer et al 2016). This leads to the question of why the

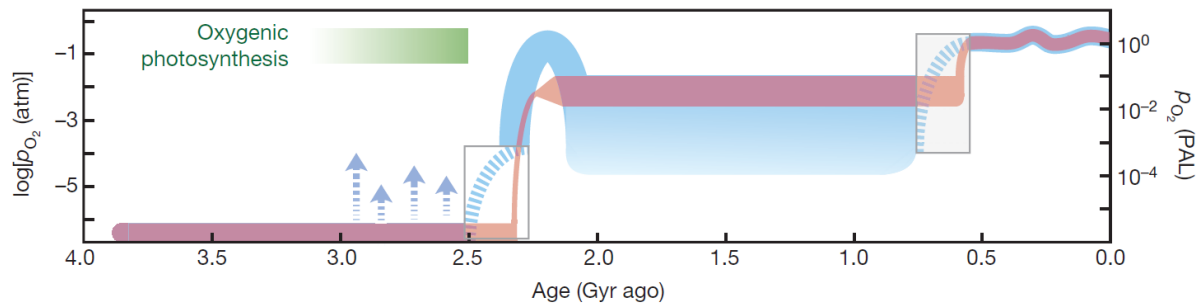


Figure 1 - Evolution of oxygen through time (from Lyons et al., 2014), the blue line and the red line represent the modern and classical views respectively.

increase in atmospheric oxygen halted until the end of the Archaean. Multiple reasons have been suggested (Kasting 2013) including :

1. Changes in recycling of carbon and sulfur.
2. Changes in volcanism from submarine to dominantly subaerial.
3. Oxidation of continents and decrease in reduced metamorphic gases.
4. Decline in the deposition of banded iron formations and decline in Ni availability.
5. Variations in the efficiency of photosynthesis

Shortly after or during the increase (2.3-2.0 Ga) of atmospheric oxygen levels, carbon isotopic ratios of marine carbonates also recorded increased values (by up to ~10‰) and this event named as Lomagundi event (LE) (Karhu and Holland 1996). Prevailing explanation for LE include enhanced oxygen production during LE which resulted enhanced organic burial incorporating ¹²C, leaving behind the marine carbonate reservoir enriched in ¹³C (Karhu and Holland 1996).

1.3.2. Nitrogen acquisition by cyanobacteria

Cyanobacteria can use the inorganic compounds of nitrogen such as N₂, NO₃⁻, NO₂⁻, and NH₄⁺ to fulfill their nitrogen requirements, but they also can use organic nitrogen sources such as urea and amino acids. However, all such nitrogen sources must be converted to the NH₄⁺ form before nitrogen assimilation (Flores and Herrero 1994). Table 1 shows some of the

main nitrogen incorporation modes by cyanobacteria as well as associated enzyme complexes and their corresponding metals. The last step of all these nitrogen assimilation pathways is the conversion of NH_4^+ to glutamine and this process is illustrated in Figure 2.

Table 1 - Key enzymes involved in nitrogen assimilation of cyanobacteria

N substrate	Product	Enzyme	Metal Cofactor
N_2	NH_3	Nitrogenase	Fe, S, Mo
NO_3^-	NO_2^-	Nitrate Reductase	Fe, Mo
NO_2^-	NH_3	Nitrite Reductase	Fe, S
NH_4^+	Glutamine ($\text{C}_2\text{H}_{10}\text{N}_2\text{O}_3$)	Glutamine Synthetase	Mn?
Urea	$\text{NH}_3, \text{H}_2\text{CO}_3$	Urease	Ni
Amines	$\text{NH}_3, \text{H}_2\text{O}_2, \text{RCHO}$	Cu-amino acid oxidase	Cu

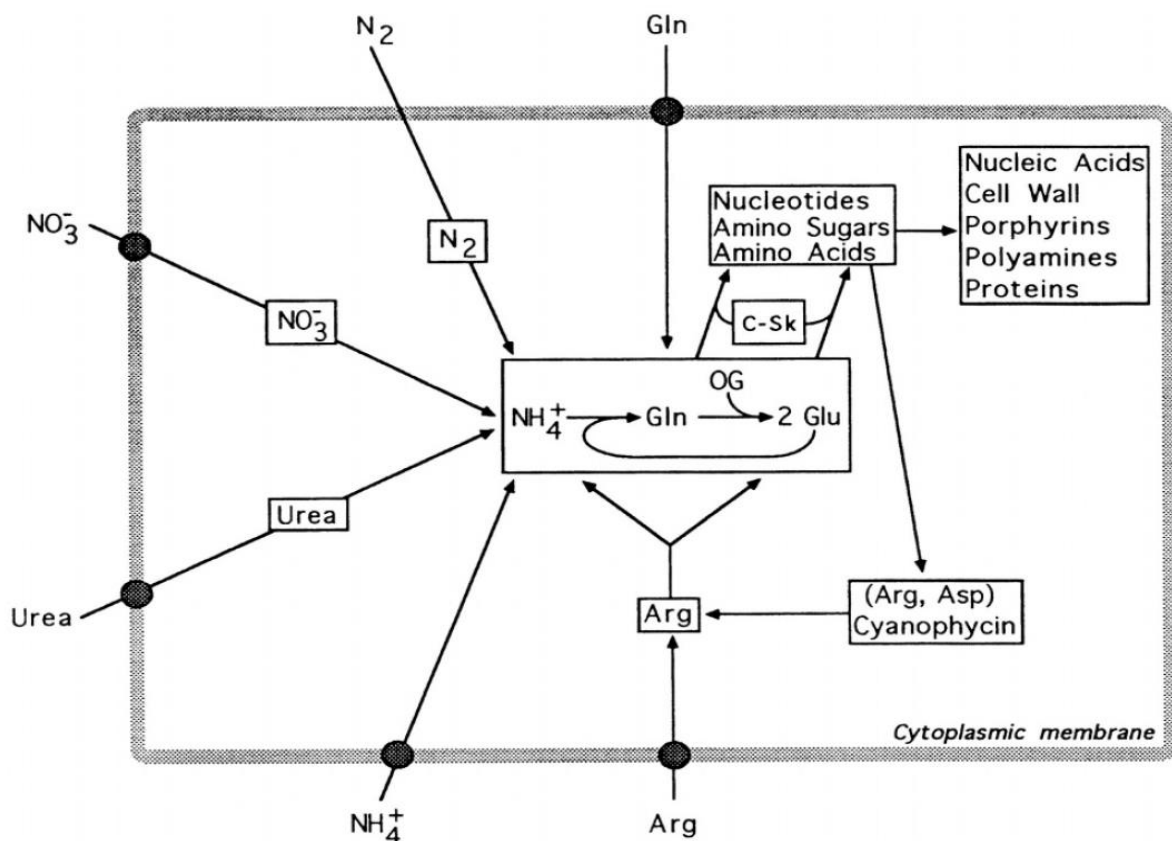


Figure 2 - Nitrogen assimilation pathways. C-Sk - Carbon skeletons; OG, 2-oxoglutarate; Gln, Glutamine; Glu, Glutamate; Arg, Arginine. (Flores and Herrero 1994)

Among these nitrogen assimilation pathways, N_2 fixation requires special adaptation of cells since the nitrogenase enzyme is extremely oxygen sensitive (Burris 1991). Therefore,

many cyanobacterial species have spatially or temporally separated functions related to oxygenic photosynthesis and nitrogen fixation. Some of them have developed specialized cells called “heterocysts” for spatially separate nitrogen fixation from oxygenic photosynthesis while others fix nitrogen during the dark period and undertake oxygenic photosynthesis during the light period (Allen et al. 2019 and references therein). However, it has been proposed that nitrogenase may have been inhibited by oxygen itself (Madigan and Background 1995). Limited primary oxygen production due to oxygen inhibition of nitrogenase (Allen et al. 2019) may have resulted a low steady-state oxygen concentration during most of the Proterozoic period. It is proposed that during this low level of oxygen, nitrogenase may have remained active such that microorganisms were not nitrogen limited. In addition to the extreme sensitivity of nitrogenase to oxygen, specific metals are required for proper functioning. In particular requires either Mo-Fe, V-Fe or only Fe are used depending on the isoenzyme (reviewed in Zerkle et al. 2006), and therefore temporal and spatial availability of these metals also may have played a role in the evolution of BNF (Glass et al. 2009). Among these isoenzymes (a group of enzymes that catalyze the same reaction but have different enzyme forms and catalytic efficiencies), the Fe-Mo nitrogenase is the most efficient in N₂ reduction. It is approximately 1.5 and 100 times more efficient than Fe-V and Fe-Fe nitrogenases, respectively (reviewed in Zerkle et al. 2006). Despite the significantly low Mo concentrations in the Archean ocean (Scott et al. 2008), it is considered as the metal co-factor of ancient nitrogenases based on the phylogenetic reconstructions with inferred ancestral sequences (Garcia et al. 2020). Generally, it was thought that nitrogenase originated in the archaea (Raymond et al. 2004) but recent studies suggest that it may have originated in bacteria (Pi et al. 2022).

It is also important to note that nitrogenase is also capable of reducing various substrates other than N₂ such as cyanide and cyanamide (Burriss 1991). Therefore, it is probable that early nitrogenases in the Earth’s distant past may have acted as a “detoxase”, i.e. protecting the microorganisms against cyanide poisoning in the ancient ocean (Fani et al. 2000). However, the age of the origin of nitrogenase evolution is still debated (Mus et al. 2019). Based on isotopes and phylogenetic analyses, it has been suggested to have originated at 2.5 Ga (Garvin et al. 2009), 3.2 Ga (Stüeken et al. 2015) or 1.5 - 2.2 Ga (Boyd et al. 2011). Nitrogenase has also been suggested to have been present in the Last Universal Common Ancestor (LUCA) of all cells (Weiss et al. 2016). However, recent studies show that earliest cyanobacteria could not have fixed N₂ and they did not have heterocysts (Hammerschmidt et al. 2021).

1.3.3. Nitrogen control and heterocyst formation

Understanding nitrogen control is extremely important when studying the microbial nitrogen assimilation process since it widely occurs among microorganisms. Nitrogen control represses the nitrogen assimilation pathways of some nitrogen sources while some other, more easily assimilated sources of nitrogen are available to the cells (Herrero et al. 2001). For example, nitrogenase synthesis is repressed in the presence of NH_4^+ , and excess ammonium can also inhibit activity or expression of nitrate reductase, nitrite reductase or glutamine synthetase (Kennedy et al. 1994; Klugkist and Haaker 1984). However, when NH_4^+ and Urea are present as reduced nitrogen sources, cyanobacteria preferentially utilize the organic nitrogen source (urea) over the inorganic nitrogen sources, and the presence of urea will repress the intake of dissolved NH_4^+ (Erratt et al. 2020).

Experimental study (Flores and Herrero, 2005) has suggested that the C/N ratio sensed by cyanobacterial cells could determine the expression of enzymes required for efficient assimilation of ammonium or alternative nitrogen sources. This expression of enzymes is mediated by a protein called NtcA and it regulates the genes that participate in nitrogen assimilation pathways (Herrero et al. 2001). Therefore, in simple words, there is no need for the production of NtcA protein in an environment where reduced nitrogen species are common. On the other hand, the development of heterocysts, which are the specialized cells for N_2 fixation, will also cease in the presence of reduced nitrogen sources as heterocyst formation is strictly regulated by the NtcA protein. Since fossil heterocysts have not been observed in rocks predating the Devonian period (~0.42 Ga) (reviewed in Allen et al. 2019), it is important to clarify how cyanobacteria fulfilled their nitrogen requirement during their evolution.

To make the problem more complicated, heterocystous cyanobacteria are absent from modern full-salinity seawater and rare in modern marine microbial mats (Hallenbeck 2010). Stal (1995) observed that heterocystous and non-heterocystous cyanobacterial growth is dependent on the presence of sulfide content and/or high O_2 concentrations in a cyanobacterial mat. It was noted that heterocystous cyanobacterial growth is limited by high sulfides and/or high oxygen concentrations in modern cyanobacterial mat. This observation questions the presence of heterocystous cyanobacteria in sulfide-rich Archaean oceans where stromatolitic microbial colonies pounded by tides may have been abundant.

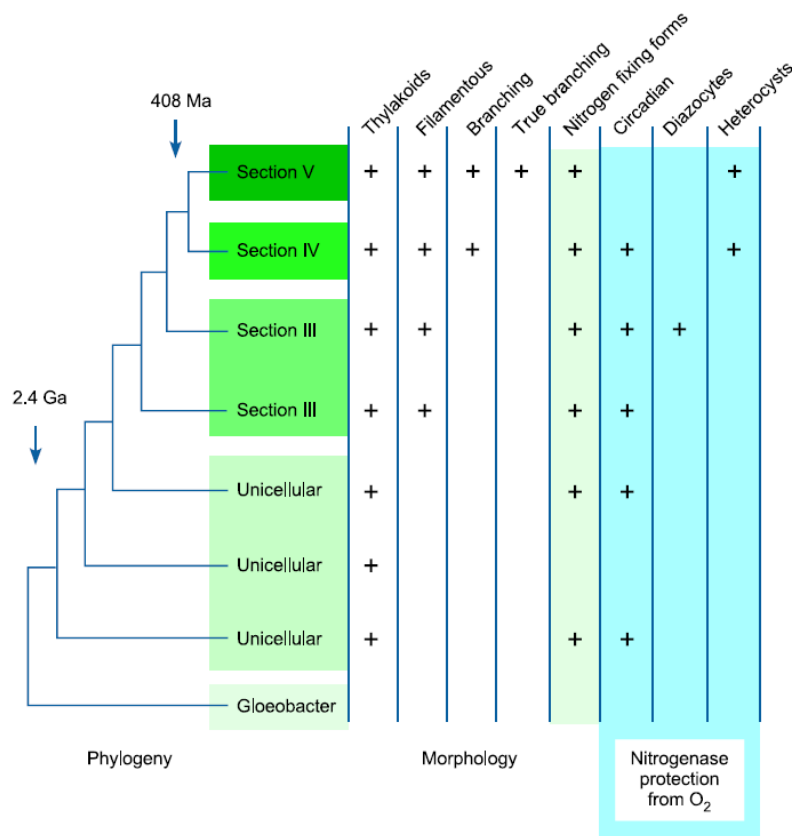


Figure 3 - Late appearance of heterocysts in cyanobacterial evolution (modified from Allan et al., 2019)

Therefore, if N₂ fixation happened on the early Earth, the following conditions must have been already present:

1. There were no or extremely limited reduced nitrogen sources available for the growth of cyanobacteria so that NtcA proteins could be expressed by the microorganisms.
2. An abundant Mo supply was present for the proper functioning of nitrogenase.
3. Heterocyst development should have already occurred or cyanobacteria had an alternative mechanism for protecting nitrogenase from oxygen.

1.3.4. Urease, urea, and Ni

Urea and urease have both set remarkable historic landmarks in molecular biology. Urea was the first synthetic organic molecule, and urease was the first enzyme ever to be crystallized. Additionally, urease was the first enzyme shown to contain Ni (two nickel ions) in its active center (Kappaun et al. 2018; Mazzei et al. 2020). Urea is readily available in most habitats because it is the principal nitrogenous waste of mammals. Therefore, many organisms, including various bacterial species of aerobes and anaerobes (Collins and D'Orazio 1993),

show urease activity. Additionally, it is also present in fungi and plants (Mobley et al. 1995; Strope et al. 2011). However, this enzyme is not found in animals (Kappaun et al. 2018).

Urease catalyzes the hydrolytic decomposition of urea, producing an ammonia molecule and a carbamate molecule (which will spontaneously decompose into another ammonia molecule and carbonic acid) (Alfano and Cavazza 2020; Mobley et al. 1995). This reaction facilitates the organism to use urea as a nitrogen source. The overall reaction will ultimately increase the pH level of the medium (Mazzei et al. 2020). It has been found that urease may have synthesized either constitutively or as a stress-related response in bacteria to counteract low environmental pH (Cotter and Hill 2003; Mackerras and Smith 1986).

Importantly, none of the nitrogen sources such as NO_3^- , N_2 , NH_4^+ , nor urea itself are able to inactivate urease enzyme except for NH_4^+ , which shows a weak inhibitory effect (Kappaun et al. 2018; Singh 1992). On the contrary, the presence of NH_4^+ and urea can repress the synthesis of nitrogenase (Ge et al. 1990; Klugkist and Haaker 1984; Zerkle et al. 2006) and therefore it can be assumed that organisms prefer these sources over the oxidized nitrogen species.

Considering the cyanobacterial nitrogen-obtaining pathways, urea assimilation probably has the highest energetic efficiency among all other pathways of nitrogen acquisition (Erratt et al. 2018) because urea can provide twice the nitrogen content and act as an additional carbon source. Utilization of urea also yield higher-quality cells by enhancing pigment synthesis (Erratt et al. 2018).

However, the excess presence of urea in the growth medium leads to various degrees of growth inhibition among cyanobacterial species (Erratt et al. 2018; Sakamoto et al. 1998). This results from excess hydrolysis of urea rather than the biosynthetic requirement, which ultimately creates excess NH_4^+ in the medium (Erratt et al. 2018; Mackerras and Smith 1986). However, the actual reason for this growth inhibition is not known (Sakamoto et al. 1998).

Regardless of the growth inhibition of cyanobacteria at high urea concentrations, urea represents a dominant organic nitrogenous compound in modern oligotrophic oceans. Laboratory culture experiments of marine cyanobacteria have shown that they require Ni in the growth medium to utilize urea as a nitrogen source, and some of them do have a high-affinity uptake system for Ni (Ge et al. 1990; Mackerras and Smith 1986; Sakamoto and Bryant 2001). The requirement of Ni for utilization of urea is straightforward because all ureases found so far

require Ni for their enzymatic activity (Collins and D'Orazio 1993), and thus providing hints for the evolution of urease in relation to the origin of life (Gan et al. 2023; Huber et al. 2003).

Since this work is mainly focused on cyanobacterial evolution in the distant past, it is important to understand the occurrences and formation mechanisms of urea in paleo environments. Despite the limited data available for the occurrence of urea in the Precambrian environment, the potential formation mechanisms of urea in such environments will be discussed below.

1.3.5. Occurrence of Urea

Urea is considered an important molecule for the origin of life (Gan et al. 2023; Salván et al. 2020; Sakurai and Yanagawa 1984; Stephen-Sherwood, Odom, and Oró 1974). Various mechanisms of the formation of urea have been discussed extensively (García et al. 2009; Lohrmann 1972; Lowe et al. 1963; Palm and Calvin 1962; Schlesinger and Miller 1983; Shorter 1978; Takano et al. 2004; Wen and Brooker 1994). Its delivery by comets and asteroids has been also suggested (Förstel et al. 2016; Todd and Öberg 2020) because of its presence in comets in solid and gas phases (Morvan et al. 2000). The formation and delivery mechanisms of urea in/to primitive Earth can be summarized as follows.

1. Heating ammonium cyanate (Wohler, 1828)
2. Electron irradiation of Methane (Palm and Calvin 1962).
3. Exposing inorganic ices of NH_3 and CO to ionizing radiation (Förstel et al. 2016)
4. The reaction between hydrocyanic acid ($=\text{HCN}$) and aqueous NH_3 (Lowe et al. 1963)
5. UV Irradiation of ammonium cyanide in the presence of Fe (Lohrmann 1972)
6. Electric discharge in inorganic gas mixtures (Schlesinger and Miller 1983)
7. Polymerization of HCN (Bermejo et al. 2013)

In addition to these mechanisms, many studies have examined the formation of urea under UV irradiation and electric discharge experiments (reviewed in (Lohrmann 1972; Sakurai and Yanagawa 1984)). Therefore, in the recent literature, it is considered that urea was readily available in the primitive Earth and gradually accumulated in the primitive oceans (Salván et al. 2020; González et al. 1989). Importantly its remarkable stability when exposed to harmful irradiation such as UV and γ -rays (Gan et al. 2023; González et al. 1989) underpins its high potential to accumulate in the primitive oceans.

In 1828, Wohler synthesized urea by evaporating a mixture of $(\text{NH}_4)_2\text{SO}_{4(\text{aq})}$ and KCN, and henceforth the mechanism for this reaction debated (Shorter 1978). It was thought that the

ammonium cyanates produced in the metathesis reaction would be rearranged into urea. Later studies revealed that initial cyanate (NCO^-) hydrolysis will generate bicarbonate, carbamate, and ammonium ions, and the excess cyanates will react with ammonium to produce urea (Wen and Brooker 1994).

Even though the complete endogenic production of urea is disfavored (Förstel et al. 2016) due to the low concentrations and lower stability of cyanates in the primitive oceans, it should be noted that these stability limits were identified based on an acidic ocean where $\text{pH} < 6$ (Miller and Orgel, 1974) however there are records for conflicting pH values for the Archean ocean in modern literature (Totton et al., 2018 and references therein). Additionally, the resulting cyanides (CN^-) from cyanate decomposition can also produce urea with the aid of irradiation by sunlight, UV, or γ -rays (García et al. 2009; Lohrmann 1972). On the other hand, some of the mechanisms mentioned above do not require cyanate at the initial step for the production of urea (ex: (Lohrmann 1972; Malhotra et al. 2005), but most of them require cyanide instead. Therefore, the formation of cyanides plays an important role in all these mechanisms, and an abundant literature is available regarding cyanide formation/delivery mechanisms for the primitive Earth (Abelson 1966; Cicerone and Zellner 1983; Kasting 1990; Pearce et al. 2022; Tian et al. 2011; Todd and Öberg 2020; Zahnle 1986). It is estimated that photolysis of N_2 in thermosphere and ionosphere ultimately produce HCN and a yield of 30 Tg/year can be calculated throughout the Archean (Tian et al. 2011). However, no one has currently explored its potential to serve as a nitrogen source for the early cyanobacteria and thus its potential to kick start atmospheric oxygenation.

1.3.6. Importance of Ni for cyanobacterial growth and growth of cyanobacteria in urea rich media

The ability of most of the Ni enzymes to produce or consume gaseous molecules and their presence in anaerobic metabolic systems hints of the ancient use of this metal in early organisms even perhaps back to the origin of life (Zamble 2017). Since Ni is near the top end of the Irving Williams series ($\text{Mg}^{2+} < \text{Ca}^{2+} < \text{Mn}^{2+} < \text{Fe}^{2+} < \text{Co}^{2+} < \text{Ni}^{2+} < < \text{Cu}^{2+} > \text{Zn}^{2+}$) it has the capability of replacing existing metals in metal centers of the enzymes, making them inactive (Wanklyn and Zamble 2017). Therefore, uncontrolled uptake of Ni ions can be toxic for the organisms.

However, the role of Ni is remarkable when considering the evolutionary perspective of life. A documented declining molar Ni to Fe ratio in banded iron formations at around 2.7 Ga

(Konhauser et al. 2009, 2015) has been attributed to a decline of Ni flux to the Precambrian oceans at the end of Archean. Since Ni serves as an essential metal cofactor for the enzyme (methyl coenzyme M reductase, MCR), which corresponds to the final step of methane production, it was inferred that this Ni decline collapsed methane production and paved the way for the ecological success of cyanobacteria.

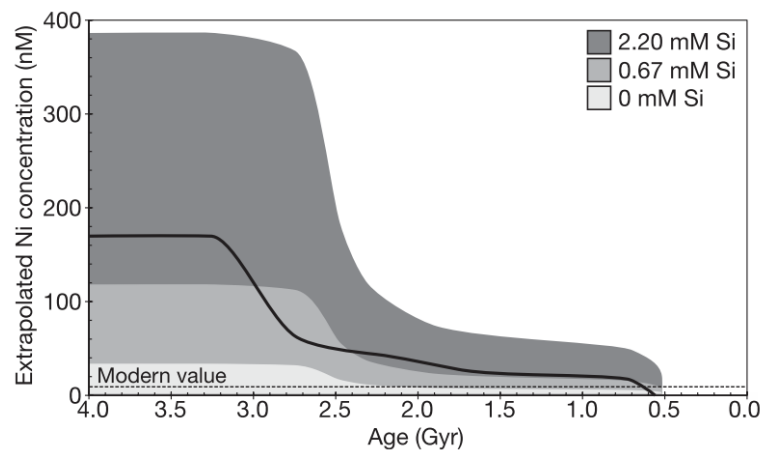


Figure 4 - Maximum dissolved Ni in sea water through time (Konhauser et al., 2009)

In cyanobacteria, Ni is mainly used by the enzymes of urease, hydrogenase and superoxide dismutases. The activity of urease enzyme is necessary to utilize urea as a nitrogen source (described above). Superoxide enzymes are required for protecting photosynthetic microorganisms from the reactive superoxide radicals they produce while hydrogenases are used in H_2 utilization. Additionally, it has been experimentally shown that decrease in Ni causes diminished cell growth of N_2 fixing cyanobacteria due to lower activity of nitrogenase and uptake hydrogenase (Zamble 2017 and references therein).

Sakamoto and Bryant (1997) noted that the high concentration of urea in the growth medium will sustain cyanobacterial (*Synechococcus sp.* PCC 7002) growth under low temperature conditions ($15\text{ }^\circ\text{C}$), whereas NO_3^- cannot. However, later it was found that growth in high urea concentrations ($>25\text{ mM}$) initiate rapid death phase of cyanobacteria especially when the medium is supplemented with high Ni and elevated CO_2 (Sakamoto et al. 1998) as they are actively involved in the catalytic center of the urease. At the same time, it was noted that addition of Ni is essential for the efficient utilization of urea (Sakamoto and Bryant 2001).

1.3.7. Oceanic Ni biogeochemistry

Among the oceanic transition metal studies conducted by the oceanographers, Ni is often neglected, and only a limited number of studies are available in relation to its role in the oceanic biosphere. This is mainly because Ni is not significantly depleted in the surface ocean like the other transition metals and therefore is not considered a bio-limiting nutrient (Figure 6). Moreover, the residual Ni portion in the photic zone is reportedly not bio available (Archer et al. 2020).

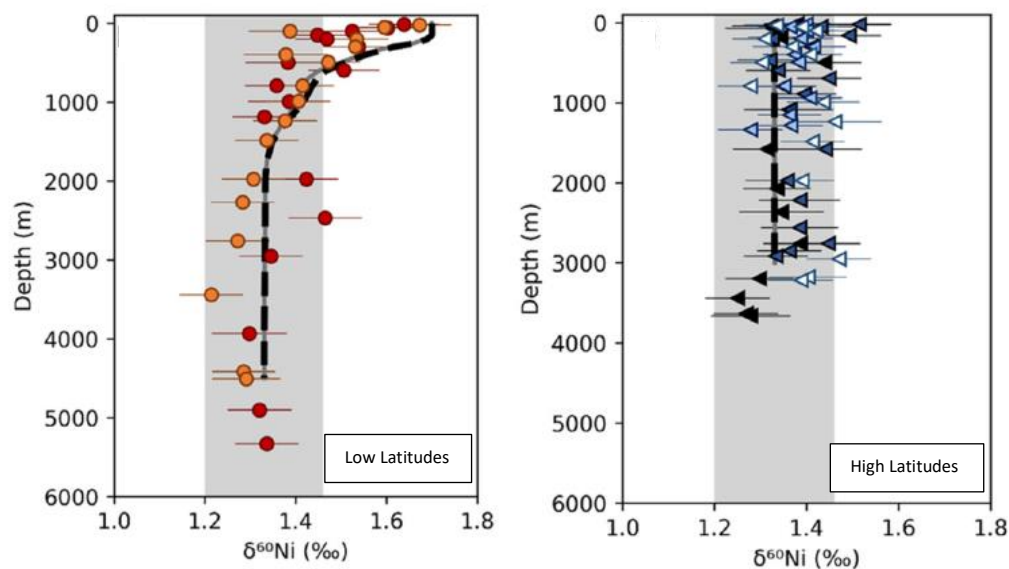


Figure 5 - Ni isotope variation in two regions (Left - Low latitudes Right - High Latitudes) of North Atlantic Ocean where the differences of the regions are mainly associated with sea water temperature, nutrient availability and the presence of diatoms (modified from Lemaitre et al. 2022)

Even though effects of Ni supplementation for laboratory grown microbial culture is known, the variations of Ni isotopic signatures in these organisms are not well studied. The only known Ni isotope fractionation study was conducted for the methanogenic Archaea (Cameron et al. 2009) which are anerobic organisms. Therefore, it is not possible to explain the observed isotope trends in the ocean (figure 5) where aerobic primary producers are present in the surface waters.

In the ocean it is also observed that Ni isotope variations differ from one locality to another in addition to the commonly observed depth profile (Figure 5). The North Atlantic Ocean shows two major trends in Ni isotopic variation where in the low latitude regions the surface water is enriched (~ 1.6 ‰) with heavier Ni isotopes while in high latitudes there is no pronounced variation in the Ni isotope profile (Lemaitre et al. 2022). Since the main differences

in these two particular regions are associated with temperature, nutrient availability and the presence of diatoms, it is important to understand which contributed to these observed variations in Ni isotope variations.

In addition to being a bio-essential element which is used by phytoplankton communities for the functioning of enzymes mentioned above, oceanic Ni also resembles the nutrient element profiles observed in the sea in which surface depletion and regeneration at depths are observed (Middag et al. 2020). However, in the surface ocean it is not completely drawn down to lower concentrations as observed for other nutrients such as NO_3^- , PO_4^{3-} , and Si (Figure 6). Possibly the remaining Ni may not be bio available but scientists are still struggling to find the source of this bio unavailable Ni fraction.

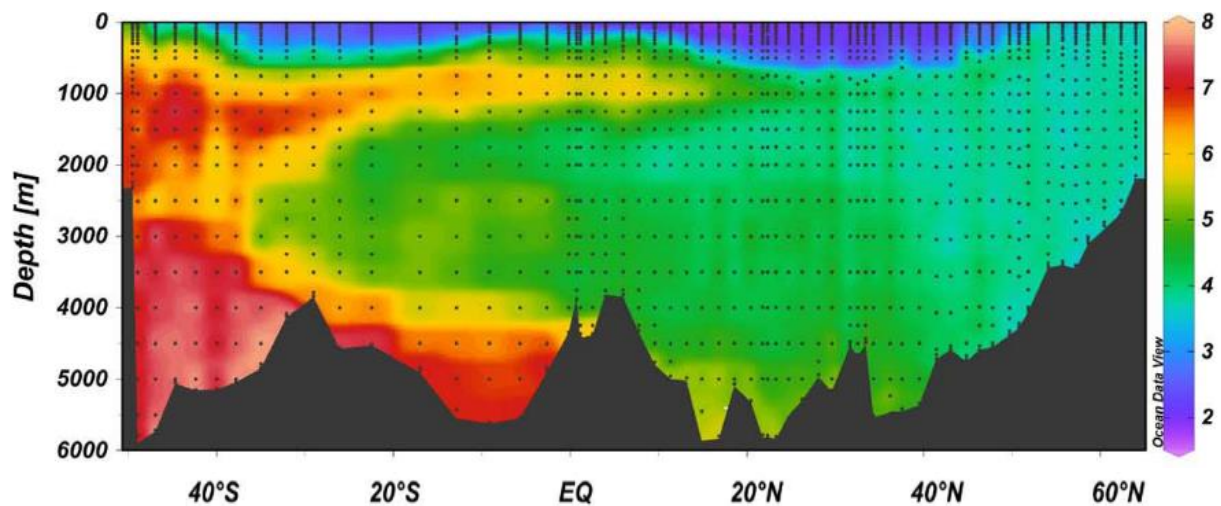


Figure 6 - The GEOTRACES GA02 section in the West Atlantic Ocean, the dissolved Ni concentration along the transect (modified after Middag et al., 2020)

1.4. References

- Abelson, Philip H. 1966. “Chemical Events on the Primitive Earth.” *Proceedings of the National Academy of Sciences* 55(6): 1365–72.
- Abramov, O., & Mojzsis, S. J. (2009). Microbial habitability of the Hadean Earth during the late heavy bombardment. *Nature*, 459(7245), 419–422.
<https://doi.org/10.1038/nature08015>
- Ader, M., Thomazo, C., Sansjofre, P., Busigny, V., Papineau, D., Laffont, R., ... Halverson, G. P. (2016). Interpretation of the nitrogen isotopic composition of Precambrian sedimentary rocks: Assumptions and perspectives. *Chemical Geology*, 429, 93–110.
<https://doi.org/10.1016/j.chemgeo.2016.02.010>

- Alfano, Marila, and Christine Cavazza. 2020. "Structure, Function, and Biosynthesis of Nickel-Dependent Enzymes." *Protein Science* 29(5): 1071–89.
- Allen, John F., Brenda Thake, and William F. Martin. 2019. "Nitrogenase Inhibition Limited Oxygenation of Earth's Proterozoic Atmosphere." *Trends in Plant Science* 24(11): 1022–31.
- Anbar, A. D., and A. H. Knoll. 2002. "Proterozoic Ocean Chemistry and Evolution: A Bioinorganic Bridge?" *Science* 297(5584): 1137–42.
- Anbar, A. D. (2001). Iron isotope biosignatures: Promise and progress. *Eos*, 82(15).
<https://doi.org/10.1029/01EO00089>
- Anbar, Ariel D. et al. 2007. "A Whiff of Oxygen before the Great Oxidation Event?" *Science* 317(5846).
- Archer, Corey, Derek Vance, Angela Milne, and Maeve C. Lohan. 2020. "The Oceanic Biogeochemistry of Nickel and Its Isotopes: New Data from the South Atlantic and the Southern Ocean Biogeochemical Divide." *Earth and Planetary Science Letters* 535: 1–11.
- Bauersachs, T., Schouten, S., Compaore, J., Wollenzien, U., Stal, L. J., & Sinninghe Damste, J. S. (2009). Nitrogen isotopic fractionation associated with growth on dinitrogen gas and nitrate by cyanobacteria. *Limnology and Oceanography*, 54(4), 1403–1411.
<https://doi.org/10.4319/lo.2009.54.4.1403>
- Bekker, A., and H. D. Holland. 2012. "Oxygen Overshoot and Recovery during the Early Paleoproterozoic." *Earth and Planetary Science Letters* 317–318: 295–304.
- Berman-frank, I., Lundgren, P., & Falkowski, P. (2003). "Nitrogen fixation and photosynthetic oxygen evolution in cyanobacteria" *Research in Microbiology*. 154, 157–164. [https://doi.org/10.1016/S0923-2508\(03\)00029-9](https://doi.org/10.1016/S0923-2508(03)00029-9)
- Bockelée-Morvan, D, DC Lis, and JE Wink. 2000. "New Molecules Found in Comet C/1995 O1 (Hale-Bopp)." *Astronomy and Astrophysics* 1114(March 1996): 1101–14.
- Boyd, E. S. et al. 2011. "A Late Methanogen Origin for Molybdenum-Dependent Nitrogenase." *Geobiology* 9(3): 221–32.

- Bradley, Harold C., and M. Starr Nichols. 1918. "Nitrogen Content of Bacterial Cells." *Journal of Biological Chemistry* 33(3): 525–29.
- Burris, R. H. 1991. "Nitrogenases." *Journal of Biological Chemistry* 266(15): 9339–42.
- Cameron, Vyllinniskii, Derek Vance, Corey Archer, and Christopher H. House. 2009. "A Biomarker Based on the Stable Isotopes of Nickel." *Proceedings of the National Academy of Sciences of the United States of America* 106(27): 10944–48.
- Catling, D. C., & Zahnle, K. J. (2020). The Archean atmosphere. *Science Advances*, 6(9). <https://doi.org/10.1126/sciadv.aax1420>
- Cicerone, R. J., and R. Zellner. 1983. "The Atmospheric Chemistry of Hydrogen Cyanide (HCN)." *Journal of Geophysical Research* 88(C15): 10689–96.
- Colín-García, M., A. Negrón-Mendoza, and S. Ramos-Bernal. 2009. "Organics Produced by Irradiation of Frozen and Liquid HCN Solutions: Implications for Chemical Evolution Studies." *Astrobiology* 9(3): 279–88.
- Collins, Carleen M., and Sarah E.F. D’Orazio. 1993. "Bacterial Ureases: Structure, Regulation of Expression and Role in Pathogenesis." *Molecular Microbiology* 9(5): 907–13.
- Cotter, Paul D., and Colin Hill. 2003. "Surviving the Acid Test: Responses of Gram-Positive Bacteria to Low PH." *Microbiology and Molecular Biology Reviews* 67(3): 429–53.
- Crowe, Sean A. et al. 2013. "Atmospheric Oxygenation Three Billion Years Ago." *Nature* 501(7468): 535–38.
- Eady, R. R. (1996). Structure-function relationships of alternative nitrogenases. *Chemical Reviews*, 96(7), 3013–3030. <https://doi.org/10.1021/cr950057h>
- Erratt, Kevin J, Irena F Creed, and Charles G Trick. 2018. "Comparative Effects of Ammonium , Nitrate and Urea on Growth and Photosynthetic Efficiency of Three Bloom-Forming Cyanobacteria." *Freshwater Biology* : 626–38.
- . 2020. "Differential Drawdown Of Ammonium, Nitrate, And Urea By Freshwater Chlorophytes And Cyanobacteria." *Journal of Phycology*, 458-468 <https://onlinelibrary.wiley.com/doi/10.1111/jpy.12960>.

- Fani, Renato, Romina Gallo, and Pietro Liò. 2000. "Molecular Evolution of Nitrogen Fixation: The Evolutionary History of the NifD, NifK, NifE, and NifN Genes." *Journal of Molecular Evolution* 51(1): 1–11.
- Flores, E, and A Herrero. 2005. "Nitrogen Assimilation and Nitrogen Control in Cyanobacteria." *Biochemical Society Transactions* 33 : 164-167
- Flores, Enrique, and Antonia Herrero. 1994. "Assimilatory Nitrogen Metabolism and Its Regulation." *The Molecular Biology of Cyanobacteria*: 487–517.
- Förstel, M. et al. 2016. "Synthesis of Urea in Cometary Model Ices and Implications for Comet 67P/Churyumov-Gerasimenko." *Chemical Communications* 52(4): 741–44.
- Gan, Dingwei et al. 2023. "Urea-Mediated Warm Ponds: Prebiotic Formation of Carbamoyl Amino Acids on the Primordial Earth." *Earth and Planetary Science Letters* 607: 118072.
- Garcia, Amanda K., Hanon McShea, Bryan Kolaczowski, and Betül Kaçar. 2020. "Reconstructing the Evolutionary History of Nitrogenases: Evidence for Ancestral Molybdenum-Cofactor Utilization." *Geobiology* 18(3): 394–411.
- Garvin, Jessica et al. 2009. "Isotopic Evidence for an Aerobic Nitrogen Cycle in the Latest Archean." *Science* 323(5917): 1045–48.
- Ge, X., K. Cain, and R. Hirschberg. 1990. "Urea Metabolism and Urease Regulation in the Cyanobacterium *Anabaena Variabilis*." *Canadian Journal of Microbiology* 36(3): 218–22.
- Glass, J. B., F. Wolfe-Simon, and A. D. Anbar. 2009. "Coevolution of Metal Availability and Nitrogen Assimilation in Cyanobacteria and Algae." *Geobiology* 7(2): 100–123.
- Gruhl, John W. 2005. "Evolution of Photosynthesis and Biospheric Oxygenation Contingent upon Nitrogen Fixation?" *International Journal of Astrobiology* 4(3–4): 251–57.
- Hallenbeck, Patrick C. 2010. *Recent Advances in Phototrophic Prokaryotes*, 675, 2010, Springer
- Hammerschmidt, Katrin et al. 2021. "The Order of Trait Emergence in the Evolution of Cyanobacterial Multicellularity." *Genome Biology and Evolution* 13(2): 1–10.

- Herrero, A., A. M. Muro-Pastor, and E. Flores. 2001. "Nitrogen Control in Cyanobacteria." *Journal of Bacteriology* 183(2): 411–25.
- Hoch, M. P., Fogel, M. L., & Kirchman, D. L. (1992). Isotope fractionation associated with ammonium uptake by a marine bacterium. *Limnology and Oceanography*, 37(7), 1447–1459. <https://doi.org/10.4319/lo.1992.37.7.1447>
- Huber, Claudia, Wolfgang Eisenreich, Stefan Hecht, and Günter Wächtershäuser. 2003. "Peptide Cycle." *Science* 301(August): 938–40.
- Kappaun, Karine, Angela Regina Piovesan, Celia Regina Carlini, and Rodrigo Ligabue-Braun. 2018. "Ureasases: Historical Aspects, Catalytic, and Non-Catalytic Properties – A Review." *Journal of Advanced Research* 13: 3–17.
- Karhu, Juha A., and Heinrich D. Holland. 1996. "Carbon Isotopes and the Rise of Atmospheric Oxygen." *Geology* 24(10): 867–70.
- Kasting, James F. 1990. "Bolide Impacts and the Oxidation State of Carbon in the Earth's Early Atmosphere." *Origins of Life and Evolution of the Biosphere* 20(3–4): 199–231.
- . 2013. "What Caused the Rise of Atmospheric O₂?" *Chemical Geology* 362: 13–25.
- Kennedy, Christina et al. 1994. 161 Ammonium Sensing in Nitrogen Fixing Bacteria: Functions of the GlnB and GlnD Gene Products. *Plant and Soil* 161, 43-57
- Klugkist, Jan, and Huub Haaker. 1984. Inhibition of Nitrogenase Activity by Ammonium Chloride in *Azotobacter Vinelandii*. *Journal of Bacteriology*, 157,148-151
- Konhauser, Kurt O. et al. 2009. "Oceanic Nickel Depletion and a Methanogen Famine before the Great Oxidation Event." *Nature* 458(7239): 750–53.
- . 2015. "The Archean Nickel Famine Revisited." *Astrobiology* 15(10): 804–15.
- Kramer, Benjamin J., et al. "Nitrogen and Phosphorus Significantly Alter Growth, Nitrogen Fixation, Anatoxin-a Content, and the Transcriptome of the Bloom-Forming Cyanobacterium, *Dolichospermum*." *Frontiers in Microbiology*, vol. 13, no. September, 2022, pp. 1–22, doi:10.3389/fmicb.2022.955032.
- Kuga, M., Carrasco, N., Marty, B., Marrocchi, Y., Bernard, S., Rigaudier, T., ... Tissandier, L. (2014). Nitrogen isotopic fractionation during abiotic synthesis of organic solid

- particles. *Earth and Planetary Science Letters*, 393, 2–13.
<https://doi.org/10.1016/j.epsl.2014.02.037>
- Kump, Lee R., and Mark E. Barley. 2007. “Increased Subaerial Volcanism and the Rise of Atmospheric Oxygen 2.5 Billion Years Ago.” *Nature* 448(7157): 1033–36.
- Leigh, J. A. (2000). Nitrogen fixation in methanogens: the archaeal perspective. *Current Issues in Molecular Biology*, 2(4), 125–131. <https://doi.org/10.21775/cimb.002.125>
- Lemaitre, Nolwenn et al. 2022. “The Essential Bioactive Role of Nickel in the Oceans: Evidence from Nickel Isotopes.” *Earth and Planetary Science Letters* 584.
- Lohrmann, R. 1972. “Formation of Urea and Guanidine by Irradiation of Ammonium Cyanide.” *Journal of Molecular Evolution* 1(3): 263–69.
- Lowe, C. U., M. W. Rees, and R. Markham. 1963. “Synthesis of Complex Organic Compounds from Simple Precursors: Formation of Amino-Acids, Amino-Acid Polymers, Fatty Acids and Purines from Ammonium Cyanide.” *Nature* 199(4890): 219–22.
- Lyons, Timothy W., Christopher T. Reinhard, and Noah J. Planavsky. 2014. “The Rise of Oxygen in Earth’s Early Ocean and Atmosphere.” *Nature* 506(7488): 307–15.
- Mackerras, A. H., and G. D. Smith. 1986. “Urease Activity of the Cyanobacterium *Anabaena cylindrica*.” *Journal of General Microbiology* 132(10): 2749–52.
- Madigan, Michael T, and Summary I Background.. *Anoxygenic Photosynthetic Bacteria*, 915-928, *Kluwer Academic Publishers*
- Malhotra, Sarla, M. Pandit, J. C. Kapoor, and D. K. Tyagi. 2005. “Photo-Oxidation of Cyanide in Aqueous Solution by the UV/H₂O₂ Process.” *Journal of Chemical Technology and Biotechnology* 80(1): 13–19.
- Marchi, S., Bottke, W. F., Elkins-Tanton, L. T., Bierhaus, M., Wuennemann, K., Morbidelli, A., & Kring, D. A. (2014). Widespread mixing and burial of Earth’s Hadean crust by asteroid impacts. *Nature*, 511(7511), 578–582. <https://doi.org/10.1038/nature13539>
- Mazzei, Luca, Francesco Musiani, and Stefano Ciurli. 2020a. “The Structure-Based Reaction Mechanism of Urease, a Nickel Dependent Enzyme: Tale of a Long Debate.” *Journal of Biological Inorganic Chemistry* 25(6): 829–45.

- Menor Salván, C. et al. 2020. “Prebiotic Origin of Pre-RNA Building Blocks in a Urea ‘Warm Little Pond’ Scenario.” *ChemBioChem* 21(24): 3504–10.
- Middag, Rob, Hein J.W. de Baar, Kenneth W. Bruland, and Steven M.A.C. van Heuven. 2020. “The Distribution of Nickel in the West-Atlantic Ocean, Its Relationship With Phosphate and a Comparison to Cadmium and Zinc.” *Frontiers in Marine Science* 7(March): 1–17.
- Miller, S.L., and Orgel, L. E., *The origins of life on the earth*, Prentice-Hall, Englewood Cliffs, NJ, 1974
- Mobley, H L, M D Island, and R P Hausinger. 1995. “Molecular Biology of Microbial Ureasases.” *Microbiological Reviews* 59(3): 451–80.
- Montoya, J. P., & Mccarthy, J. J. (1995). Isotopic fractionation during nitrate uptake by phytoplankton grown in continuous culture. *Journal of Plankton Research*, 17(3), 439–464. <https://doi.org/10.1093/plankt/17.3.439>
- Moore, Eli K et al. 2017. “Metal Availability and the Expanding Network of Microbial Metabolisms in the Archaean Eon.” *Nature Publishing Group* (August).
- Mus, Florence, Daniel R. Colman, John W. Peters, and Eric S. Boyd. 2019. “Geobiological Feedbacks, Oxygen, and the Evolution of Nitrogenase.” *Free Radical Biology and Medicine* 140: 250–59.
- Navarro-González, R., A. Negrón-Mendoza, and E. Chacón. 1989. “The γ -Irradiation of Aqueous Solutions of Urea. Implications for Chemical Evolution.” *Origins of Life and Evolution of the Biosphere* 19(2): 109–18.
- Nisbet, Euan G., and R. Ellen R. Nisbet. 2008. “Methane, Oxygen, Photosynthesis, Rubisco and the Regulation of the Air through Time.” *Philosophical Transactions of the Royal Society B: Biological Sciences* 363(1504): 2745–54.
- Nishizawa, M., Miyazaki, J., Makabe, A., Koba, K., & Takai, K. (2014). Physiological and isotopic characteristics of nitrogen fixation by hyperthermophilic methanogens: Key insights into nitrogen anabolism of the microbial communities in Archean hydrothermal systems. *Geochimica et Cosmochimica Acta*, 138, 117–135. <https://doi.org/10.1016/j.gca.2014.04.021>

- Palm, Christof, and Melvin Calvin. 1962. "Primordial Organic Chemistry. I. Compounds Resulting from Electron Irradiation." *Journal of the American Chemical Society* 84(11): 2115–21.
- Pearce, Ben K. D. et al. 2022. "Toward RNA Life on Early Earth: From Atmospheric HCN to Biomolecule Production in Warm Little Ponds." *The Astrophysical Journal* 932(1): 9.
- Pearce, Ben K.D., Chao He, and Sarah M. Hörst. 2022. "An Experimental and Theoretical Investigation of HCN Production in the Hadean Earth Atmosphere." *ACS Earth and Space Chemistry* 6(10): 2385–99.
- Pennock, J. R., Velinsky, D. J., Ludlam, J. M., Sharp, J. H., & Fogel, M. L. (1996). Isotopic fractionation of ammonium and nitrate during uptake by *Skeletonema costatum*: Implications for $\delta^{15}\text{N}$ dynamics under bloom conditions. *Limnology and Oceanography*, 41(3), 451–459. <https://doi.org/10.4319/lo.1996.41.3.0451>
- Pi, Hong Wei et al. 2022. "Origin and Evolution of Nitrogen Fixation in Prokaryotes." *Molecular Biology and Evolution* 39(9).
- Planavsky, Noah J. et al. 2014. "Low Mid-Proterozoic Atmospheric Oxygen Levels and the Delayed Rise of Animals." *Science* 346(6209).
- Raymond, Jason, Janet L. Siefert, Christopher R. Staples, and Robert E. Blankenship. 2004. "The Natural History of Nitrogen Fixation." *Molecular Biology and Evolution* 21(3): 541–54.
- Rucker, Holly R., and Betül Kaçar. 2023. "Enigmatic Evolution of Microbial Nitrogen Fixation: Insights from Earth's Past." *Trends in Microbiology*: 1–11.
- Ruiz-Bermejo, Marta, María Paz Zorzano, and Susana Osuna-Esteban. 2013. "Simple Organics and Biomonomers Identified in HCN Polymers: An Overview." *Life* 3(3): 421–48.
- Sakamoto, Toshio, and Donald A. Bryant. 1997. "Growth at Low Temperature Causes Nitrogen Limitation in the Cyanobacterium *Synechococcus* Sp. PCC 7002." *Archives of Microbiology* 169(1): 10–19.

- . 2001a. “Requirement of Nickel as an Essential Micronutrient for the Utilization of Urea in the Marine Cyanobacterium *Synechococcus* Sp. PCC 7002.” *Microbes and Environments* 16(3): 177–84.
- Sakamoto, Toshio, Victoria B. Delgaizo, and Donald A. Bryant. 1998. “Growth on Urea Can Trigger Death and Peroxidation of the Cyanobacterium *Synechococcus* Sp. Strain PCC 7002.” *Applied and Environmental Microbiology* 64(7): 2361–66.
- Sakurai, Michiharu, and Hiroshi Yanagawa. 1984. “Prebiotic Synthesis of Amino Acids from Formaldehyde and Hydroxylamine in a Modified Sea Medium.” *Origins of Life* 14(1–4): 171–76.
- Schirrmeister, Bettina E., Muriel Gugger, and Philip C.J. Donoghue. 2015. “Cyanobacteria and the Great Oxidation Event: Evidence from Genes and Fossils.” *Palaeontology* 58(5): 769–85.
- Schirrmeister, Bettina E., Patricia Sanchez-Baracaldo, and David Wacey. 2016. “Cyanobacterial Evolution during the Precambrian.” *International Journal of Astrobiology* 15(3): 187–204.
- Schlesinger, Gordon, and Stanley L. Miller. 1983. “Prebiotic Synthesis in Atmospheres Containing CH₄, CO, and CO₂ - II. Hydrogen Cyanide, Formaldehyde and Ammonia.” *Journal of Molecular Evolution* 19(5): 383–90.
- Scott, C., Lyons, T. W., Bekker, A., Shen, Y., Poulton, S. W., Chu, X., & Anbar, A. D. (2008). *Tracing the stepwise oxygenation of the Proterozoic ocean*. 452(March), 27–31. <https://doi.org/10.1038/nature06811>
- Shorter, J. 1978. “The Conversion of Ammonium Cyanate into Urea - A Saga in Reaction Mechanisms.” *Chemical Society Reviews* 7(1): 1–14.
- Singh, Surendra. 1992. “Regulation of Urease Cellular Levels in the Cyanobacteria *Anacystis Nidulans* and *Nostoc Muscorum*.” *Biochemie und Physiologie der Pflanzen* 188(1): 33–38.
- Sleep, N. H., Zahnle, K. J., Kasting, J. F., & Morowitz, H. J. (1989). Annihilation of ecosystems by large asteroid impacts on the early Earth. *Nature*, 342(6246), 139–142. <https://doi.org/10.1038/342139a0>

- Stephen-Sherwood, E., D. G. Odom, and J. Oró. 1974. "The Prebiotic Synthesis of Deoxythymidine Oligonucleotides." *Journal of Molecular Evolution* 3(4): 323–30.
- Strope, Pooja K., Kenneth W. Nickerson, Steven D. Harris, and Etsuko N. Moriyama. 2011. "Molecular Evolution of Urea Amidolyase and Urea Carboxylase in Fungi." *BMC Evolutionary Biology* 11(1).
- Stüeken, Eva E., Roger Buick, Bradley M. Guy, and Matthew C. Koehler. 2015a. "Isotopic Evidence for Biological Nitrogen Fixation by Molybdenum-Nitrogenase from 3.2 Gyr." *Nature* 520(7549): 666–69.
- Takano, Yoshinori et al. 2004. "Pyrolysis of Complex Organics Following High-Energy Proton Irradiation of a Simple Inorganic Gas Mixture." *Applied Physics Letters* 85(9): 1633–35.
- Tian, Feng, J. F. Kasting, and K. Zahnle. 2011a. "Revisiting HCN Formation in Earth's Early Atmosphere." *Earth and Planetary Science Letters* 308(3–4): 417–23.
- Todd, Zoe R., and Karin I. Öberg. 2020a. "Cometary Delivery of Hydrogen Cyanide to the Early Earth." *Astrobiology* 20(9): 1109–20.
- Totton, K., Joshua, et al. "Constraining the Climate and Ocean PH of the Early Earth with a Geological Carbon Cycle Model." *Proceedings of the National Academy of Sciences of the United States of America*, vol. 115, no. 16, 2018, pp. 4105–10, doi:10.1073/pnas.1721296115.
- Ueno, Y., Johnson, M. S., Danielache, S. O., Eskebjerg, C., Pandey, A., & Yoshida, N. (2009). Geological sulfur isotopes indicate elevated OCS in the Archean atmosphere, solving faint young sun paradox. *Proceedings of the National Academy of Sciences of the United States of America*, 106(35), 14784–14789. <https://doi.org/10.1073/pnas.0903518106>
- Waser, N. A. D., Harrison, P. J., Nielsen, B., Calvert, S. E., & Turpin, D. H. (1998). Nitrogen isotope fractionation during the uptake and assimilation of nitrate, nitrite, ammonium, and urea by a marine diatom. *Limnology and Oceanography*, 43(2), 215–224. <https://doi.org/10.4319/lo.1998.43.2.0215>
- Weiss, Madeline C. et al. 2016. "The Physiology and Habitat of the Last Universal Common Ancestor." *Nature Microbiology* 1(9): 1–8.

- Wen, Nanping, and M H Brooker. 1994. "Rate Constants for Cyanate Hydrolysis to Urea: A Raman Study NANPING." *Can J. Chem* 72: 1099–1106.
- Wolf-gladrow, D. (2006). *THE GLOBAL NITROGEN CYCLE Overview : Schlesinger*. 1–36.
- Wolfe, J. M., & Fournier, G. P. (2018). Horizontal gene transfer constrains the timing of methanogen evolution. *Nature Ecology and Evolution*, 2(5), 897–903.
<https://doi.org/10.1038/s41559-018-0513-7>
- Zahnle, K. J. 1986. "Photochemistry of Methane and the Formation of Hydrocyanic Acid (HCN) in the Earth's Early Atmosphere." *Journal of Geophysical Research* 91(D2): 2819–34.
- Zamble, Deborah. 2017. "Introduction to the Biological Chemistry of Nickel." *RSC Metallobiology* 2017-Janua(10): 1–11. <http://dx.doi.org/10.1039/9781782624981-00001>.
- Zeer-Wanklyn, Conor J., and Deborah B. Zamble. 2017. "Microbial Nickel: Cellular Uptake and Delivery to Enzyme Centers." *Current Opinion in Chemical Biology* 37: 80–88.
- Zerkle, A. L., C. H. House, R. P. Cox, and D. E. Canfield. 2006. "Metal Limitation of Cyanobacterial N₂ Fixation and Implications for the Precambrian Nitrogen Cycle." In *Geobiology*, , 285–97.
- Zerkle, A. L., Junium, C. K., Canfield, D. E., & House, C. H. (2008). Production of ¹⁵N-depleted biomass during cyanobacterial N₂-fixation at high Fe concentrations. *Journal of Geophysical Research: Biogeosciences*, 113(3), 1–9.
<https://doi.org/10.1029/2007JG000651>
- Zhang, X., Sigman, D. M., Morel, F. M. M., & Kraepiel, A. M. L. (2014). Nitrogen isotope fractionation by alternative nitrogenases and past ocean anoxia. *Proceedings of the National Academy of Sciences of the United States of America*, 111(13), 4782–4787.
<https://doi.org/10.1073/pnas.1402976111>

Chapter 2: Development of a sequential ion exchange chromatography technique to separate transition metals

**Abstract and the contents of this chapter are published in Goldschmidt 2023 as a poster presentation.*

<https://doi.org/10.7185/gold2023.18756>

2.1. Abstract

To carry out precise isotope measurements by TIMS and MC-ICP-MS, it is important to isolate the desired element in the purest form while reducing matrix elements to avoid interferences and matrix effects. This is generally achieved by ion exchange chromatography and most of these procedures were developed to isolate a single element. Developing a sequential ion exchange element separation technique capable of separating multiple elements has the advantage of enabling an investigation of the relationships between multiple isotope systems in the same fraction, which is especially important when the sample amount is limited. In this study, a sequential separation method for multiple elements, including transition elements (Ti, V, Cr, Fe, Ni, Cu, Zn, Cd, W \pm Mo), Mg and Ca was developed. The method also can be extended to separate the rare earth elements (REEs), which are important for geochemistry and cosmochemistry. For the separation techniques anion exchange resin (AG1X8), cation exchange resin (AG50WX8) and DGA resin were used. Oxalic acid was the only organic acid used throughout the procedure while the other reagents used were commonly available inorganic acids. Resin volumes were kept minimal (maximum 1 ml), but can be modified accordingly.

2.2. Introduction

To measure precise isotopic ratios, it is mandatory to obtain a pure fraction of the desired element by removing the sample matrix irrespective of the instrument. Ion exchange chromatography techniques are commonly followed during sample preparation for the removal of matrix elements and to obtain a pure sample. These techniques are tailored specifically to the particular element of interest since matrix effects and possible elemental/molecular interferences vary from one element to another. However, when the sample amount is limited it is beneficial to follow an ion exchange separation scheme which can separate multiple elements from the same sample aliquot. Utilizing such a procedure rules out the effects arising due to sample heterogeneity. Ability to purifying multiple elements in a single sample create

possibility to understand the co-variation of isotope signatures of each element and this may be especially useful in the differentiation of the biotic signatures from abiotic signatures.

In this study, a sequential ion exchange chromatography technique was developed to separate multiple elements (Ti, V, Cr, Fe, Ni, Cu, Zn, Cd, W, Mg, Ca \pm Mo and rare earth elements [REE]) from a single sample aliquot. To achieve the separation, AG1-X8 anion exchange resin, AG50W-X8 cation exchange resin and DGA resin were used. In addition to the commonly used inorganic acids, oxalic acid was utilized as an organic reagent was used. To evaluate the accuracy and reproducibility of the developed methods, geological standards and meteorites with a range of compositions were tested and the results are presented here.

2.3. Materials and Methods

Sample digestion, ion chromatography and mass spectrometry were carried out at the Pheasant Memorial Laboratory (PML) for Geochemistry and Cosmochemistry, Institute for Planetary Materials, Okayama University. All the experiments were carried out in a class 10 clean bench maintained at 24 ± 0.5 °C.

2.3.1. Reagents and materials

Guaranteed grade 46% HF (Fujifilm Wako Pure Chemical Co.), EL grade 70% HNO₃ (Kanto Chemical Co. Inc.), and Electronic industry (EL) grade 36% HCl (Kanto Chemical Co. Inc.) were distilled by a PFA sub-boiling distillation apparatus, which will be referred to here as 1D HF, 1D HNO₃ and 1D HCl, respectively. The reagents that were further distilled are denoted with the prefix 2D. HCl, HF, and HNO₃ that were used in the ion chromatography procedure were prepared by diluting 1D HCl, 1D HF, and 1D HNO₃ with water (≥ 18.2 M Ω cm) prepared by a Milli-Q system (Merck Millipore, France). Guaranteed grade oxalic acid dihydrate (H₂C₂O₄·2H₂O) (Fujifilm Wako Pure Chemical Co.) was diluted to make 0.05 mol L⁻¹ oxalic acid solution. The 30% H₂O₂ (Kanto Chemical Co. Inc.) was used as it is. The multi element standard solutions (MES) were prepared using atomic absorption spectrometry reagent (AAS) (Kanto Chemical Co. Japan and Fujifilm WAKO chemicals, Japan) of the transition elements (Ni, Cr, V, Ti, Fe, Co, Mo, W, Cu, Zn, Cd) and group 1, 2 and 3 elements (Na, K, Mg, Al, Ca). The concentration of each element in MES solution was adjusted to 1 μ g/ ml.

Anion exchange resin (AG1-X8 200-400 mesh, Bio-Rad, USA) and cation exchange resin (AG50W-X8 200-400 mesh, Bio-Rad, USA) were pre-washed several times with water and 6 mol L⁻¹ HCl and stored. DGA Normal resin (N,N,N',N'-tetra-n-octyldiglycolamide,

Eichrom Technologies, USA) was suspended in 3 mol L⁻¹ HNO₃, decanted several times and stored.

The developed technique was evaluated by analyzing geological reference materials including dunite [JP-1 (GSJ)], basalt [BHVO-2 (USGS)], andesite [AGV-2 (USGS)], rhyolite [RGM-1 (USGS)], shale [SCO-1 (USGS)], stream sediment [JSd-1 (GSJ)], and Allende meteorite.

2.3.2. Sample Preparation

Powdered rock samples of 40 to 70 mg were weighed into PFA vials (Savillex, USA) and 1:1 mixture of 2D HNO₃ and 2D HF was added and agitated in an ultrasonic bath for 12 hours. Then samples were heated on a hotplate at 120 °C for 7 days. The digested samples were evaporated to dryness at 120 °C and repeatedly dissolved in 1ml of 1D HCl to remove the fluorides. After drying, aqua regia was added to the samples and heated on a hotplate at 170 °C for 5 days and then evaporated to dryness. To decompose any organic matter remaining in the JSD-1 (sediment) and SCO-1 (shale) reference materials, 1 ml of 30% H₂O₂ was added and heated on a hotplate at 70 °C for 6 hours and dried. All the digested samples were diluted with 0.5 mol L⁻¹ HNO₃ and stored.

2.3.3. Determination of distribution coefficients

The distribution coefficients of chloro- and nitrate complexes of the studied transition metals and ion exchange resins were determined by a batch method. First, 1 g of dry resin particles of AG1-X8 and AG50W-X8 was placed into 30 ml vials. Then multi-element standard (MES) solution dissolved in 1 ml of each acids was added into the vial (Table 2), and equilibrated for 6 hours at room temperature. Then the mixture was centrifuged and supernatant solution was pipetted out, dried and dissolved in 0.5 mol L⁻¹ HNO₃ and analyzed by inductively coupled plasma spectrometry (ICP-MS).

Distribution coefficient was calculated as follows

$$K_D = \frac{C_{resin}}{C_{supernatant}}$$

Element concentration of the resin was obtained from

$$C_{resin} = \frac{C_{MES} \times 1 g - C_{supernatant} \times 1 g}{1g}$$

C stands for the concentration in $\mu\text{g/g}$

Table 2 - Concentration of acids used for determining K_d and the corresponding resins used.

Acid	Acid concentration (mol L^{-1})	Resin
HCl	0.1	AG50W-X8
	0.2	
	0.3	
	0.4	
	0.5	
	1	AG1-X8 AG50W-X8
	4	
	6	
	8	
	11.7	
HNO ₃	0.1	AG50W-X8
	0.2	
	0.3	
	0.4	
	2	AG1-X8 AG50W-X8
	3	
	8	
	15.7	

2.3.4. Chemical Separation

Based on the distribution coefficients obtained in this study and referring to the available literature, a sequential multi-element separation technique was developed. A flow chart of the separation method is presented in Figure 9 and the detailed description is summarized in Table 7.

2.4. Results

2.4.1. Distribution coefficients (K_D)

i. Anion exchange resin AG1-X8

The distribution coefficients between anion exchange resin (AG1-X8) and nitrates of the tested elements were below 5 for all the elements in the 2-8 mol L⁻¹ HNO₃. However, when 15.7 mol L⁻¹ HNO₃ was used, the K_d value for W increased to 49 while that for other elements were below 8. However, when HCl was used, varying K_d values were obtained upon changing the acid concentration (Figure 7).

Table 3 - K_d values for AG1-X8 and nitrates of the transition elements

K_d values for AG1-X8 and nitrates of the transition elements				
	2 mol L ⁻¹ HNO ₃	3 mol L ⁻¹ HNO ₃	8 mol L ⁻¹ HNO ₃	15 mol L ⁻¹ HNO ₃
V	3.3	3.0	3.3	6.1
Cr	1.4	0.5	1.0	0.3
Co	3.2	3.0	3.2	6.0
Cu	3.2	2.9	3.3	6.3
Ni	3.3	2.9	3.4	6.4
Cd	3.1	2.8	3.1	5.9
W	3.6	4.8	3.6	49.1
Zn	3.0	2.7	3.1	5.9
Mo	3.8	3.2	3.4	8.1
Fe	3.3	2.9	3.6	5.7

Table 4 - K_d values for AG1-X8 and chlorides of the transition elements

K_d values for AG1-X8 and chlorides of the transition elements					
	1 mol L ⁻¹ HCl	4 mol L ⁻¹ HCl	6 mol L ⁻¹ HCl	8 mol L ⁻¹ HCl	11.7 mol L ⁻¹ HCl
V	0.1	2.8	3.5	3.5	4.6
Cr	0.1	0.0	0.4	0.4	0.4
Co	0.0	2.8	5.2	14.1	14.5
Cu	0.0	3.6	7.2	8.6	7.2
Ni	0.1	2.8	3.4	3.0	4.5
Cd	75.9	170	56.1	31.3	8.1
W	1.3	4.0	9.9	30.0	17.6
Zn	18.9	98.7	46.0	33.3	13.8
Mo	0.4	32.4	42.6	48.6	27.2
Fe	0.1	34.2	167	2009	1074

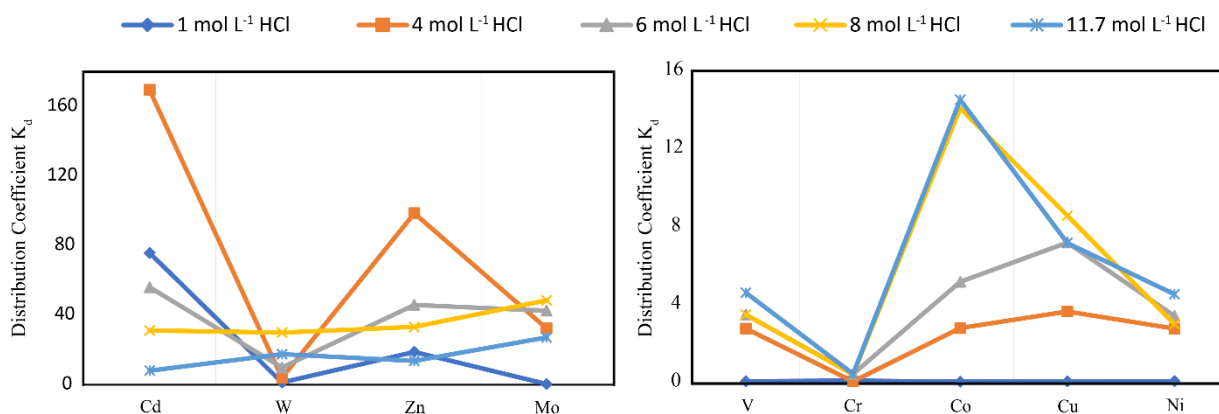


Figure 7 -Variation of K_d values with the HCl concentration on the AG1X8 resin

The K_d value for Fe on to the AG1-X8 increases with the molarity of HCl, with the highest K_d value was obtained at 8 mol L^{-1} HCl.

ii. Cation exchange resin AG50W-X8

Distribution coefficients of chlorides and nitrates of the transition metals are low at high ($>1 \text{ mol L}^{-1}$) concentrations of HCl and HNO_3 acids. However, differences in K_d values at low acid concentrations were observed (Tables 5 & 6).

Table 5 - K_d values for AG50W-X8 and chlorides of the studied transition elements

K_d values for AG50W-X8 and chlorides of the transition elements										
	0.1 M HCl	0.2 M HCl	0.3 M HCl	0.4 M HCl	0.5 M HCl	1 M HCl	4 M HCl	5 M HCl	8 M HCl	11.7 M HCl
V	106.8	37.8	21.7	11.5	2.2	0.6	0.1	0.0	0.1	0.2
Cr	333.1	157.8	83.5	46.4	29.3	7.0	0.1	0.0	2.0	0.9
Co	6323.0	2840.5	117.3	284.4	35.0	3.1	0.0	0.0	3.9	14.8
Cu	475.0	131.4	56.6	25.7	5.1	1.3	0.1	0.0	0.3	0.2
Ni	477.5	124.4	60.5	27.0	4.7	1.3	0.1	0.0	0.1	0.1
Cd	2.9	3.0	2.7	2.5	0.0	0.0	0.8	0.6	0.2	0.0
W	116.9	22.6	8.3	4.1	0.1	0.0	0.8	0.5	0.1	0.0
Zn	2.4	2.5	2.3	2.2	0.0	0.0	0.1	0.1	0.0	0.1
Mo	459.5	126.8	57.5	26.3	5.0	1.3	0.1	0.0	0.3	0.2
Fe	406.2	115.4	51.6	23.0	4.2	1.0	0.1	0.0	0.2	0.2

Table 6 - K_d values for AG50W-X8 and nitrates of the transition elements

K_d values for AG50W-X8 and nitrates of the transition elements								
	0.1 M HNO ₃	0.2 M HNO ₃	0.3 M HNO ₃	0.4 M HNO ₃	2 M HNO ₃	3 M HNO ₃	8 M HNO ₃	15.7 M HNO ₃
V	107	37.8	21.7	11.5	2.2	0.6	0.1	0.0
Cr	333	158	83.5	46.4	29.3	7.0	0.1	0.0
Co	6323	2840	117	284	35.0	3.1	0.0	0.0
Cu	475	131	56.6	25.7	5.1	1.3	0.1	0.0
Ni	478	124	60.5	27.0	4.7	1.3	0.1	0.0
Cd	2.9	3.0	2.7	2.5	0.0	0.0	0.8	0.6
W	117	22.6	8.3	4.1	0.1	0.0	0.8	0.5
Zn	2.4	2.5	2.3	2.2	0.0	0.0	0.1	0.1
Mo	460	127	57.5	26.3	5.0	1.3	0.1	0.0
Fe	406	115	51.6	23.0	4.2	1.0	0.1	0.0

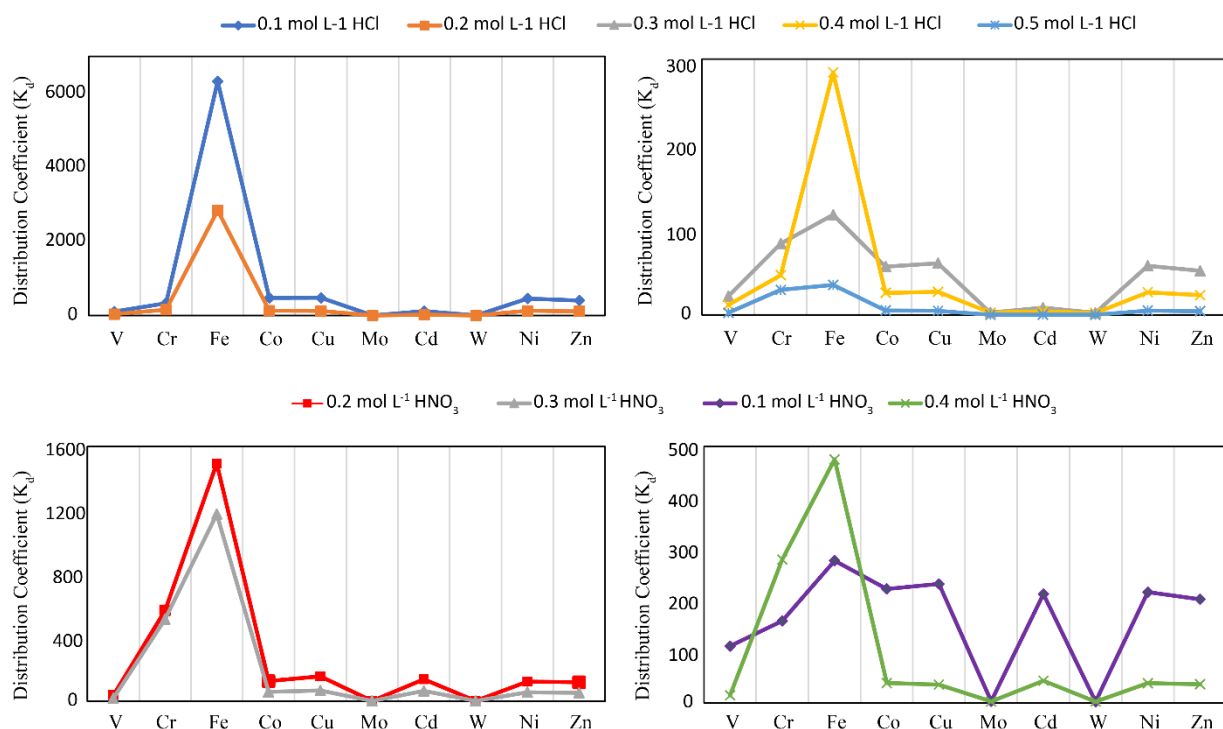


Figure 8 - Variation of K_d values with HCl and HNO₃ concentration on the AGIX8 resin

2.4.2. Element separation methods

Yields for the digested geological reference materials are shown in Table 8 and the elution profiles constructed for each separation step is in Figure 10-17.

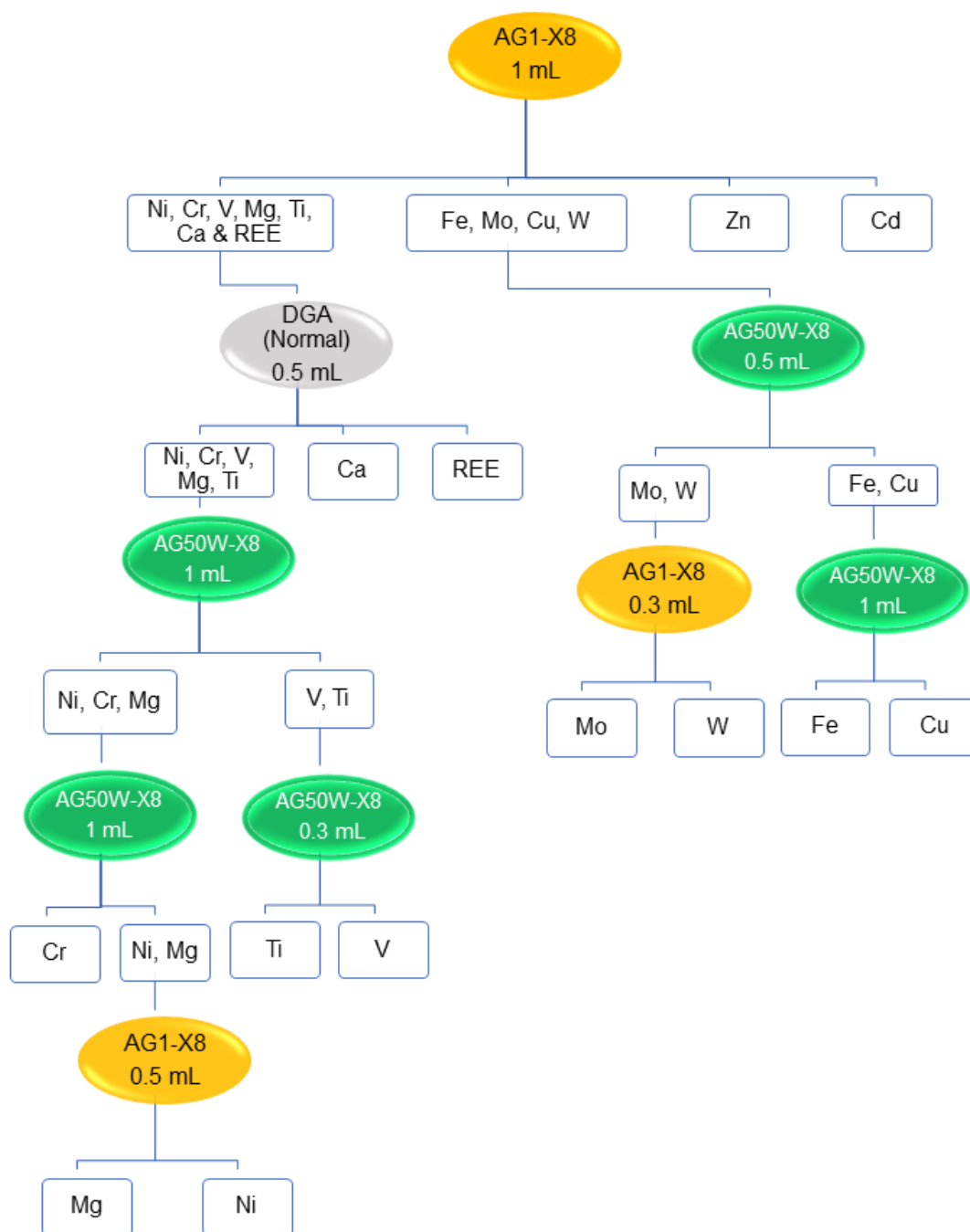


Figure 9 -Flow chart for the developed sequential element separation technique

Table 7 - Sequential element separation procedure

Procedure	Reagent	Volume (mL)
Step 1 Separation of Zn and Cd		
Resin	AG1-X8 (200-400 mesh)	1
Cleaning Resin	3 mol L ⁻¹ HNO ₃	8
	H ₂ O	8
	6 mol L ⁻¹ HCl	8
Conditioning	8 mol L ⁻¹ HCl	2
Sample Loading	8 mol L ⁻¹ HCl	1
Ni, Cr, V, Ti, Ca, Mg Fraction	8 mol L ⁻¹ HCl	4
Cu, Fe, W Fraction	0.5 mol L ⁻¹ HCl	10
Zn Fraction	0.1 mol L ⁻¹ HBr in 0.5 mol L ⁻¹ HNO ₃	5
Cd Fraction	3 mol L ⁻¹ HNO ₃	5
Step 2 Separation of REE, Ca and Sr		
Resin	DGA Normal	0.5 ml
Cleaning Resin	3 mol L ⁻¹ HNO ₃	3
	6 mol L ⁻¹ HCl	3
	H ₂ O	6
Conditioning	1 mol L ⁻¹ HNO ₃	3
Loading and collection of Ni, Cr, V, Ti, Mg and Li	1 mol L ⁻¹ HNO ₃	3
Ca and Sr	15 mol L ⁻¹ HNO ₃	3
Th	3 mol L ⁻¹ HNO ₃ + 0.2 mol L ⁻¹ HF	6
REE	0.05 mol L ⁻¹ HCl	6
Step 3 Separation of Cr from Al, V, Ti		
Resin	AG50W-X8 (200-400 mesh)	1
Cleaning resin	3 mol L ⁻¹ HNO ₃	8
	6 mol L ⁻¹ HCl	8

	H ₂ O	8
Conditioning	0.5 mol L ⁻¹ HNO ₃	4
Sample Loading	0.1 mol L ⁻¹ HNO ₃	1
Al, V, Ti Fraction	1 mol L ⁻¹ HF	12
Cr fraction	10.5 mol L ⁻¹ HCl	4
	4 mol L ⁻¹ HCl	2
Step 4 – Separation of V from Ti and Al		
Resin	AG50W-X8 (200-400 mesh)	0.3
Cleaning resin	3 mol L ⁻¹ HNO ₃	3
	H ₂ O	3
	6 mol L ⁻¹ HCl	3
Conditioning	0.5 mol L ⁻¹ HCl + H ₂ O ₂ [1% (V/V)]	3
Sample Loading	0.5 mol L ⁻¹ HCl	1
V fraction	0.5 mol L ⁻¹ HCl + H ₂ O ₂ [1% (V/V)]	3
Ti and Al Fraction	6 mol L ⁻¹ HCl	6
Step 5 – Separation of Al and Ti		
Resin	AG50W-X8 (200-400 mesh)	1
Cleaning resin	3 mol L ⁻¹ HNO ₃	9
	6 mol L ⁻¹ HCl	5
	H ₂ O	16
Conditioning	0.05 mol L ⁻¹ H ₂ C ₂ O ₄	4
Loading and Collection of Ti	0.1 mol L ⁻¹ HCl + 0.05 mol L ⁻¹ H ₂ C ₂ O ₄	3
	1 mol L ⁻¹ HCl	2
Al fraction	2 mol L ⁻¹ HCl	6
Step 6 – Separation of Cr from Ni and Mg		
Resin	AG50W-X8 (200-400 mesh)	1

Cleaning Resin	3 mol L ⁻¹ HNO ₃	8
	6 mol L ⁻¹ HCl	8
	H ₂ O	16
Conditioning	0.05 mol L ⁻¹ Oxalic acid	1
Sample Loading + Cr fraction	0.05 mol L ⁻¹ Oxalic acid	3
Remaining Cr fraction	0.5 mol L ⁻¹ HCl	2
Na fraction	1 mol L ⁻¹ HCl	5
Ni, Mg, K	2 mol L ⁻¹ HCl	5
Step 7 – Separation of Ni from Mg		
Resin	AG1-X8 (200-400 mesh)	0.5
Cleaning Resin	3 mol L ⁻¹ HNO ₃	8
	6 mol L ⁻¹ HCl	5
	H ₂ O	16
Conditioning	0.05 mol L ⁻¹ Oxalic acid	4
Loading	0.05 mol L ⁻¹ Oxalic acid	1
Mg fraction	0.02 mol L ⁻¹ HCl	5
	0.04 mol L ⁻¹ HCl	2.5
Ni fraction	0.2 mol L ⁻¹ HCl	2.5
Step 8 - Separation of Cu and Fe from Mo and W		
Resin	AG50W-X8 (200-400 mesh)	0.3
Cleaning Resin	3 mol L ⁻¹ HNO ₃	3
	H ₂ O	3
	6 mol L ⁻¹	3
Conditioning	0.5 mol L ⁻¹ HCl	2
Sample Loading and Fe, Mo, W	0.5 mol L ⁻¹ HCl	1
Mo and W fraction	0.5 mol L ⁻¹ HCl	3
Fe and Cu fraction	2.8 mol L ⁻¹ HCl	3
Step 9 – Separation of Cu and Fe		
Resin	AG50W-X8	1

Cleaning Resin	3 mol L ⁻¹ HNO ₃	8
	6 mol L ⁻¹ HCl	8
	H ₂ O	8
Conditioning	0.5 mol L ⁻¹ HNO ₃	4
Sample Loading	0.1 mol L ⁻¹ HNO ₃	1
Fe fraction	1 mol L ⁻¹ HF	6
Cu Fraction	10.5 mol L ⁻¹ HCl	4
Step 10 – Separation of Mo and W		
Resin	AG1-X8	0.3
Cleaning Resin	3 mol L ⁻¹ HNO ₃	3
	H ₂ O	3
	6 mol L ⁻¹ HCl	3
Conditioning	2.8 mol L ⁻¹ HCl	1
W fraction	2.8 mol L ⁻¹ HCl	3
Mo Fraction	0.5 mol L ⁻¹ HCl	3
Shaded steps were adopted from the existing scientific literature		

In step 1 of the purification procedure, 1 ml of AG1-X8 anion exchange resin was loaded into a polypropylene (PP) column having an internal diameter (ID) of 5 mm, and a bed volume height (h) of 50 mm. The sample was heated at 120 °C for 2 hours and cooled down to room temperature before loading into the resin. All the fractions collected were evaporated at 120° C.

For the second step, 0.5 ml of DGA Normal resin was packed in a PP column similar to the one used in step 1. The Ca containing fraction collected in step 1 was dissolved in 1 ml of 1 mol L⁻¹ HNO₃ and heated at 120 °C for 1 hour and cooled down to room temperature before adding into the column. Resulting fractions were dried again at 120 °C. Since the use of 15 mol L⁻¹ HNO₃ can damage the DGA resin, the fraction containing Ca and Sr was heated along with the eluent acid at 170 °C after collection to destroy the organic residue coming from the resin.

Step 3 was designed to separate Cr from Al, Ti and V. This step is similar to the second step in Ratnayake et al. (2023). The sample was heated for 2 hours on a hotplate at 120 °C and

cooled before loading to the resin. Sometimes it was difficult to add the whole sample to the resin due to the stickiness caused by the presence of excess Ti as TiO_2 . In those instances, the residue was dissolved in 0.5 ml of 0.05 mol L^{-1} HF and loaded on to the column. The collected fractions were dried at $120 \text{ }^\circ\text{C}$.

The dried Al, V and Ti fractions from step 3 were dissolved in 1 ml of 0.5 mol L^{-1} HCl solution and heated on a hotplate at $120 \text{ }^\circ\text{C}$ for 3 hours and cooled to room temperature before loading on to the resin. In this step 0.3 ml of AG50W-X8 was loaded into a PP column (ID $\sim 3.5 \text{ mm}$, h $\sim 30 \text{ mm}$). The immediately eluting V fraction was collected with 3 ml of 0.5 mol L^{-1} HCl + H_2O_2 [1% (V/V)]. The HCl- H_2O_2 mixture was made just before the column chemistry was undertaken in order to avoid H_2O_2 oxidation. Then Ti and Al were collected with 6 mol L^{-1} HCl.

Ti and Al can be separated in step 5 with AG50W-X8 cation exchange resin using oxalic acid and HCl mixtures. Samples containing Al and Ti were dissolved in 0.1 mol L^{-1} HCl and 0.05 mol L^{-1} oxalic acid mixture and heated at $110 \text{ }^\circ\text{C}$ for 4.5 hours, cooled to room temperature and loaded onto the 1 ml PP column. Immediately eluting Ti fraction was collected with another 2 ml of 1 mol L^{-1} HCl and Al fraction was eluted with 2 mol L^{-1} HCl. All the fractions were evaporated at $80 \text{ }^\circ\text{C}$ to avoid sample loss and remaining oxalates were oxidized by adding 20 drops of 1D HNO_3 and heating for 6 hours at $150 \text{ }^\circ\text{C}$.

The separation procedure of Cr from Ni and Mg (Step 6) follows Ratnayake et al. (2023), and oxalic acid was used as a chelating agent to assist the chemical separation. Samples were dissolved in 3 mL of oxalic acid heated for 1 hour and cooled to room temperature before loading on to the resin. Cr which was eluting immediately was collected with an additional 2 ml of 0.5 mol L^{-1} HCl. Then the majority of Na can be washed out from the resin using 1 mol L^{-1} HCl. Finally, Ni, Mg and K were collected with 2 mol L^{-1} HCl. All collected fractions were dried at $80 \text{ }^\circ\text{C}$. Oxalates were oxidized using similar procedure to that of step 5.

In the subsequent step 7, Ni was separated from Mg following Ratnayake et al. (2021). Anion exchange resin AG1-X8 was used in this step, where 0.5 ml of resin was loaded on to a 1 ml of PP column. The dried sample was heated at $120 \text{ }^\circ\text{C}$ for 4 hours and cooled down to room temperature before loading on to the resin. All the eluents were treated in a similar way as in Step 5 and 6.

The fraction including Cu, Fe, Mo and W obtained at step 1 was further purified in step 8. To separate Cu and Fe from Mo and W, 0.3 ml of AG50W-X8 resin was used. The fraction collected in step 1 was dried and dissolved in 1 ml of 0.5 mol L⁻¹ HCl and heated at 120 °C for 2 hours. The solution was loaded on to the resin, which was packed in a 0.3 ml PP column (ID ~3.5 mm, h ~30 mm) after cooling down to room temperature. The Mo and W fraction was eluted with an additional 3 ml of 0.5 mol L⁻¹ HCl and then Fe and Cu were eluted together with 3 ml of 2.8 mol L⁻¹ HCl.

Step 9 consisted of purifying Fe and Cu fractions. This step is similar to step 3. However only 6 ml of 1 mol L⁻¹ HF was used to elute Fe. The Cu fraction was eluted with 4 ml of 10.5 mol L⁻¹ HCl.

In the final step, purification of the Mo and W fraction was achieved with 0.3 ml of AG1-X8 resin. The column used for this step was similar to the one used in step 8. The Mo and W fraction from step 8 was dried and dissolved in 2.8 mol L⁻¹ HCl, then heated at 120 °C for 2 hours and cooled to room temperature before loading on to the column. W fraction was eluted with an additional 3 ml of 2.8 mol L⁻¹ HCl and the Mo fraction was collected with 3 ml of 0.5 mol L⁻¹ HCl.

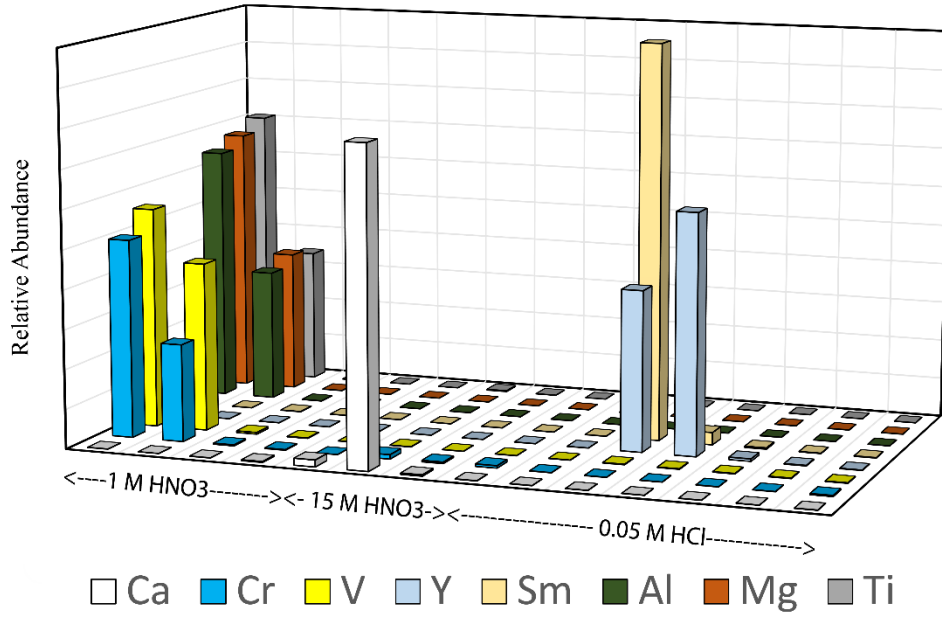


Figure 10 - Elution profile for the separation of Ca and REE fraction in step 2.

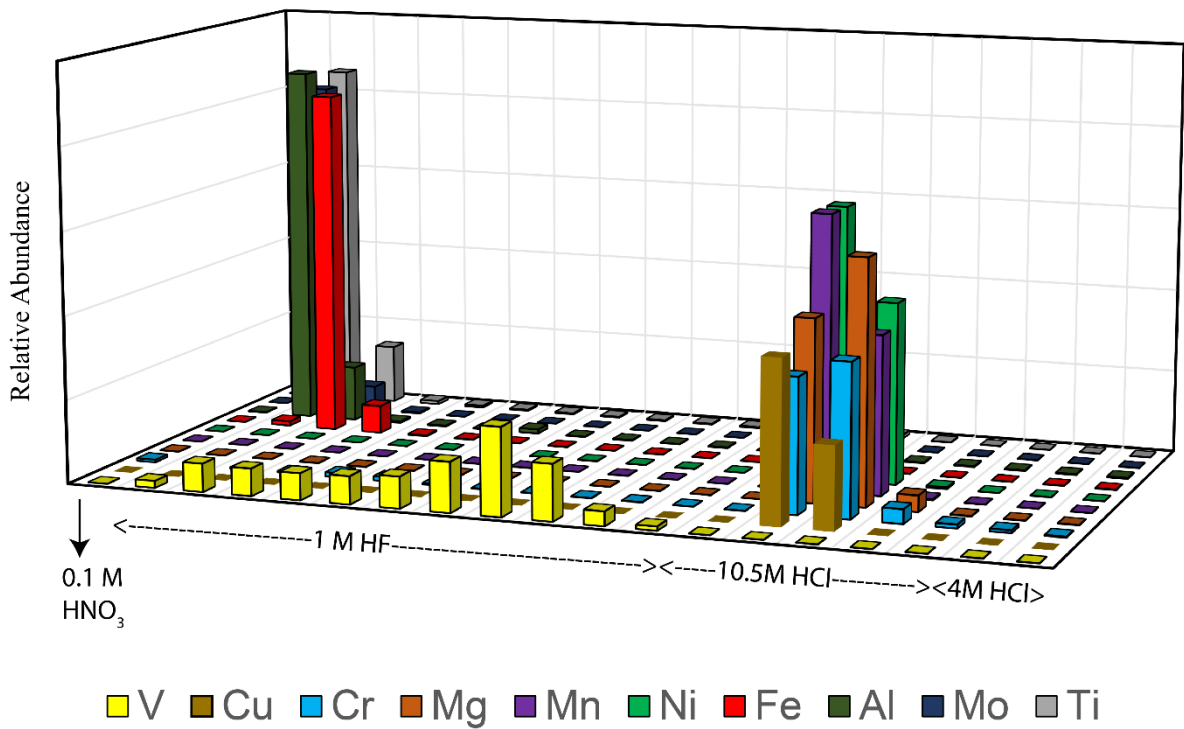


Figure 11 - Elution profile for the steps 3 and 9 where separation of Cr from Al, V and Ti and the separation of Fe from Cu.

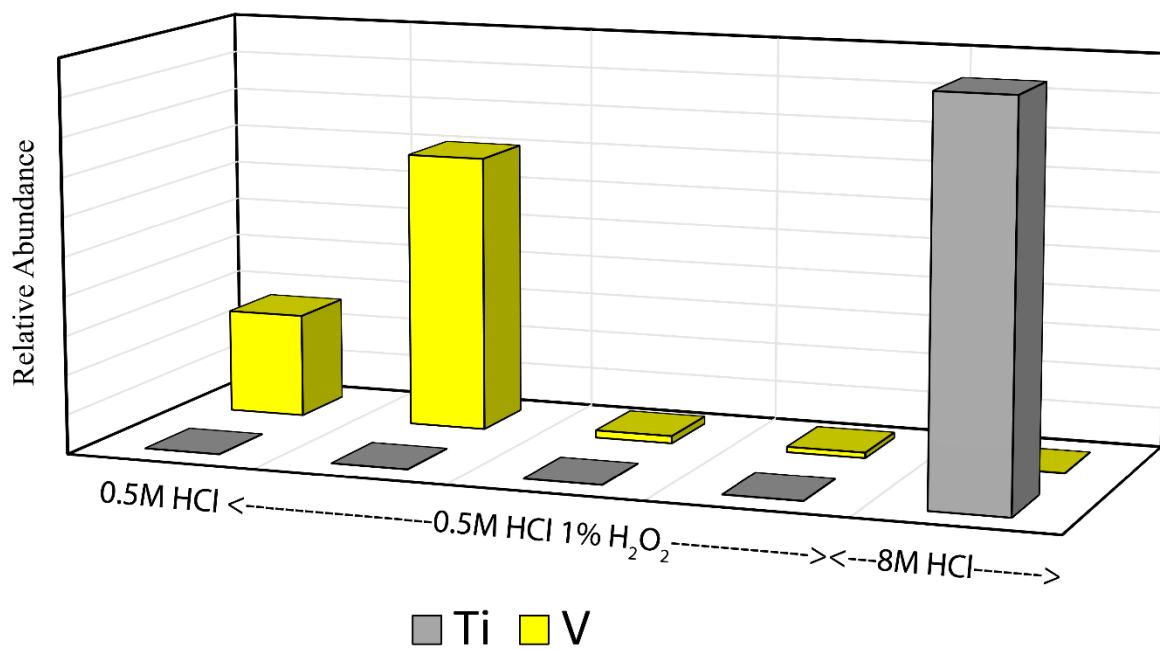


Figure 12 - Elution profile for the separation of V from Ti in step 4.

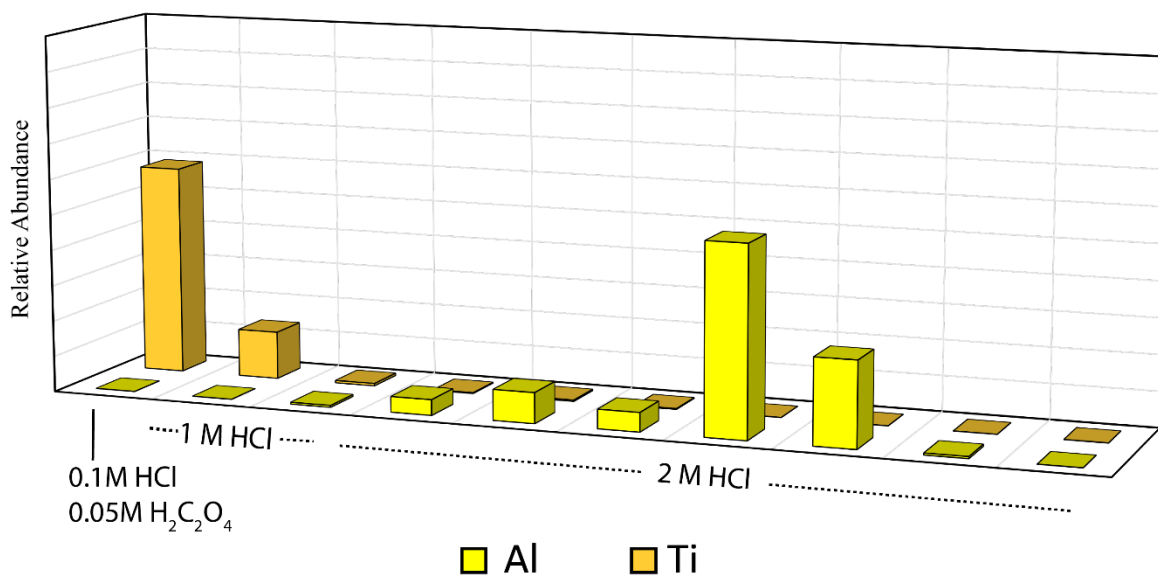


Figure 13 - Elution profile for Step 5 where Al and Ti was separated from each other.

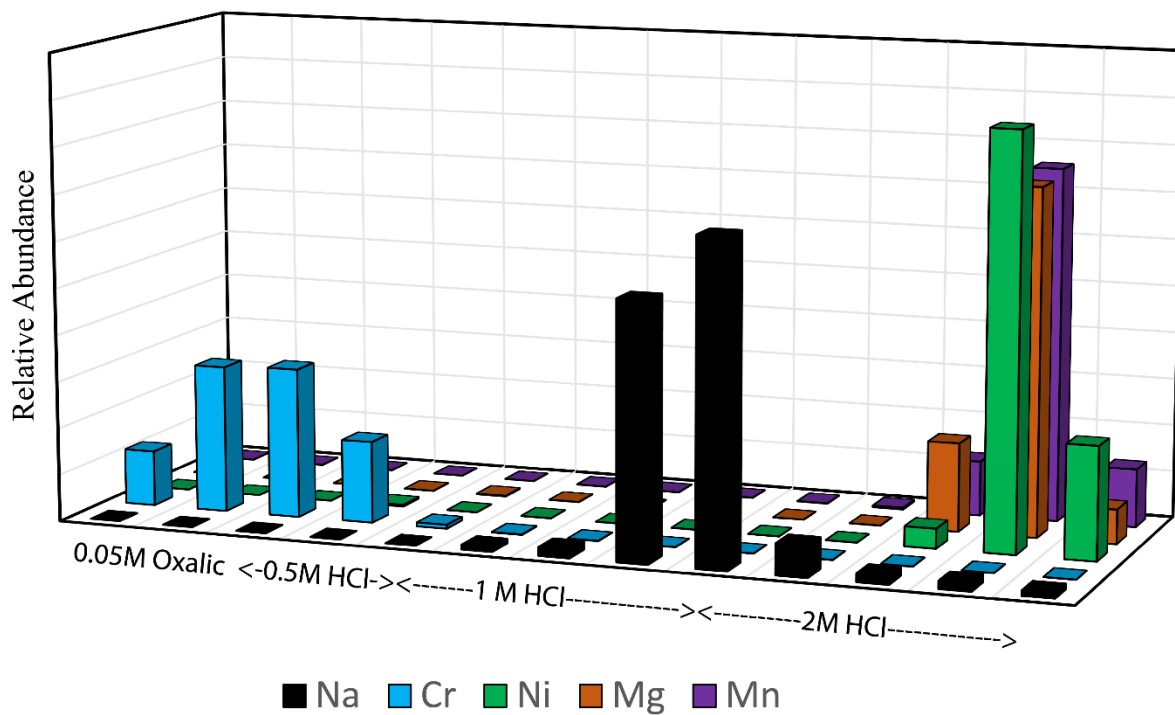


Figure 14 - Elution profile for Step 6 : separation of Cr from Ni and Mg

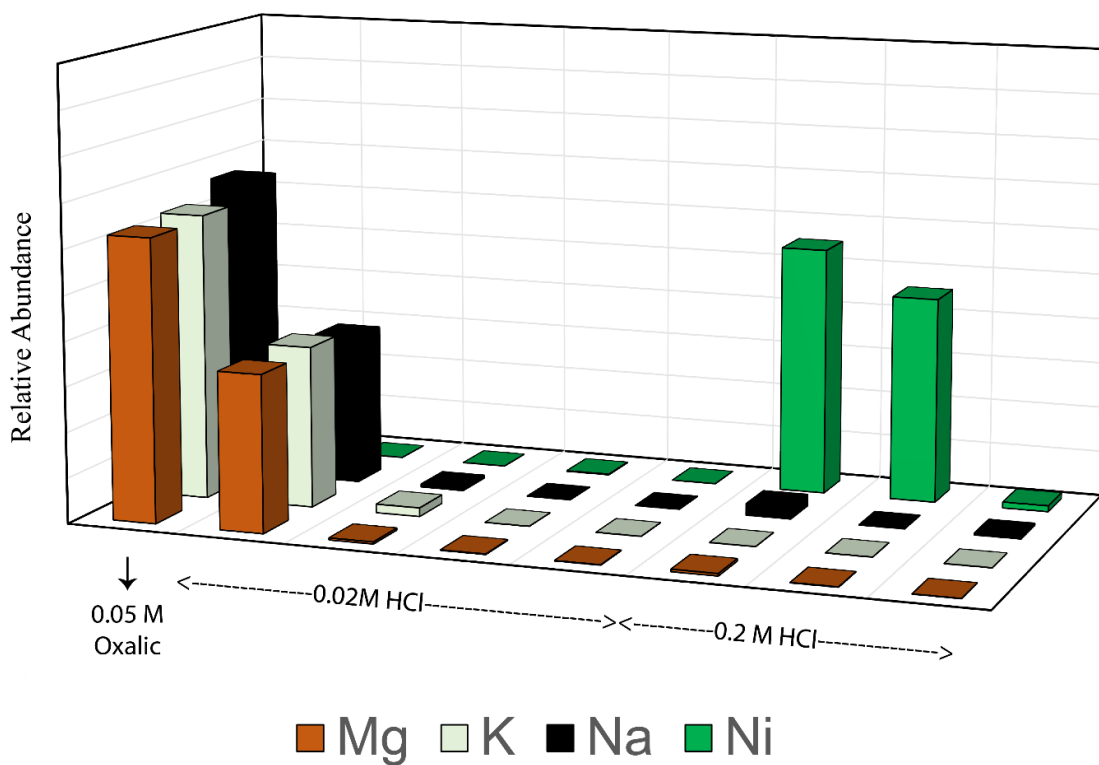


Figure 15 - Elution profile for the separation of Ni from Mg in step 7.

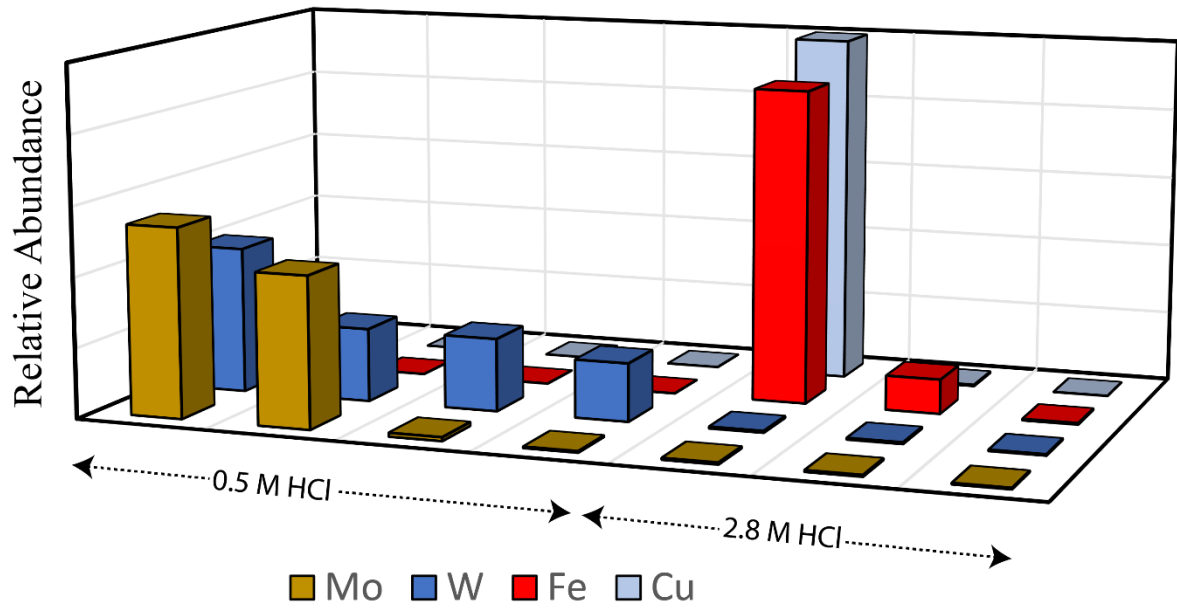


Figure 16 – Elution profile for the separation of Cu and Fe from Mo and W in step 8.

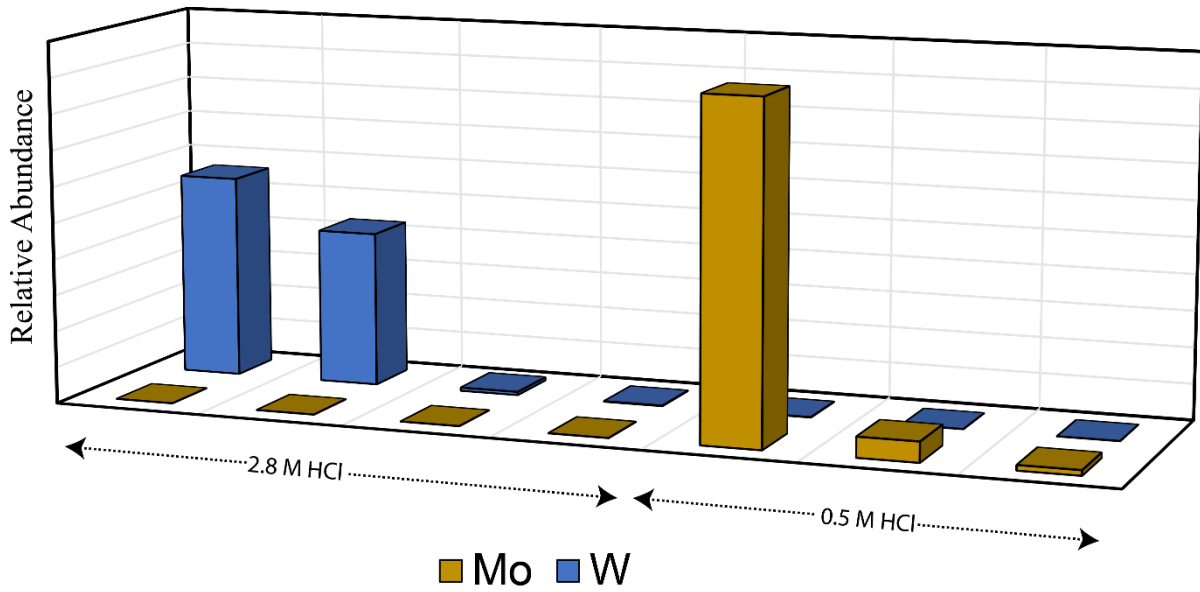


Figure 17 - Elution profile for Step 10 where Mo and W were separated.

Table 8 - Yields of the separated elements from the geological reference materials and the multi-element standard solution.

Element Rock	Ni	Cr	Zn	Ca	V	Sm	Nd	Fe	Cu	Mo	Cd	W
JP-1	98	90	100	90	81	-	-	100	91	Not measured.		
SCO-1	100	-	100	94	60	-	-	100	88			
RGM-1	94	96	100	92	47	-	-	91	86			
AGV-2	99	91	100	100	88	-	-	100	100			
BHVO-2	97	-	100	92	71	92	91	100	96			
JSD-1	98	97	100	100	45	100	100	100	98			
Allende	95	90	100	100	100	-	-	100	96			
Multi element standard	99	92	100	100	100	100	100	100	98	97	97	95
(-) Not checked												

2.5. Discussion

Heating with concentrated HCl result the formation of neutral and positively charged chloro-complexes of Ni, Cr, V, Ti, Ca and Mg. Therefore, these elements were immediately eluted when the sample solution was loaded to the anion exchange resin AG1-X8. On the other hand, Fe, Cu, Co, Mo, W, Zn and Cd form chloro-complexes having net negative charge and thus adsorb onto the anion exchange resin. This is also expressed by the relatively high K_d values present in Fe, Cu, Co, Mo, W, Zn and Cd for 8 mol L⁻¹ HCl (Table 4). Zn and Cd, which have a high K_d at all tested HCl concentrations, remained adsorbed even when 0.5 mol L⁻¹ HCl was used to elute the Fe fraction from the anion exchange resin in step 1. To elute Zn while retaining Cd in the resin, a mixture of 0.1 mol L⁻¹ HBr and 0.5 mol L⁻¹ HNO₃ was used because Cd adsorbs strongly to the anion exchange resins with HBr (Strelow et al. 1978), whereas Zn elutes because of its low K_d at 0.5 mol L⁻¹ HNO₃.

Step 2 of the separation procedure was adopted from the DGA resin instruction manual (Eichrom Technologies, USA) and a detailed explanation for the separation procedure can be found there. Step 3 of the separation procedure is similar to step 2 of the published Cr separation procedure (Ratnayake et al. 2023) and for detailed explanation please refer to chapter 4 of this thesis.

Vanadium naturally displays oxidation numbers from +2 to +5 in compounds and it only has two stable isotopes (⁵¹V and ⁵⁰V). Thus, the double spike technique cannot be used to avoid isotopic fractionation during sample preparation and 100% yield is mandatory. Therefore, obtaining a single oxidation state is important before undertaking column chemistry to maximize the yield and avoid isotopic fractionation during the ion exchange chromatography. Moreover, complete separation of V from Ti is mandatory since ⁵⁰Ti⁺ can interfere with ⁵⁰V⁺ during isotope analysis. Separation of V from Ti and Al was achieved using the cation exchange resin and the sample was heated for a longer period to obtain a single oxidation state for both V and Ti. Variable yields (from 45% to 100%) were obtained in this study for V in the geological reference materials and especially, the yields were low for the samples which had high Ti content. But for the meteorite sample and the MES solution 100% yields were obtained. Thus, it was found that the vanadium yield was matrix dependent. V loss may have been associated with step 3, where the formation of multiple V complexes was evidenced from multiple elution peaks (Figure 11). Therefore, re-examination of the vanadium yield for each step is necessary.

Step 5 and 6 are similar in chemistry used to separate elements. Initially the elements were adsorbed onto the resin by forming metal oxalate complexes. In step 5, the cationic Al oxalate complexes ($[\text{AlC}_2\text{O}_4]^+$) get adsorbed and anionic Ti oxalate complexes elute immediately when the sample solution was loaded to the resin. However, Al also can form anionic oxalate complexes such as $[\text{Al}(\text{C}_2\text{O}_4)_2]^-$ and $[\text{Al}(\text{C}_2\text{O}_4)_3]^{3-}$ (Krishnamurty et al. 1970). But their stability is lower than the mono-oxalate complex (Krishnamurty et al. 1970) and therefore heating for long periods is necessary during this step to allow formation of the cationic Al oxalate complex only. However, the elution profile of Al contains 2 peaks, which may indicate the presence of the isolated Al^{3+} cation in addition to the complexed oxalate form. Step 6 is similar to step 3 of the developed Cr separation procedure (Ratnayake et al. 2023), and the chemistry behind the elution of Cr is discussed in chapter 4. After removing Cr from the resin, Na can partially elute from the resin using 1 mol L^{-1} HCl and Mg, Ni and K, which were adsorbed either as cationic oxalate complexes, or their pure ionic forms were eluted with the use of 2 mol L^{-1} HCl. Anion exchange resin AG1-X8 was used to separate Ni from Mg and this step is similar to the step 2 of the developed Ni separation procedure (Ratnayake et al. 2021) and chemistry behind this separation step is explained in chapter 3.

The formation constants of Fe-fluoride complexes are higher than those of Cu-fluoride complexes (Brown 1964). Therefore, addition of HF to the cation exchange resin releases the adsorbed Fe, forming anionic fluoro-complexes and therefore a complete removal of Fe can be achieved. Additionally, the K_d value between the Cu and Fe fluoro-complexes and cation exchange resin will decrease with increasing HF concentration (Brown 1964). Therefore, separation of Cu and Fe was achieved by using 1 mol L^{-1} HF in step 9. Then, Cu fraction was eluted with the addition of concentrated HCl allowing the formation of anionic chloro complexes as in step 1 of this separation method.

Based on the variations of the K_d values obtained between anion exchange resin AG1-X8, and metal chlorides were used to develop the final separation step (step 10). Tungsten elution can be achieved even with the use of 4 or 6 mol L^{-1} HCl because of its low K_d values in these acid molarities. The W and Mo yields of the natural samples were not evaluated in this study due to the low abundances of these elements in natural samples. But the yields $>95\%$ in MES solution indicate the effectiveness of the separation technique even though the matrix effects should be evaluated.

2.6. Conclusions

In this study, a sequential element separation method was developed using the commonly available acids and ion exchange resins. Oxalic acid, an organic reagent was used in addition to the inorganic acids to separate elements in the ion exchange chromatography. The yields for the transition elements excluding V and Cu in geological reference materials were above 90%. Separation of transition elements in the Allende meteorite sample were also >90% and therefore this method is applicable for the analysis of the samples which are either precious or when the availability of the sample amount is limited. Impurities in purified Ni and Cr fractions were evaluated and presented in (Ratnayake et al. 2021) and (Ratnayake et al. 2023) respectively.

Credit author statement –

- Dilan M. Ratnayake (Conceptualization, Methodology, Investigation, Writing original Draft)
- Ryoji Tanaka (Writing – Review & Editing, Supervision, Resources)
- Eizo Nakamura (Supervision)

2.7. References

- Brown, R. B. (1964). The effect of hydrofluoric acid on the cation exchange behavior of metal ions.
- Krishnamurty, K. V., Harris, G. M., & Sastri, V. S. (1970). The chemistry of the metal oxalato complexes. *Chemical Reviews*, 70(2), 171–197.
<https://doi.org/10.1021/cr60264a001>
- Ratnayake, D. M., Tanaka, R., & Nakamura, E. (2021). Novel nickel isolation procedure for a wide range of sample matrices without using dimethylglyoxime for isotope measurements using MC-ICP-MS. *Analytica Chimica Acta*, 1181.
<https://doi.org/10.1016/j.aca.2021.338934>
- Ratnayake, D. M., Tanaka, R., & Nakamura, E. (2023). Determination of mass-dependent chromium isotopic compositions in geological samples by double spike-total evaporation-thermal ionization mass spectrometry (DS-TE-TIMS). *Analytica Chimica Acta*, 1278. <https://doi.org/10.1016/j.aca.2023.341723>
- Strelow, F. W. E., Weinert, C. H. S. W., & Eloff, C. (1978). Distribution Coefficients and Anion Exchange Behavior of some elements in hydrobromic-nitric acid mixtures. *Analytical Chemistry*, 50(9), 1359–1361. <https://doi.org/10.1021/ac60322a001>

Chapter 3: Novel nickel isolation procedure for a wide range of sample matrices without using dimethylglyoxime for isotope measurements using MC-ICP-MS

This chapter is published as an article in Analytica Chimica Acta <https://doi.org/10.1016/j.aca.2021.338934>

3.1. Abstract

Nickel isotope ratios have traditionally been used as an important tracer in cosmochemistry, and recently, it has gained attention in geochemistry, biochemistry, and environmental sciences with the development of MC-ICP-MS. Purification of Ni before isotope measurement is mandatory for obtaining precise data, which has been commonly achieved with ion-exchange chromatography, employing dimethylglyoxime (DMG) as a chelating agent for Ni. However, it has been pointed out that the use of DMG can adversely affect the isotope measurement due to insufficient Ni recovery and mass bias during measurement caused by the remaining DMG. Ni isolation procedures without the usage of DMG were innovated, but they have disadvantages such as the necessity of complex separation methods, high Ni blank, and matrix-dependent Ni recovery. Here, we present a simple Ni isolation procedure without using DMG but with the aid of oxalic acid along with common inorganic acids, achieving near-complete recovery of Ni with low blanks [0.7 ± 0.3 ng (2SD, $n = 4$)] only using three ion exchange column steps. To validate our method and strengthen the Ni isotope database of reference materials, $^{60}\text{Ni}/^{58}\text{Ni}$ of 20 geological reference materials, covering wide matrix compositions, were measured by MC-ICP-MS using the double-spike method. The results have shown that high recovery of Ni, independent of the sample matrix elements was achieved ($98 \pm 4\%$) and the $^{60}\text{Ni}/^{58}\text{Ni}$ was measured with a 2SD of 0.006-0.084‰ from samples containing 100-200 ng Ni.

3.2. Introduction

Nickel has five naturally occurring isotopes, ^{58}Ni , ^{60}Ni , ^{61}Ni , ^{62}Ni , and ^{64}Ni , and their variations have been widely used as valuable tracers in cosmochemistry, geochemistry, biochemistry, and environmental sciences. Mass-independent Ni isotope variation formed by stellar nucleosynthesis and the decay of the short-lived ^{60}Fe nuclide with a half-life of 2.62 million years (Rugel et al., 2009) are being used to unravel the origin and evolution of the early solar system materials (Cook et al., 2006; Morand & Allègre, 1983; Quitte et al., 2007; Shukolyukov & Lugmair, 1991; Steele et al., 2011; Tang & Dauphas, 2012, 2014). On the other hand, mass-dependent Ni isotope fractionation occurs in various conditions. Nickel behaves like a

moderate siderophile element forming Ni^{2+} and Ni^0 under the oxidized and reduced conditions, respectively. These redox-controlled mass dependent Ni isotope fractionation could be occurred by metal-silicate interaction processes during core formation or impact processes of planetary bodies (Elliott & Steele, 2017). In the Earth's surface environment, significant mass-dependent isotope fractionation occurs in aqueous Ni species because of the differences in bonding environment (Fujii et al., 2011). Weathering processes also can create significant fractionation in Ni isotopes (Estrade et al., 2015; Ratié et al., 2015) which is apparent with isotopically heavier compositions in river water and seawater (Cameron & Vance, 2014). Ni isotopes also have been used as a potential biomarker (Cameron et al., 2009) where the methanogenic bacteria utilize it as a micro-nutrient creating an isotopic fractionation between cells and the media, enriching lighter isotopes of Ni. Additionally, Ni isotope fractionation has been also observed in higher plants even though their Ni requirement is very low (Deng et al., 2014). Thus, there is a need to establish a highly accurate method of Ni isotope analysis for various types of samples. High precision Ni isotope analyses are recently performed by MC-ICP-MS. To obtain accurate Ni isotopic data, separating Ni from spectral and non-spectral interferences is a prerequisite. However, the separation of Ni from natural samples is challenging because the partitioning behavior of Ni^{2+} onto the ion exchange resin is similar to that of some major cations (Gall et al., 2012). Therefore, the most commonly used method for Ni separation is to selectively chelate Ni ions from matrix elements by using organic bidentate ligand, dimethylglyoxime ($(\text{CH}_3\text{CNOH})_2$, DMG), under alkaline condition. Because of this specific selectivity of Ni to form $\text{Ni}(\text{DMG})_2$ complex, a Ni-specific resin containing DMG in the pore spaces was also introduced (Quitté & Oberli, 2006). However, the usage of DMG for Ni separation has several disadvantages. Chelation of Ni by DMG highly depends on the sample pH, and the change in pH makes low recovery of Ni, chelating unwanted elements such as Fe, Mn, Co, Cu, Pd, and Pt other than Ni and introduce impurities such as Ca to the Ni fraction (Ali et al., 2019; Burger et al., 1965; Chen et al., 2009; Klaver & Coath, 2019; Lee & Diehl, 1950). Moreover, the slow reaction kinetics of Ni and DMG complexation also causes low recovery of Ni during flow-through conditions in columns (Wu et al., 2019). Acetone-HCl mixtures were often used to elute the Ni-DMG complexes by ion exchange, but the high volatility of tetracarbonyl Ni species may result in loss of Ni (Klaver et al., 2020; Victor, 1986). Complete decomposition of DMG is also required to prevent loss of Ni in the following ion exchange step(s) (Gall et al., 2012). Also, residual DMG affects the instrumental mass bias during MC-ICP-MS measurements (Klaver & Coath, 2019). To overcome these problems

caused by DMG, several procedures have been invented by minimizing the amount of DMG (Gall et al., 2012; Klaver et al., 2020; Wu et al., 2019) or avoiding the usage of DMG (Beunon et al., 2020; Chen et al., 2009; Tang & Dauphas, 2012). However, there are several drawbacks for the procedures that do not require DMG including the matrix dependence of the recovery and elution of Ni (Beunon et al., 2020), the necessity of long (up to 8 steps) and repetitive column procedures (Tang & Dauphas, 2012), and high Ni (>1 ng) blank levels. This paper presents a novel Ni isolation procedure which can be applied to geological samples with a wide compositional variation without using any repetitive, time consuming, long column procedures avoiding the usage of DMG, expensive resins or customized laboratory equipment and therefore it is a simple method. We have used oxalic acid (H₂C₂O₄) as the only organic reagent along with the common inorganic reagents: HCl, HF, and HNO₃, employed three-column steps using common cation and anion exchange resins, and the procedure yields ~98% recovery of Ni with low blank level. To examine the applicability of the developed method, $\delta^{60}\text{Ni}$ values [$\delta^{60}\text{Ni} = ({}^{60}\text{Ni}/{}^{58}\text{Ni}_{\text{sample}}/{}^{60}\text{Ni}/{}^{58}\text{Ni}_{\text{NIST986}} - 1) * 1000$] of 20 reference materials, covering an expansive matrix composition (acidic to ultramafic igneous rocks, schist, shales, marine mud, and sediment) with a wide range of Ni mass fractions (~3 $\mu\text{g g}^{-1}$ to ~2350 $\mu\text{g g}^{-1}$) were measured by MC-ICP-MS using the double-spike method.

3.3. Experimental

Sample digestion, chemical separation, and mass spectrometric analysis were carried out at the Pheasant Memorial Laboratory (PML) for Geochemistry and Cosmochemistry, Institute for Planetary Materials, Okayama University (Nakamura et al., 2003).

3.3.1. Reagents and materials

High purity water ($\geq 18.2 \text{ M}\Omega \text{ cm}^{-1}$) was prepared using a Milli-Q system (Merck Millipore, France). Guaranteed-grade 46% HF (FUJIFILM Wako Pure Chemical Co.), electronics industry (EL)-grade 70% HNO₃ (Kanto Chemical Co., Inc.), and EL-grade 36% HCl (Kanto Chemical Co. Inc.) diluted to 6 mol L⁻¹ HCl were distilled by a PFA sub-boiling distillation apparatus, which will be referred as 1D HF, 1D HNO₃, and 1D HCl, respectively. HCl and HNO₃ used in the chromatography were prepared by diluting non-distilled EL-grade HCl and HNO₃ with water, respectively. 1 mol L⁻¹ HF was prepared by diluting 1D HF with water. Guaranteed grade oxalic acid dihydrate (Fujifilm Wako Pure Chemical Co.) was diluted to make 0.05 mol L⁻¹ oxalic acid solution. Ni standard solution was prepared by dissolving the NIST SRM 986 Ni metal powder in 1D HNO₃, dried, and then diluted with 0.5 mol L⁻¹ HNO₃.

^{61}Ni (99.44%) and ^{62}Ni (98.45%) enriched Ni metal powders provided by Oak Ridge National Laboratory (USA) were dissolved in $0.5 \text{ mol L}^{-1} \text{ HNO}_3$ using the same method for Ni standard solution, and they were mixed to make ^{61}Ni - ^{62}Ni double spike (DS) solution. To optimize the purification procedure and to examine the matrix and interference effects, multi-element standard solutions were prepared by diluting the standard solutions for atomic absorption spectrometry (100 to $1000 \text{ } \mu\text{g mL}^{-1}$, Kanto Chemical Co. Inc.). The applicability and effectiveness of the developed separation procedure was evaluated by analyzing 20 reference materials with a Ni mass fraction between $\sim 3 \text{ } \mu\text{g g}^{-1}$ and $\sim 2350 \text{ } \mu\text{g g}^{-1}$. These include three peridotites [JP-1 (GSJ), PCC-1 (USGS), DTS-1 (USGS)], three dolerites [W-2 (USGS), DNC-1 (USGS), TDB-1 (CCRMP)] two serpentinites [UB-N (ANRT), MUH-1 (IAG)], two basalts [JB-1b (GSJ), BCR-2 (USGS)], two andesites [JA-2 (GSJ), AGV-2 (USGS)], two shales [SCo-1 (USGS), SGR-1 (USGS)], two sediment samples [MAG-1 (USGS), JSD-1 (GSJ)], one sample each from rhyolite [RGM-1 (USGS)], schist [SDC-1 (USGS)], granodiorite [GSP-1 (USGS)] and komatiite [OKUM (IAG)].

3.3.2. Sample preparation and digestion

Approximately 100 mg of a powdered rock sample, weighed in a 7 mL PFA vial (Savillex, USA), was digested using 1D HF and 1D HNO_3 (1:1) mixture in an ultra-sonic bath for two days, followed by heating at $160 \text{ }^\circ\text{C}$ for another two days. The digested samples were evaporated to dryness at $120 \text{ }^\circ\text{C}$, then further digested with aqua regia for another two days at $160 \text{ }^\circ\text{C}$. After evaporating the samples to dryness at $120 \text{ }^\circ\text{C}$, they were repeatedly dissolved (at least twice) in 1 mL of 6 mol L^{-1} 1D HCl and dried at $120 \text{ }^\circ\text{C}$. Then 1 mL of 1D HNO_3 was added to the samples and further ultrasonicated until solutions become clear. Finally, samples were evaporated to dryness at $120 \text{ }^\circ\text{C}$ and dissolved in 7 mL of $0.5 \text{ mol L}^{-1} \text{ HNO}_3$.

3.3.3. Chemical separation

Nickel separation was performed using a three-step column chemistry method as summarized in *Table 9*. All experiments were carried in class 10 clean bench and the temperature was maintained at $21 \pm 1 \text{ }^\circ\text{C}$. A sample aliquot containing 200 ng of nickel was mixed with the ^{61}Ni - ^{62}Ni DS in a 7 mL PFA vial according to the optimized ratio of Ni in DS and sample (0.66:0.34). The sample-DS mixture was slowly heated to dryness at $90 \text{ }^\circ\text{C}$ allowing sample-spike equilibration, followed by dissolving in 1 mL of $0.5 \text{ mol L}^{-1} \text{ HNO}_3$. Sample was heated at $120 \text{ }^\circ\text{C}$ for 2 h, and finally cooled to room temperature. In the first separation step, 1 mL of AG50W-X8 cation-exchange resin (Bio-Rad Laboratories, USA, 200-

400 mesh size) was packed in a polypropylene (PP) column (ID ~ 5 mm, h = 50 mm), then cleaned and conditioned. 1 mL of sample solution dissolved in 0.5 mol L⁻¹ HNO₃ was loaded onto the resin. Then, Sn, Al, Ti, Fe, and V were eluted. Finally, Ni along with group 1 and group 2 elements was collected. The Ni fraction was evaporated to dryness at 120 °C, re-dissolved in H₂O, evaporated to dryness, dissolved in 1 mL of 0.05 mol L⁻¹ oxalic acid, and heated at 120 °C for 4 h, and finally cooled to room temperature. In the second separation step, 0.5 mL of AG1-X8 anion exchange resin (Bio-Rad Laboratories, USA, 200-400 mesh size) was packed in a PP column (ID ~5 mm, h = 50 mm), then cleaned and conditioned. Sample solution dissolved in 1 mL of 0.05 mol L⁻¹ oxalic acid was loaded on the resin. Then, group 1 and group 2 elements were eluted. Finally, Ni was collected. The Ni fraction was slowly evaporated to dryness at 80 °C, dissolved in 0.2 mL of 8 mol L⁻¹ HCl and heated at 120 °C for 2 h, then cooled to room temperature.

Table 9 - Nickel separation procedure

Procedure	Reagent	Amount (mL)
<i>Step 1: Separating Ni from Sn, Ti, Al, V, and Ca</i>		
Resin	AG50w-X8 (200-400 mesh)	1
Cleaning resin	3 mol L ⁻¹ HNO ₃	8
	6 mol L ⁻¹ HCl	8
	H ₂ O	8
Conditioning	0.5 mol L ⁻¹ HNO ₃	4
Sample Loading	0.5 mol L ⁻¹ HNO ₃	1
Fe, Al, Ti, V, Sn fraction	1 mol L ⁻¹ HF	10
Ni Collection	10.5 mol L ⁻¹ HCl	3.5
<i>Step 2: Separating Ni from group 1 and group 2 elements</i>		
Resin	AG1-X8 (200-400 mesh)	0.5
Cleaning Resin	3 mol L ⁻¹ HNO ₃	8
	6 mol L ⁻¹ HCl	5
	H ₂ O	16
Conditioning	0.05 mol L ⁻¹ Oxalic acid	4
Sample Loading	0.05 mol L ⁻¹ Oxalic acid	1
Group 1 & 2 elements	0.02 mol L ⁻¹ HCl	5
	0.04 mol L ⁻¹ HCl	2.5
Ni Collection	0.2 mol L ⁻¹ HCl	2.5
<i>Step 3: Purifying Ni from Cu, Zn, and Co</i>		
Resin	AG1-X8 (200-400 mesh)	0.1

Cleaning Resin	3 mol L ⁻¹ HNO ₃	3
	H ₂ O	3
	6 mol L ⁻¹ HCl	3
Sample Loading	8 mol L ⁻¹ HCl	0.2
Ni Collection	8 mol L ⁻¹ HCl	0.3

In the third separation step, 0.1 mL of AG1-X8 resin was packed in a PP column (ID ~3.5 mm, h = 10 mm), then cleaned and conditioned. Note that even if we have used a different column, the column used for the 1st and 2nd steps filled with 0.1 mL of AG1-X8 resin also can be used in this step without changing the eluent volumes. 0.2 mL of sample solution dissolved in 8 mol L⁻¹ HCl was loaded on the resin. Ni which immediately elutes was recovered with an additional 0.3 mL of 8 mol L⁻¹ HCl. The purified Ni fraction was evaporated to dryness, then re-dissolved in 0.6 mL of 1D HNO₃ and heated to decompose oxalates and any organic matter derived from resins and finally dissolved in 2 mL of 0.5 mol L⁻¹ HNO₃.

3.3.4. Mass spectrometry

Mass fractions of Ni and matrix elements during ion chromatographic calibrations were measured using a sector field type ICP-MS (ELEMENT XR, Thermo Scientific, Germany) with wet plasma conditions. The tuning condition was optimized to obtain an optimum mass resolution of ~4000 and ~9000 for medium and high-resolution modes, respectively. The concentration of elements was measured by the calibration curve method (for the determination of impurities in the purified Ni fractions) as well as the isotope dilution method (for the yield calculation of representative samples). Nickel isotopic compositions were measured by MC-ICP-MS (Neptune Plus, Thermo Scientific, Germany) with dry plasma condition using an APEX IR desolvator (Elemental Scientific Inc., USA) (*Table 10*). N₂ gas was mixed with the sample aerosol within the desolvator to improve the signal intensity, stability and to reduce the oxide interferences (e.g. ⁴⁰Ar¹⁸O⁺ on ⁵⁸Ni⁺). The potential interferences of ⁵⁸Fe⁺ on ⁵⁸Ni⁺ and ⁶⁴Zn⁺ on ⁶⁴Ni⁺ were corrected by measuring ⁵⁶Fe⁺ and ⁶⁶Zn⁺ on the center cup. The gain calibration was performed once a day at the beginning of the analytical session. The electronic baseline measurement was performed before each measurement. The measurement was performed in medium resolution mode. The Ni masses were resolved from the interferences (e.g. ⁴⁰Ar¹⁸O⁺) on the low mass side of the Ni plateau peak. The ⁵⁶Fe mass was also resolved from ⁴⁰Ar¹⁶O⁺ on the low mass side of the Fe plateau peak. The double spike method was applied for the measurement and the on-peak-zero baseline was measured before each sample or standard. As mentioned elsewhere, the instrument mass bias that occurred among each

analytical session was calibrated by bracketing the NIST SRM 986 double spike mix solution before and after each sample. After analyzing the standard or sample, the autosampler probe was cleaned in two individual 0.5 mol L⁻¹ HNO₃ solutions. Data acquisition comprised of 40 scans with 4.194 s integration time was performed. The sensitivity of ⁵⁸Ni⁺ was 50-60 V per 1 µg g⁻¹ Ni for medium resolution, and typically, 100 ng g⁻¹ of Ni solution both for standard and sample were measured.

3.3.5. Double spike calibration

The optimum proportion of each spike in the ⁶¹Ni-⁶²Ni double-spike was simulated using a MATLAB code published elsewhere (Rudge et al., 2009). The isotopic composition of the double-spike was calibrated using a certified Ni standard NIST SRM 986 and certified Cu standard IRMM-647. The calibration procedure was based on the method described for Mo isotope (Siebert et al. 2001). For the calibration, Cu was doped for both standard and double spike solutions, and the mass fraction of Ni and Cu was adjusted to 0.3 µg g⁻¹ for both solutions. In addition, Cu-doped double spike-standard mixture solution containing 0.3 µg g⁻¹ of Ni and Cu, dissolved in 0.5 mol L⁻¹ HNO₃ with variable double spike/standard ratio (0.5, 0.9, 1.4, 1.7, and 3.9) was prepared.

Table 10 - Instrumental parameters and settings for the analysis of Ni isotopes on MC-ICP-MS

Parameter	Setting
RF Power	1200 W
Sample Cone	Normal Ni
Skimmer Cone	X Ni
Desolvator	APEX IR (Elemental Scientific, USA)
APEX IR Temperature configuration	100 °C Heating and -3 °C Cooling
Nebulizer	Self-Aspirating PFA microflow (Elemental Scientific, USA)
Aspiration Rate	50 µL min ⁻¹
Resolution	Medium
Analyte Concentration	100 ng g ⁻¹
Analyte Base	0.5 mol L ⁻¹ HNO ₃
Number of Blocks	1
Number of Cycles/ block	40
Integration Time	4.194 seconds

Idle Time	2.000 seconds							
Cup Configuration								
Cup	L3	L2	L1	C	H1	H2	H3	H4
Species	⁵⁸ Ni	⁵⁹ Co	⁶⁰ Ni	⁶¹ Ni	⁶² Ni	⁶³ Cu	⁶⁴ Ni	⁶⁵ Cu
				⁵⁶ Fe				
				⁶⁶ Zn				

First, the Cu-doped Ni standard and the Cu-doped double spike solutions were measured. The measurements of the standards and the double spike solution were performed five times for each sequence. To minimize the memory effect, the APEX-IR desolvating nebulizer was removed from the connecting line and washed by diluted HNO₃ and water between the nickel standard and the double spike measurements without turning off the plasma. Then the isotopic ratios of the standard and the double spike were optimized by measuring the standard-double spike mixture solutions. The result of the isotopic ratio in standard and double spike are shown in *Table 11*. The optimum proportion of the double-spike in the double-spike-sample mixture was calculated as 0.66 (Rudge et al., 2009).

3.4. Results and discussion

3.4.1. Chemical separation

The main innovation of this study is the development of a Ni separation procedure employing metal oxalate complexes. When using oxalic acid, it is necessary to consider (1) a reduction in the amount of oxalic acid because it contains a non-negligible amount of Ni (0.958 ng g⁻¹ in 0.5 mol L⁻¹ oxalic solution), and (2) to prevent the formation of sparingly soluble oxalate complexes, which may occur with some elements. To achieve this, it is necessary to optimize the number of oxalates needed to increase the solubility of the complexes (Krishnamurty & Harris, 1961) while reducing the blanks. Therefore, Al, Fe, Ti, Sn, and Ca were removed from the Ni fraction in step 1 (Figure 18).

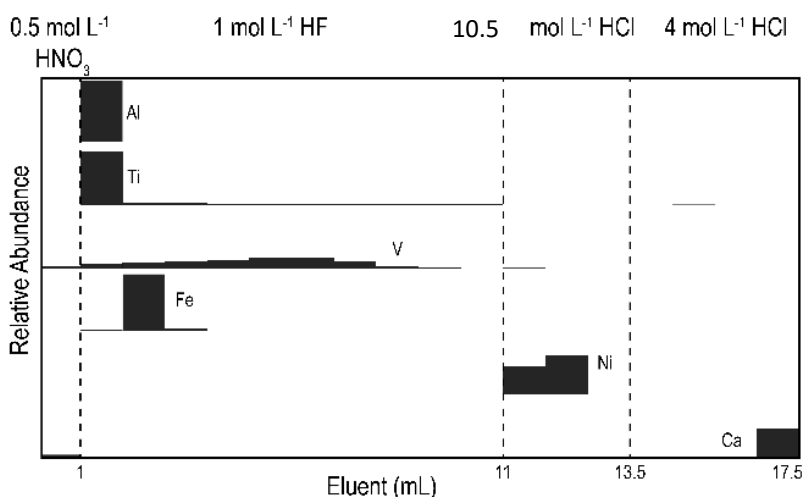


Figure 18 - Elution profile for step 1: Separating Ni from Fe, V, Al, Ti, and Ca

The formation constants of the fluoro complexes of Ni^{2+} and most of the divalent cations (e.g. Mn^{2+} , Mg^{2+} , Cu^{2+} , Zn^{2+} , Cd^{2+} , and Pb^{2+}) are lower than that of Al^{3+} , Fe^{3+} , Zr^{4+} , VO^{2+} , Sn^{4+} (Brown, 1964). Thus, by using 1 mol L^{-1} HF as an eluant solution to the cation exchange resin, the latter elements were separated from Ni. The retained Ni^{2+} in the resin was completely eluted by adding 10.5 mol L^{-1} HCl solution with most of the univalent and divalent cations while retaining Ca^{2+} in the resin (Nelson et al., 1964). Removing the Al, Ca, Ti and Fe from the Ni fraction significantly reduced the amount of oxalic acid required in step 2. Removal of Ca is also important in preventing the precipitation of Ca oxalate (CaC_2O_4), which may interfere with the ion separation in step 2.

Table 11 - Ni isotope ratios for NIST SRM 986 and DS

Isotope	NIST SRM 986 (2SD)	Double Spike (2SD)
$^{60}\text{Ni}/^{58}\text{Ni}$	$\equiv 0.385166$	1.1876 ± 0.0010
$^{61}\text{Ni}/^{58}\text{Ni}$	0.0167457 ± 0.0000012	116.31 ± 0.10
$^{62}\text{Ni}/^{58}\text{Ni}$	0.0533661 ± 0.0000022	132.44 ± 0.11
$^{64}\text{Ni}/^{58}\text{Ni}$	0.0135680 ± 0.0000009	0.2590 ± 0.0004

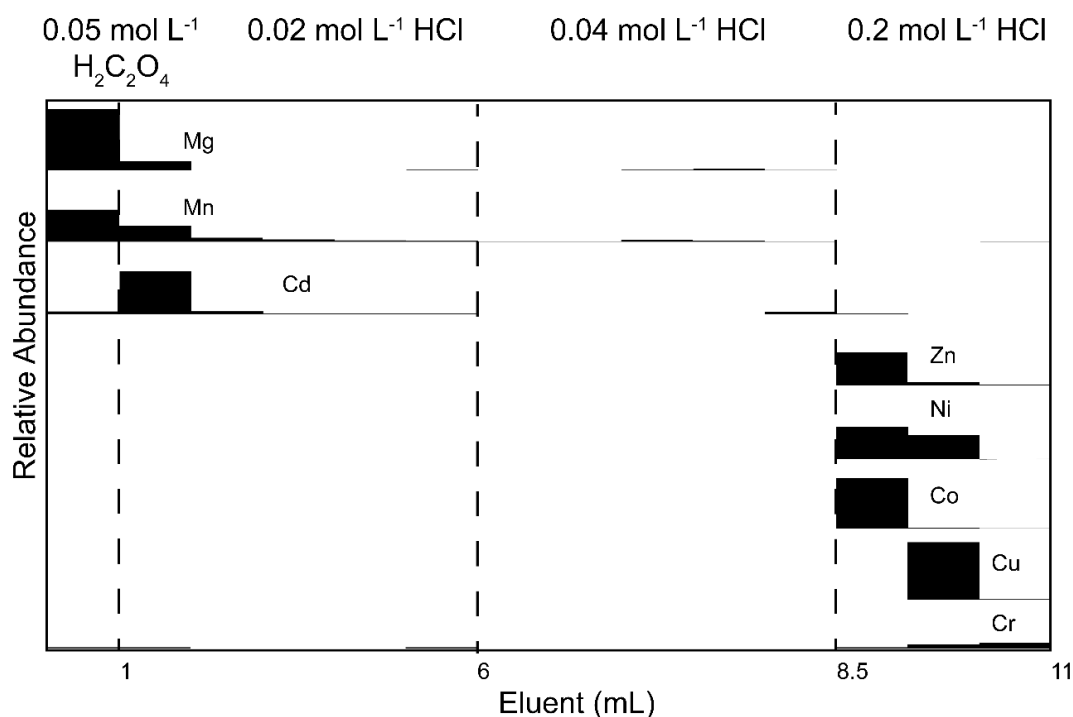


Figure 19 - Elution profile for step 2: Separating Ni from Group 1 and Group 2 elements.

In step 2, Ni was separated from univalent and divalent cations and Cr by using the ability to form oxalate metal complexes (Figure 19). Oxalic acid has been used as a chelating agent (Krishnamurty & Harris, 1961) and an oxalic - HCl solution was conventionally used for the separation of multi-valent elements from divalent elements (Strelow et al., 1972). In the case of Ni separation, oxalic HCl solution was used to remove divalent and higher valence ions from a cation exchange resin, followed by collecting Ni by DMG-acetone-HCl solution (Gall et al., 2012). However, the recovery of Ni was dependent on the sample matrix, resulting in lower Ni yields for samples having a high matrix to Ni ratio, and yielding a high level of Ni blank ranging from 0.5 ng to 2.5 ng (Gall et al., 2012). In this study, oxalic acid was used as the loading solution for an anion exchange resin (AG-1X8), after allowing to form anionic oxalate complexes for Ni while neutral and cationic oxalate complexes for the majority of remaining Group 1 and Group 2 elements (Krishnamurty & Harris, 1961). To prevent the formation of Ni chloro complexes it is essential to remove chloride ions adsorbed in the resin and convert it to oxalate and OH⁻ forms. Washing the resin with an excess amount of H₂O is necessary because the selectivity of the OH⁻ for AG-1X8 is 22 times lower than that of the Cl⁻ (Bio-Rad, 2000). After loading the sample on the resin, 0.02 mol L⁻¹ and 0.04 mol L⁻¹ of HCl were used to effectively elute the remaining group 2 elements and Mn which forms multiple oxalate complexes (Krishnamurty & Harris, 1961). Nickel was subsequently eluted along with

Co, Cu, and Zn by adding 0.2 mol L⁻¹ HCl. The distribution coefficients of oxalate complexes of Al, Ti, and V are higher than that of Ni (Strelow et al., 1972). Hence, even if any residual Al, Ti, and V were present after the first step, they can be completely separated from Ni cut in step 2.

Initially, we have decomposed resulting oxalates in the Ni cut with concentrated HNO₃ (Kubota, 1982). However, there was no difference in the elution curve and Ni recovery during ion exchange whether the loading solution in step 3 was HNO₃-attacked or not. Thus, further decomposition of oxalates is not necessary before step 3. Finally, the remained transition metals (Co, Cu, Zn and minor Cd) were separated from Ni by the same anion exchange resin, AG-1X8. Anionic Ni chloro complex is not formed in high molarity HCl (Moore & Kraus, 1952) while stable Co, Zn, and Cu anionic chloro complexes of [CoCl₄]²⁻ (Kauffman et al., 1989), [ZnCl₃]⁻, [ZnCl₄]²⁻ (Gallardo et al., 2008) and [CuCl₃]⁻, [CuCl₄]²⁻ (Marechal & Albarede, 2002) are formed respectively. Since Co has the potential to form ⁵⁹Co¹H⁺ in the plasma which can interfere with ⁶⁰Ni⁺ and ⁶⁴Zn⁺ can interfere with ⁶⁴Ni⁺, it is desirable to remove Co and Zn from the Ni fraction. The highest distribution coefficient for Co chloro complex is at 9 mol L⁻¹ HCl with Dowex-1 anion exchange resin (Moore & Kraus, 1952). However, since such a high molarity HCl can damage the resin, 8 mol L⁻¹ HCl was used to purify Ni using 0.1 mL of AG-1X8 resin (Figure 20). If necessary, the retained transition metals (Co, Cu, Zn, and minor amount of Cd) can be eluted subsequently by modifying the method described elsewhere (Yamakawa et al., 2009).

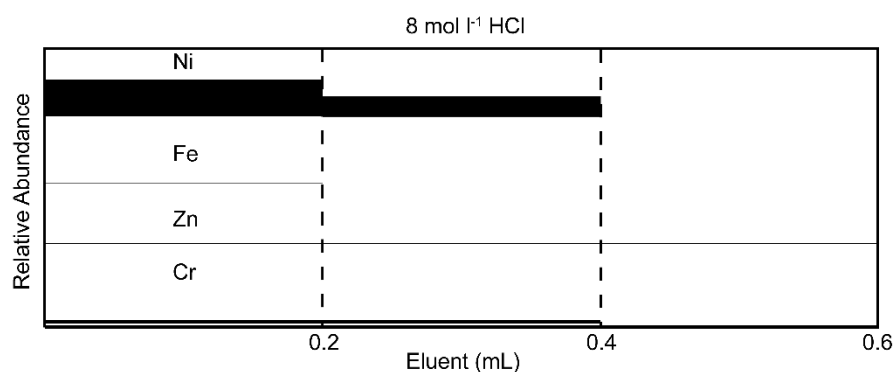


Figure 20 - Elution profile for step 3: Separating Ni from remaining transition metals

3.4.2. Recovery yields and procedural blanks

Recovery yields of Ni examined using the representative geological samples are: peridotite (JP-1, 98%), diabase (TDB-1, 100%), basalt (BCR-2, 97%), andesite (AGV-2, 99%), rhyolite (RGM-1, 94%), shale (SCO-1, 100%), marine mud (MAG-1, 95%), and sediment

(JSD-1, 98%), yielding $98 \pm 4\%$ (2SD, N = 8). Thus, the recovery of Ni does not depend on matrix compositions. The total procedural blank of Ni carried out from sample decomposition to full chemical separation, yielded 0.7 ± 0.3 ng solution was $<0.4\%$ of Ni in the sample, thus, the blank is negligible (2SD, N = 4 for 200 ng of Ni). The blank contribution to the sample for Ni isotope measurement. As the Ni blank from the reagents used in column chemistry yielded 0.5 ng, 0.2 ng was derived from others.

3.4.3. Evaluation of the procedure for the removal of interfering elements

Possible interferences that can affect Ni isotope measurements have been extensively discussed in previous studies. Elements such as Fe, Zn, Mg, Ca, Al, Cr, Na, Ti, Co, K, V, Cu, Cd, S, P can produce spectral interferences by forming doubly charged species (e.g. $^{116}\text{Cd}^{2+}$, $^{116}\text{Sn}^{2+}$ etc.), poly-atomic molecules combining with O, N, and Ar (e.g. $^{42}\text{Ca}^{16}\text{O}^+$, $^{46}\text{Ti}^{14}\text{N}^+$, $^{36}\text{Ar}^{24}\text{Mg}^+$, etc.) or isobaric species such as $^{58}\text{Fe}^+$ and $^{64}\text{Zn}^+$ (Beunon et al., 2020; Gall et al., 2012; Quitté & Oberli, 2006; Wu et al., 2019). To evaluate the presence of interfering species in the purified Ni fractions, they were analyzed for impurities and found that X/Ni (X = Fe, Zn, Cr, Cu, Co, Ti, Ca, Sn, Cd, Mn) ratios for all sample matrices are < 0.2 with an exception of Mg which was not completely purified (*Table 12* and Appendix B)

Table 12 - Ni mass fraction and $\delta^{60}\text{Ni}$ value of reference materials

Sample	[Ni] ($\mu\text{g g}^{-1}$)	$\delta^{60}\text{Ni}$	$\pm 2\text{SD}$	N	Element/Ni after purification [#]		
					Fe/Ni	Zn/Ni	Mg/Ni
<i>Peridotite</i>							
JP-1	2327	0.114	± 0.030	3	<0.01	<0.01	2.25
PCC-1	2343	0.131	± 0.016	3	0.02	0.02	2.96
DTS-1	2333	-0.086	± 0.008	3	0.01	<0.01	0.10
<i>Diabase</i>							
DNC-1	258.4	0.142	± 0.044	3	<0.01	<0.01	0.09
W-2	70.4	0.344	± 0.034	3	<0.01	<0.01	0.50
TDB-1	90.8	0.161	± 0.045	3	BDL	<0.01	2.82
<i>Serpentinite</i>							
UBN	1964	0.115	± 0.014	3	0.03	0.02	0.04
MUH-1	2152	0.131	± 0.051	3	0.02	0.02	3.26
<i>Komatiite</i>							
OKUM	889	0.130	± 0.026	3	<0.01	<0.01	1.96
<i>Basalt</i>							
BCR-2	12.0	0.228	± 0.030	3	<0.01	<0.01	0.24
JB-1b	148	0.164	± 0.015	3	<0.01	0.01	2.07
<i>Andesite</i>							
AGV-2	17.9	0.035	± 0.082	3	<0.01	<0.01	0.36
JA-2	128.4	0.218	± 0.014	3	BDL	0.05	0.10
<i>Rhyolite</i>							
RGM-1	3.0	-0.099	± 0.084	4	BDL	<0.01	0.07
<i>Granodiorite</i>							
GSP-1	6.9	0.185	± 0.017	3	0.02	0.03	6.68
<i>Schist</i>							
SDC-1	32.9	0.147	± 0.006	3	BDL	<0.01	0.31
<i>Shale</i>							
SCO-1	26.2	0.089	± 0.054	3	<0.01	<0.01	1.25
SGR-1	29.3	0.445	± 0.014	3	BDL	BDL	0.12
<i>Marine mud</i>							
MAG-1	49.2	0.225	0.031*	2	<0.01	BDL	0.97
<i>Sediment</i>							
JSD-1	7.2	0.153	± 0.044	3	<0.01	<0.01	0.32

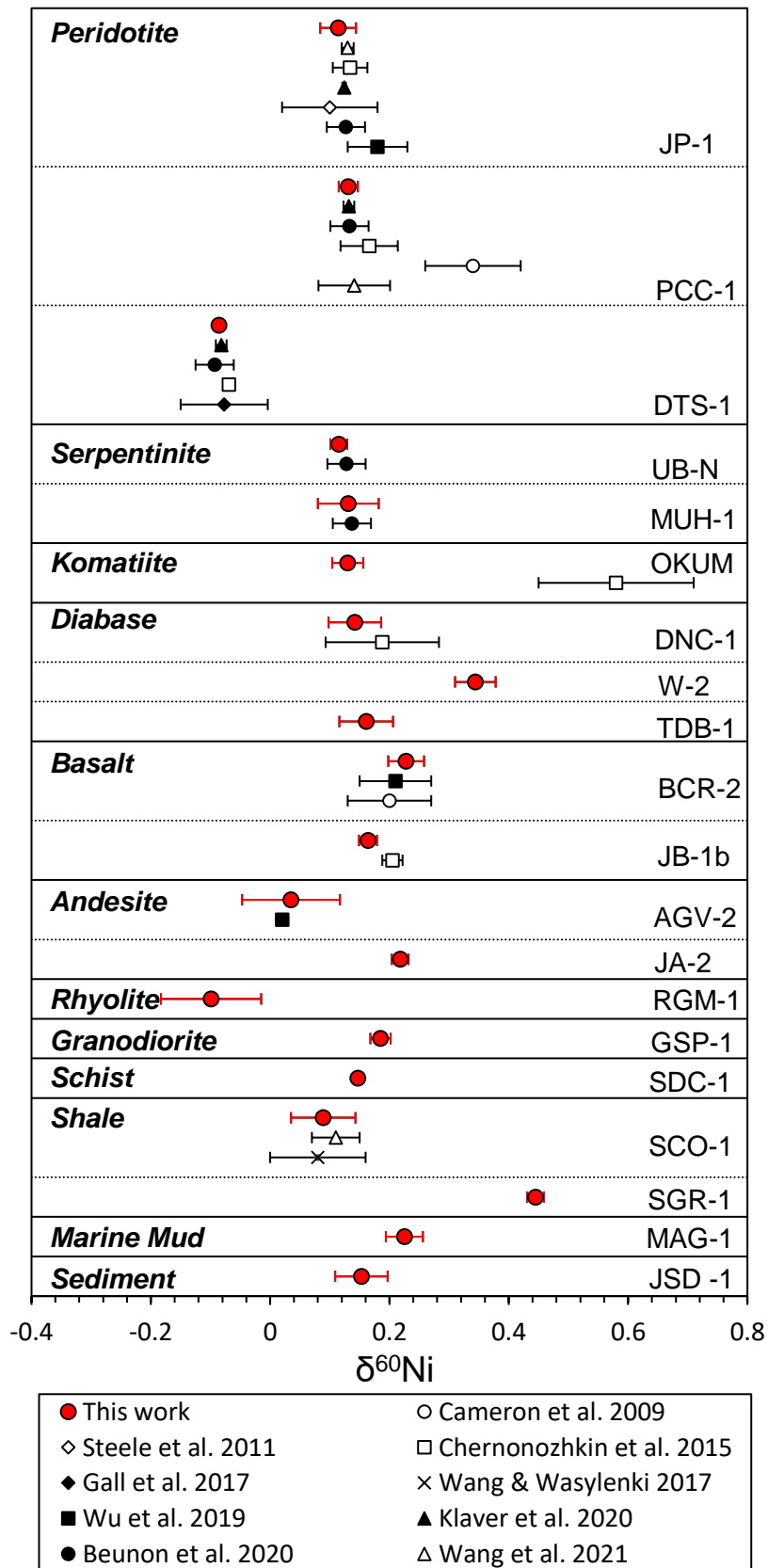


Figure 21 - $\delta^{60}\text{Ni}$ values for the geological samples analyzed in this study in comparison with literature data.

The reason for this insufficient purification of Mg is the multiple anionic complexes that form with oxalic acid which is difficult to elute completely by using low molarity acids. Incomplete removal of Mn was known to produce a significant matrix effect to the $^{60}\text{Ni}/^{58}\text{Ni}$ measurement if the atomic ratio Mn/Ni was >0.4 (Wu et al., 2019). In contrast, the presence of Mg does not affect the $\delta^{60}\text{Ni}$ measurement even atomic ratio of Mg/Ni ~ 5 (Beunon et al., 2020). To examine the effects of Mn and Mg in the purified Ni fraction, we performed the doping experiment, adding Mg or Mn (up to Mn/ Ni = 2 and Mg/Ni = 8) into NIST SRM 986 with different proportions. There was no systematic difference in the measured isotopic ratios, revealing that presence of those elements up to the levels measured does not affect the isotopic compositions. The formation of the doubly charged species was evaluated by aspirating $10 \mu\text{g g}^{-1}$ solutions of Cd, Sn, and Te to the plasma and observed that they are insignificant compared to the signal of Ni species. Moreover, the corresponding species were effectively removed from the Ni fraction (Appendix A2). The samples having high Fe/Ni ~ 11000 and Zn/Ni ~ 10 (BCR-2) have resulted in pure Ni fractions with Element/Ni ≤ 0.01 , removing the interfering species, assuring the effectiveness of the purification procedure.

3.4.4. Ni isotope compositions of reference materials

To demonstrate the applicability of our technique to various sample matrices and to contribute the Ni isotope database of the reference standards, Ni separation and isotope measurement for 20 reference standards including 9 new samples which have not been previously analyzed for Ni isotopes, were performed. Results are presented in *Table 12* and a detailed version is presented with Appendix B. In general, our measured $\delta^{60}\text{Ni}$ values are indistinguishable within the uncertainty of the previously published values with high and intermediate Ni mass fractions ($>12 \mu\text{g g}^{-1}$, *Table 12* and Figure 21) validating the effectiveness of the novel purification procedure. Our $\delta^{60}\text{Ni}$ values of OKUM (komatiite) and JB-1b (basalt) are lower than that of the published values. These discrepancies may derive either from sample heterogeneities themselves, matrix effects, or low recovery yields. Unfortunately, the recovery yields and the level of impurities in the purified Ni fractions are not discussed per each sample for the published data (Chernonozhkin et al., 2015), therefore evaluation is not possible and further inter laboratory comparisons are warranted for these samples. Our method has shown to achieve nearly complete recovery and effective separation of matrix elements from Ni even from samples with low Ni mass fraction (Ni = $3 - 7 \mu\text{g g}^{-1}$; RGM-1, GSP-1, JSD-1) and with rich in organic matter (MAG-1). Therefore, the Ni isotope values of these low-Ni and organic-rich samples measured in this study are considered to be highly accurate.

3.5. Conclusions

A simple and novel method for isolating Ni from geological samples by 3 column step ion exchange method was developed. In this method, Ni was separated from univalent and divalent cations using a minimum amount of oxalic acid without using conventionally used DMG, Ni specific resins, or repetitive column steps with pH adjustments. This method only requires 100-200 ng Ni containing sample which is significantly (6-8 times) lower than the current methods published and low blank purification is also guaranteed. Moreover, the recovery of Ni yields $98 \pm 3 \%$, which does not depend on the sample matrix.

Credit author statement –

- *Dilan M. Ratnayake (Conceptualization, Methodology, Investigation, Writing original Draft)*
- *Ryoji Tanaka (Writing – Review & Editing, Supervision, Resources)*
- *Eizo Nakamura (Supervision)*

3.6. References

- Ali, S. Y., Reddy, K. D., & Manna, A. K. (2019). Structural, Electronic, and Spectral Properties of Metal Dimethylglyoximate $[M(\text{DMG})_2; M = \text{Ni}^{2+}, \text{Cu}^{2+}]$ Complexes: A Comparative Theoretical Study. *Journal of Physical Chemistry A*, 123(42), 9166–9174. <https://doi.org/10.1021/acs.jpca.9b06762>
- Beunon, H., Chernonozhkin, S. M., Mattielli, N., Goderis, S., Doucet, L.-S., Debaille, V., & Vanhaecke, F. (2020). Innovative two-step isolation of Ni prior to stable isotope ratio measurements by MC-ICP-MS: Application to igneous geological reference materials. *Journal of Analytical Atomic Spectrometry*, 2213–2223. <https://doi.org/10.1039/d0ja00163e>
- Bio-Rad. (2000). AG1, AG MP-1 and AG 2 Strong Anion Exchange Resin Instruction Manual. 23.
- Brown, R. B. (1964). The effect of hydrofluoric acid on the cation exchange behavior of metal ions.
- Burger, K., Ruff, I., & Ruff, F. (1965). Some theoretical and practical problems in the use of organic reagents in chemical analysis—IV. *Journal of Inorganic and Nuclear Chemistry*, 27(1), 179–190. [https://doi.org/10.1016/0022-1902\(65\)80208-1](https://doi.org/10.1016/0022-1902(65)80208-1)

- Cameron, V., & Vance, D. (2014). Heavy nickel isotope compositions in rivers and the oceans. *Geochimica et Cosmochimica Acta*, 128, 195–211. <https://doi.org/10.1016/j.gca.2013.12.007>
- Cameron, V., Vance, D., Archer, C., & House, C. H. (2009). A biomarker based on the stable isotopes of nickel. *Proceedings of the National Academy of Sciences of the United States of America*, 106(27), 10944–10948. <https://doi.org/10.1073/pnas.0900726106>
- Chen, J. H., Papanastassiou, D. A., & Wasserburg, G. J. (2009). A search for nickel isotopic anomalies in iron meteorites and chondrites. *Geochimica et Cosmochimica Acta*, 73(5), 1461–1471. <https://doi.org/10.1016/j.gca.2008.11.040>
- Chernonozhkin, S. M., Goderis, S., Lobo, L., Claeys, P., & Vanhaecke, F. (2015). Development of an isolation procedure and MC-ICP-MS measurement protocol for the study of stable isotope ratio variations of nickel. *Journal of Analytical Atomic Spectrometry*, 30(7), 1518–1530. <https://doi.org/10.1039/c5ja00080g>
- Cook, D. L., Wadhwa, M., Janney, P. E., Dauphas, N., Clayton, R. N., & Devis, A. M. (2006). High precision measurements of non-mass-dependent effects in nickel isotopes in meteoritic metal via multicollector ICPMS. *Analytical Chemistry*, 78(24), 8477–8484. <https://doi.org/10.1021/ac061285m>
- Deng, T. H. B., Cloquet, C., Tang, Y. T., Sterckeman, T., Echevarria, G., Estrade, N., Morel, J. L., & Qiu, R. L. (2014). Nickel and zinc isotope fractionation in hyperaccumulating and nonaccumulating plants. *Environmental Science and Technology*, 48(20), 11926–11933. <https://doi.org/10.1021/es5020955>
- Elliott, T., & Steele, R. C. J. (2017). The Isotope Geochemistry of Ni. *Non-Traditional Stable Isotopes*, 82, 511–541. <https://doi.org/10.2138/rmg.2017.82.12>
- Estrade, N., Cloquet, C., Echevarria, G., Sterckeman, T., Deng, T., Tang, Y., & Morel, J. (2015). Weathering and vegetation controls on nickel isotope fractionation in surface ultramafic environments (Albania). *Earth and Planetary Science Letters*, 423, 24–35. <https://doi.org/10.1016/j.epsl.2015.04.018>
- Fujii, T., Moynier, F., Dauphas, N., & Abe, M. (2011). Theoretical and experimental investigation of nickel isotopic fractionation in species relevant to modern and ancient

- oceans. *Geochimica et Cosmochimica Acta*, 75(2), 469–482.
<https://doi.org/10.1016/j.gca.2010.11.003>
- Gallardo, V., Navarro, R., Saucedo, I., Ávila, M., & Guibal, E. (2008). Zinc(II) extraction from hydrochloric acid solutions using amberlite XAD-7 impregnated with cyphos IL 101 (tetradecyl(trihexyl)phosphonium chloride). *Separation Science and Technology*, 43(9–10), 2434–2459. <https://doi.org/10.1080/01496390802119002>
- Gall, L., Williams, H., Siebert, C., & Halliday, A. (2012). Determination of mass-dependent variations in nickel isotope compositions using double spiking and MC-ICPMS. *Journal of Analytical Atomic Spectrometry*, 27(1), 137–145.
<https://doi.org/10.1039/c1ja10209e>
- Kauffman, G. B., Adams, M. L., & Tuttle, T. R. (1989). The separation of cobalt from nickel by anion exchange chromatography. *Journal of Chemical Education*, 66(2), 166–167.
<https://doi.org/10.1021/ed066p166>
- Klaver, M., & Coath, C. D. (2019). Obtaining Accurate Isotopic Compositions with the Double Spike Technique: Practical Considerations. *Geostandards and Geoanalytical Research*, 43(1), 5–22. <https://doi.org/10.1111/ggr.12248>
- Klaver, M., Ionov, D. A., Takazawa, E., & Elliott, T. (2020). ScienceDirect The non-chondritic Ni isotope composition of Earth ' s mantle. 268, 405–421.
<https://doi.org/10.1016/j.gca.2019.10.017>
- Krishnamurty, K. V., & Harris, G. M. (1961). The chemistry of the metal oxalato complexes. *Chemical Reviews*, 61(3), 213–246. <https://doi.org/10.1021/cr60211a001>
- Kubota, M. (1982). Decomposition of oxalic acid with nitric acid. *Journal of Radioanalytical Chemistry*, 75(1–2), 39–49. <https://doi.org/10.1007/BF02519972>
- Lee, F. T., & Diehl, H. (1950). Proceedings of the Iowa Academy of Science The Colorimetric Determination of Cobalt with Dimethylglyoxime and Benzidine The Colorimetric Determination of Cobalt with. 57, 187–191.
- Marechal, C., & Albarede, F. (2002). Ion-exchange fractionation of copper and zinc isotopes . *Geochimica et Cosmochimica Acta*, 66(9), 1499–1509.

- Moore, G. E., & Kraus, K. A. (1952). Anion Exchange Studies. IV.1,2 Cobalt and Nickel in Hydrochloric Acid Solutions. *Journal of the American Chemical Society*, 74(3), 843–844. <https://doi.org/10.1021/ja01123a520>
- Morand, P., & Allègre, C. J. (1983). Nickel isotopic studies in meteorites. *Earth and Planetary Science Letters*, 63(2), 167–176. [https://doi.org/10.1016/0012-821X\(83\)90034-1](https://doi.org/10.1016/0012-821X(83)90034-1)
- Nakamura, E., Makishima, A., Moriguti, T., Kobayashi, K., Sakaguchi, C., Yokoyama, T., Tanaka, R., Kuritani, T., & Takei, H. (2003). Comprehensive geochemical analyses of small amounts (< 100 mg) of extraterrestrial samples for the analytical competition related to the sample return mission MUSES-C. The Institute of Space and Astronautical Science Report. S.P.: The First Open Competition for the MUSES-C Asteroidal Sample Preliminary Examination Team, 16, 49–101.
- Nelson, F., Murase, T., & Kraus, K. A. (1964). Ion exchange procedures. I. Cation exchange in concentration HCl and HClO₄ solutions. *Journal of Chromatography A*, 13(C), 503–535. [https://doi.org/10.1016/s0021-9673\(01\)95146-5](https://doi.org/10.1016/s0021-9673(01)95146-5)
- Quitte, G., Halliday, A. N., Meyer, B. S., Markowski, A., Latkoczy, C., & Gunther, D. (2007). Correlated Iron 60, Nickel 62, and Zirconium 96 in Refractory Inclusions and the Origin of the Solar System. *The Astrophysical Journal*, 655(1), 678–684. <https://doi.org/10.1086/509771>
- Quitté, G., & Oberli, F. (2006). Quantitative extraction and high precision isotope measurements of nickel by MC-ICPMS. *Journal of Analytical Atomic Spectrometry*, 21(11), 1249–1255. <https://doi.org/10.1039/b607569j>
- Ratié, G., Jouvin, D., Garnier, J., Rouxel, O., Miska, S., Guimarães, E., Cruz Vieira, L., Sivry, Y., Zelano, I., Montarges-Pelletier, E., Thil, F., & Quantin, C. (2015). Nickel isotope fractionation during tropical weathering of ultramafic rocks. *Chemical Geology*, 402, 68–76. <https://doi.org/10.1016/j.chemgeo.2015.02.039>
- Rudge, J. F., Reynolds, B. C., & Bourdon, B. (2009). The double spike toolbox. *Chemical Geology*, 265(3–4), 420–431. <https://doi.org/10.1016/j.chemgeo.2009.05.010>
- Rugel, G., Faestermann, T., Knie, K., Korschinek, G., Poutivtsev, M., Schumann, D., Kivel, N., Günther-Leopold, I., Weinreich, R., & Wohlmuther, M. (2009). New measurement

- of the Fe60 half-life. *Physical Review Letters*, 103(7), 14–17.
<https://doi.org/10.1103/PhysRevLett.103.072502>
- Shukolyukov, A., & Lugmair, G. W. (1991). Live Iron-60 in the Early Solar System.
- Siebert, C., Nögler, T. F., & Kramers, J. D. (2001). Determination of molybdenum isotope fractionation by double-spike multicollector inductively coupled plasma mass spectrometry. *Geochemistry, Geophysics, Geosystems*, 2(7).
<https://doi.org/10.1029/2000GC000124>
- Steele, R. C. J., Elliott, T., Coath, C. D., & Regelous, M. (2011). Confirmation of mass-independent Ni isotopic variability in iron meteorites. *Geochimica et Cosmochimica Acta*, 75(24), 7906–7925. <https://doi.org/10.1016/j.gca.2011.08.030>
- Strelow, F. W. E., Weinert, C. H. S. W., & Eloff, C. (1972). Distribution Coefficients and Anion Exchange Behavior of Elements in Oxalic Acid-Hydrochloric Acid Mixtures. 44(14), 2352–2356.
- Tang, H., & Dauphas, N. (2012). Abundance, distribution, and origin of ⁶⁰Fe in the solar protoplanetary disk. *Earth and Planetary Science Letters*, 359–360, 248–263.
<https://doi.org/10.1016/j.epsl.2012.10.011>
- Tang, H., & Dauphas, N. (2014). ⁶⁰Fe-⁶⁰Ni chronology of core formation in Mars. *Earth and Planetary Science Letters*, 390, 264–274. <https://doi.org/10.1016/j.epsl.2014.01.005>
- Victor, A. H. (1986). Separation of nickel from other elements by cation-exchange chromatography in dimethylglyoxime/hydrochloric acid/acetone media. *Analytica Chimica Acta*, 183(C), 155–161. [https://doi.org/10.1016/0003-2670\(86\)80083-6](https://doi.org/10.1016/0003-2670(86)80083-6)
- Wu, G., Zhu, J. M., Wang, X., Han, G., Tan, D., & Wang, S. J. (2019). A novel purification method for high precision measurement of Ni isotopes by double spike MC-ICP-MS. *Journal of Analytical Atomic Spectrometry*, 34(8), 1639–1651.
<https://doi.org/10.1039/c9ja00077a>
- Yamakawa, A., Yamashita, K., Makishima, A., & Nakamura, E. (2009). Chemical separation and mass spectrometry of Cr, Fe, Ni, Zn, and Cu in terrestrial and extraterrestrial materials using thermal ionization mass spectrometry. *Analytical Chemistry*, 81(23), 9787–9794. <https://doi.org/10.1021/ac901762a>

Appendix A

A.1. Ni Double-spike Calibration

The optimum proportion of each spike in the ^{61}Ni - ^{62}Ni double-spike was simulated using a MATLAB code published elsewhere (Rudge et al., 2009). The isotopic composition of the double-spike was calibrated using a certified Ni standard NIST SRM 986 and certified Cu standard IRMM-647. The calibration procedure was based on the method described for Mo isotope (Siebert et al., 2001). For the calibration, Cu was doped for both standard and double spike solutions, and the mass fraction of Ni and Cu was adjusted to $0.3 \mu\text{g g}^{-1}$ for both solutions. In addition, Cu-doped double spike-standard mixture solution containing $0.3 \mu\text{g g}^{-1}$ of Ni and Cu, dissolved in $0.5 \text{ mol l}^{-1} \text{ HNO}_3$ with variable double spike/standard ratio (0.5, 0.9, 1.4, 1.7, and 3.9) was prepared.

The measurement was performed in two steps. First, the Cu-doped Ni standard and the Cu-doped double spike solutions were measured. The measurements of the standards and the double spike solution were performed five times for each sequence. To minimize the memory effect, the APEX-IR desolvating nebulizer was removed from the connecting line and washed by diluted HNO_3 and water between the nickel standard and the double spike measurements without turning off the plasma.

The true and measured Ni isotope ratios of isotope i and j of the Ni standard solution and the double spike, $R_{Nistd \text{ or } NiDS}^{i/j}$ and $r_{NiDS \text{ or } NiDS}^{i/j}$, respectively, were expressed by the exponential law:

$$R_{Nistd}^{i/j} = r_{Nistd}^{i/j} \left(\frac{M_i}{M_j} \right)^{f_{Ni}} \quad \text{Eq. (A1)}$$

$$R_{NiDS}^{i/j} = r_{NiDS}^{i/j} \left(\frac{M_i}{M_j} \right)^{f_{Ni}} \quad \text{Eq. (A2)}$$

Where M_i and M_j are the absolute atomic masses of isotope i and j , respectively, where $j = 58$ and $i = 60, 61, 62,$ and 64 . Similarly, the true and measured Cu isotope ratio of isotope ^{65}Cu and ^{63}Cu , $R_{Cu}^{65/63}$ and $r_{Cu}^{65/63}$, respectively, were expressed as:

$$R_{Cu}^{65/63} = r_{Cu}^{65/63} \left(\frac{M_{65}}{M_{63}} \right)^{f_{Cu}} \quad \text{Eq. (A3)}$$

where M_{65} and M_{63} are absolute atomic masses ^{65}Cu and ^{63}Cu , respectively.

The f_{Ni} and f_{Cu} values for each measurement were tentatively measured using the fixed values of $R_{Nistd}^{60/58} = 0.385199$ and $R_{Cu}^{65/63} = 0.44560$ (ERM certificate), respectively. The measured $\frac{f_{Cu}}{f_{Ni}}$ values among the measurements were identical within the internal precision of each measurement, thus the average value of $\frac{f_{Cu}}{f_{Ni}}$ in Cu-doped standard and the obtained f_{Cu} value in Cu-doped double spike were used for the determination of f_{Ni} for each double spike measurement.

Second, the isotopic ratios of the standard and the double spike were optimized by measuring the standard-double spike mixture solutions. The optimization was performed by changing the $R_{Nistd}^{60/58}$ and $R_{Cu}^{65/63}$ values for equations (A1), (A2), and (A3) to achieve the average absolute value of $\delta^{60}Ni$ values in standard-double spike mixtures to be minimized. The ^{58}Ni , ^{60}Ni , ^{61}Ni , and ^{62}Ni were used for the data reduction to determine the $\delta^{60}Ni$ value using the double spike reduction method described elsewhere (Albarède et al., 2004). The optimum proportion of the double-spike in the double-spike-sample mixture was calculated as 0.66 (Rudge et al., 2009).

A.3. References

- Albarède, F., Telouk, P., Blichert-Toft, J., Boyet, M., Agranier, A., & Nelson, B. (2004). Precise and accurate isotopic measurements using multiple-collector ICPMS. *Geochimica et Cosmochimica Acta*, 68(12), 2725–2744. <https://doi.org/10.1016/j.gca.2003.11.024>
- Rudge, J. F., Reynolds, B. C., & Bourdon, B. (2009). The double spike toolbox. *Chemical Geology*, 265(3–4), 420–431. <https://doi.org/10.1016/j.chemgeo.2009.05.010>
- Siebert, C., Nögler, T. F., & Kramers, J. D. (2001). Determination of molybdenum isotope fractionation by double-spike multicollector inductively coupled plasma mass spectrometry. *Geochemistry, Geophysics, Geosystems*, 2(7). <https://doi.org/10.1029/2000GC000124>
- Menor Salván, C. et al. 2020. “Prebiotic Origin of Pre-RNA Building Blocks in a Urea ‘Warm Little Pond’ Scenario.” *ChemBioChem* 21(24): 3504–10.
- Tian, Feng, J. F. Kasting, and K. Zahnle. 2011. “Revisiting HCN Formation in Earth’s Early Atmosphere.” *Earth and Planetary Science Letters* 308(3–4): 417–23. <http://dx.doi.org/10.1016/j.epsl.2011.06.011>.

Appendix B : Ni Isotopic Composition of Geological Reference Materials

Sample Name	Sample Type	[Ni] ($\mu\text{g g}^{-1}$)	$\delta^{66}\text{Ni}$	2SD	N*	Metal/Ni Ratio After Purification														Reference
						Fe/Ni	Zn/Ni	Cr/Ni	Cu/Ni	Co/Ni	Ti/Ni	Na/Ni	Ca/Ni	Sr/Ni	Al/Ni	Cd/Ni	Mg/Ni	Mn/Ni		
JP-1		2327	0.114	0.030	3	<0.001	<0.001	0.002	<0.001	<0.001	<0.001	0.005	0.011	BDL	0.001	<0.001	2.250	0.026	This Study	
			0.13	0.01	-														Wang et al. 2021	
			0.134	0.029	1														Chernozhukhin et al. 2015	
			0.124	0.003	12														Klaver et al. 2020	
			0.1	0.08	58														Steele et al. 2011	
			0.127	0.032	7														Beannon et al. 2020	
		2480	0.18	0.05	6														Wu et al. 2019	
PCC-1		2343	0.131	0.016	3	0.023	0.015	0.010	BDL	BDL	BDL	BDL	BDL	BDL	0.009	BDL	2.964	0.021	This Study	
			0.132	0.009	8														Klaver et al. 2020	
	Peridotite		0.133	0.032	3														Beannon et al. 2020	
			0.166	0.048	8														Chernozhukhin et al. 2015	
			0.34	0.08															Cameron et al. 2009	
		2325	0.141	0.06	17														Gall et al. 2017	
DTS-1		2333	-0.086	0.008	3	0.010	0.002	BDL	BDL	BDL	BDL	BDL	BDL	BDL	0.005	BDL	0.099	0.010	This Study	
			-0.082	0.009	8														Klaver et al. 2020	
			-0.093	0.032	3														Beannon et al. 2020	
			-0.069	0.006	2														Chernozhukhin et al. 2015	
		2360	-0.077	0.073	32														Gall et al. 2017	
DNC-1		258.4	0.142	0.044	3	0.001	0.003	0.005	<0.001	0.001	BDL	0.193	0.106	BDL	0.008	BDL	0.092	0.043	This Study	
			0.188	0.095	5														Chernozhukhin et al. 2015	
W-2	Database	70.4	0.344	0.034	3	0.003	0.002	0.017	0.001	0.001	BDL	0.129	0.07	BDL	0.009	BDL	0.500	0.100	This Study	
TDB-1		90.8	0.161	0.045	3	BDL	0.002	0.029	<0.001	<0.001	BDL	0.108	0.187	BDL	0.020	BDL	2.821	0.300	This Study	
UBN		1964	0.115	0.014	3	0.025	0.015	0.017	BDL	0.001	BDL	0.079	0.331	BDL	0.008	BDL	0.036	0.016	This Study	
			0.128	0.032	8														Beannon et al. 2020	
MUH-1	Serpentine	2152	0.131	0.051	3	0.023	0.017	0.008	BDL	BDL	BDL	0.312	0.312	BDL	0.006	BDL	3.262	0.026	This Study	
			0.137	0.032	8														Beannon et al. 2020	

Sample Name	Sample Type	[Ni]/($\mu\text{g g}^{-1}$)	$\delta^{60}\text{Ni}$	2SD	N*	Mean/Ni Ratio After Purification														Reference
						Fe/Ni	Zn/Ni	Cr/Ni	Cu/Ni	Co/Ni	Ti/Ni	Na/Ni	Ce/Ni	Sr/Ni	Al/Ni	Cd/Ni	Mg/Ni	Mn/Ni		
OKUM	Basalt	889	0.130	0.026	3	0.003	0.002	0.002	0.001	BDL	BDL	0.115	0.068	BDL	0.007	BDL	1.963	0.067	This Study	
			0.58	0.13																Chernozhukin et al. 2015
BCR-2			12.0	0.228	0.030	3	0.001	<0.001	0.002	0.002	0.004	BDL	0.024	0.167	BDL	0.003	<0.001	0.240	0.088	This Study
			9.5	0.21	0.06	5														Wu et al. 2019
				0.2	0.07															Cameron et al. 2009
JB1-b		148.0	0.164	0.015	3	0.002	0.005	0.013	0.001	0.002	BDL	0.176	0.462	BDL	0.016	BDL	2.070	0.634	This Study	
				0.205	0.017	1														Chernozhukin et al. 2015
AGV-2	Andesite	17.9	0.035	0.082	3	<0.001	<0.001	0.001	0.001	<0.001	BDL	0.013	0.072	BDL	0.003	<0.001	0.356	0.140	This Study	
			20.2	0.02	0.01	3														Wu et al. 2019
JA-2			128.4	0.218	0.014	3	BDL	0.048	0.059	BDL	BDL	BDL	BDL	0.033	BDL	0.007	BDL	0.099	0.032	This Study
GSP-1	Granodiorite	6.9	0.185	0.017	3	0.020	0.032	0.004	0.001	0.002	BDL	0.174	0.673	BDL	0.099	BDL	6.682	0.825	This Study	
RGM-1	Rhyolite	3.0	-0.099	0.084	4	BDL	0.005	0.024	0.002	BDL	BDL	0.262	BDL	BDL	0.410	BDL	0.067	0.065	This Study	
SDC-1	Schist	32.9	0.147	0.006	3	BDL	<0.001	0.014	0.001	BDL	BDL	0.018	0.022	BDL	0.004	BDL	0.310	0.150	This Study	
SCO-1	Shale	26.2	0.089	0.054	3	0.001	<0.001	0.003	0.001	<0.001	BDL	0.043	0.098	BDL	0.003	<0.001	1.245	0.166	This Study	
				0.11	0.04															Wang et al. 2021
				0.08	0.08															Wang and Wasylenki 2017
SGR-1		29.3	0.445	0.014	3	BDL	BDL	0.017	BDL	0.055	BDL	BDL	0.205	BDL	BDL	BDL	0.118	0.035	This Study	
MAG-1	Marme mud	49.2	0.225	0.031**	2	<0.001	BDL	0.003	0.001	<0.001	BDL	0.014	0.02	BDL	0.003	<0.001	0.971	0.033	This Study	
JSD-1	Sediment	7.2	0.153	0.044	3	0.001	<0.001	0.007	0.001	<0.001	BDL	0.011	0.044	BDL	0.009	<0.001	0.320	0.209	This Study	

* Number of different sample aliquots processed through the ion exchange columns.

**Relative Percent Difference

BDL = Below Detection Limit

Chapter 4: Determination of mass-dependent chromium isotopic compositions in geological samples by double spike-total evaporation-thermal ionization mass spectrometry (DS-TE-TIMS)

This chapter is published as an article in Analytica Chimica Acta.

<https://doi.org/10.1016/j.aca.2023.341723>

4.1. Abstract

Background: Chromium isotopes have been used to trace geochemical and cosmochemical processes in the past. However, the presence of multivalent Cr species has made it difficult to isolate Cr from geological samples, particularly for samples with a low Cr mass fraction.

Results: Here, a simple three-step ion exchange chromatography procedure is presented to separate Cr from various sample matrices, ranging from ultramafic to felsic rocks. Throughout each of the column chromatography steps, 1 ml of cation exchange resin AG50W-X8 (200-400 mesh) was used as the stationary phase and oxalic acid as a chelating agent, was used in addition to the inorganic acids. This method yielded high recoveries of Cr [$93 \pm 8\%$ (2SD, N = 7)] regardless of the lithology. The total procedural blank of Cr was <0.5 ng. We also developed a double spike-total evaporation thermal ionization mass spectrometry (DS-TE-TIMS) technique that significantly reduced sample consumption to ~ 20 ng of Cr per each measurement of mass-dependent $^{53}\text{Cr}/^{52}\text{Cr}$.

Significance: This study achieved a 2SD external precision of 0.02 ‰ for the analysis of NIST NBS3112a and of 0.01 to 0.07 ‰ for the geological samples. This study enabled high-precision Cr isotope analysis in geological samples with various matrix and Cr compositions using relatively small sample volumes.

Key Words – Cr isotopes, DS-TE-TIMS, cation exchange resin, low blank, high precision

4.2. Introduction

Chromium is a moderately compatible and slightly siderophile element with four naturally occurring isotopes: ^{50}Cr , ^{52}Cr , ^{53}Cr , and ^{54}Cr , which have relative abundances of 4.35%, 83.79%, 9.50%, and 2.36%, respectively (De Laeter et al. 2003; Rosman and Taylor 1998). The abundances of ^{53}Cr and ^{54}Cr isotopes are important tracers in cosmochemistry that provide temporal and spatial information on early solar system processes (Lugmair and Shukolyukov

1998; Qin et al. 2010; Qin and Wang 2017; Trinquier et al. 2008; Yamakawa et al. 2010; Zhu (朱柯) et al. 2021). Chromium is sensitive to redox reactions that cause mass-dependent isotopic fractionation, which can often be observed in both biotic and abiotic processes. Moreover, sorption and coprecipitation processes also fractionate Cr isotopes due to the changes in bonding environments.

Isolating Cr from the sample is necessary for precise measurement of isotopic variations. However, multiple oxidation states and the sluggish reaction kinetics of Cr complexes have made Cr isolation difficult. Therefore, rigorous sample pretreatment procedures were followed to obtain single valence species of Cr before ion-exchange chromatography (Hibiya et al. 2019; Larsen et al. 2016; J. M. Zhu et al. 2018a). These procedures include storing the sample with HNO₃ and H₂O₂ for more than five days (Larsen et al. 2016), adjusting pH and adding reagents such as (NH₄)₂S₂O₈, KMnO₄, H₂O₂, H₂SO₃, NH₂OH.HCl and NH₄OH ((Larsen et al. 2016) and references therein, (Li et al. 2017; J. M. Zhu et al. 2018a)) to achieve the desired valence state of Cr.

However, the aforementioned oxidants and reductants have many disadvantages. For example, the use of sulfur compounds can introduce SO₄²⁻ ions into the solution, which reduces the ionization efficiency of Cr in TIMS (Ball and Bassett 2000; Li et al. 2017; C. Y. Liu et al. 2019a). While NH₂OH.HCl was found to be an effective reducing agent, its instability and toxicity made procedures it was used in cumbersome. Furthermore, additional oxidizing-reducing reagents, such as H₂O₂ and (NH₄)₂S₂O₈ (Zhu et al. 2018a), were often required in subsequent steps to obtain a pure Cr fraction. Meanwhile, KMnO₄ was found to be unsuitable for Fe-Mn nodules and low-Cr samples, because it generated MnO₂ (from the excess KMnO₄) that could adsorb and coprecipitate Cr (Wei et al. 2018), yielding a low recovery of Cr (Zhu et al. 2018a).

On the other hand, the usage of oxidants and reductants is always influenced by the matrix. The addition of a double spike prior to column chemistry is preferred, in order to correct the isotopic fractionation due to low recoveries during ion-exchange chromatography. However, a high recovery yield is still necessary to minimize the errors in double spike inversion (Wang and Johnson 2021). Therefore, the development of a simple Cr recovery method that was independent of the matrix, and which resulted in high recovery, was required.

Mass-dependent Cr isotopic compositions of geological or extraterrestrial samples were measured using either the double spike (DS) method or standard-sample-bracketing (SSB) method (Halicz et al. 2008; Schiller et al. 2014) using the thermal ionization mass spectrometry (TIMS) or multi-collector inductively coupled plasma mass spectrometry (MC-ICP-MS). The Cr mass used for such isotope measurements by the DS-MC-ICP-MS, SSB-MC-ICP-MS and DS-TIMS techniques range from ~60 to 180 ng (Sossi, Moynier, and Van Zuilen 2018; Q. Zhang et al. 2018; J. M. Zhu et al. 2018a), ~25 to 60 μg (Halicz et al. 2008), and ~1 to 2 μg (Frei et al. 2009; Li et al. 2016a; C. Y. Liu et al. 2019b), respectively. Furthermore, the aforementioned analytical techniques are only effective when the Cr mass fraction in the sample is high enough. Nevertheless, the isolation of Cr is difficult in samples that have a low Cr mass fraction and/or when the available sample is precious and limited.

This paper presents a simple Cr isolation procedure that does not require rigorous sample pretreatment and allows the recovery of >90% of Cr from geological samples, ranging from ultramafic to felsic rocks with Cr mass fractions between ~4000 and ~2 $\mu\text{g g}^{-1}$. We used oxalic acid as a chelating agent for the separation procedure, in addition to commonly used inorganic acids. We also applied a DS-TE (total evaporation) TIMS method that lowered the sample consumption to ~20 ng per analysis (typically a total of ~60 to 140 ng for triplicate to septuplicate measurements from one sample), while maintaining high precision. The technique reported here, enables the precise analysis of Cr isotopes in a small amount of sample and will be particularly advantageous for future studies of felsic samples and precious samples, such as those returned from asteroids e.g. (Nakamura et al. 2022).

4.3. Materials and Methods

Sample digestion, ion chromatography, and mass spectrometry were carried out at the Pheasant Memorial Laboratory (PML) for Geochemistry and Cosmochemistry, Institute for Planetary Materials, Okayama University (Nakamura et al. 2003).

4.3.1. Reagents and Materials

Electronic industry (EL) grade 36% HCl (Kanto Chemical Co. Inc.), EL grade 70% HNO₃ (Kanto Chemical Co. Inc.), and guaranteed grade 46% HF (FUJIFILM Wako Pure Chemical Co.) were distilled using a PFA sub-boiling distillation apparatus, and will be referred to as 1D HCl, 1D HNO₃ and 1D HF respectively. Reagents that were further distilled are denoted as 2D. The HCl, HF, and HNO₃ that were used in the ion chromatography procedure were prepared by diluting 1D HCl, 1D HF, and 1D HNO₃ with water ($\geq 18.2 \text{ M}\Omega$

cm) prepared by a Milli-Q system (Merck Millipore, France). Guaranteed grade oxalic acid dihydrate (Fujifilm Wako Pure Chemical Co.) was diluted to make 0.05 mol L⁻¹ oxalic acid solution. The 30% H₂O₂ (Kanto Chemical Co. Inc.) was used as it is. Cation exchange resin (AG50W-X8 200-400 mesh, Bio-Rad, USA) was pre-washed several times with water and 6 mol L⁻¹ HCl and stored.

For method validation, several geological reference materials that contain ~2 to 4000 µg g⁻¹ Cr were analyzed. These included dunite [JP-1 (GSJ) and DTS-1 (USGS)], harzburgite [PCC-1 (USGS) and MUH-1 (IAG)], serpentinite [UB-N (ANRT)], komatiitic basalt [OKUM (IAG)], basalt [BHVO-2 (USGS) and BCR-2 (USGS)], andesite [AGV-2 (USGS), JA-2 (GSJ)], rhyolite [RGM-1 (USGS)], syenite [STM-1 (USGS)], stream sediment [JSd-1 (GSJ)], and dolomite [JDo-1 (GSJ)].

A double spike method using a ⁵⁰Cr-⁵⁴Cr enriched double spike (hereafter described as a double spike or DS) was applied to correct mass bias during sample preparation and mass spectrometry (Ellis, Johnson, and Bullen 2002). The double spike was prepared by dissolving ⁵⁰Cr-enriched (97.4 ± 0.2 mol %) and ⁵⁴Cr-enriched (95.5 ± 0.1 mol %) metal powders purchased from ISOFLEX USA Inc. The mixing ratio of the ⁵⁰Cr- and the ⁵⁴Cr-enriched spike was optimized using MATLAB code in the double-spike toolbox (Rudge, Reynolds, and Bourdon 2009). After dissolving and mixing the spikes, the DS was stored in 6 mol L⁻¹ HCl with a Cr mass fraction of ~1000 µg g⁻¹. For routine analysis, the DS was diluted to ~4 µg g⁻¹ with 6 mol L⁻¹ HCl. The mass fraction of Cr in the DS was calibrated using Cr standard solution (Kanto Chemical, Japan) and a value of 3.77 ± 0.01 µg g⁻¹ (N = 18, 2SD) was determined.

The Nb-H₃PO₄ activator used in this study was prepared by modifying the Nb₂O₅-H₃PO₄ activator described elsewhere (Li et al. 2016a). In this study, a Nb₂O₅ suspension (Li et al. 2016b) was not used. Instead, Nb₂O₅ was dissolved in the solution added to the TIMS filament, to minimize Nb heterogeneity on the filament. The activator was prepared by dissolving Nb₂O₅ (Kanto Chemical., high purity grade, >99.95%) in HF-HNO₃-H₃PO₄ solution, to give 1 wt.% of Nb in 0.5 mol L⁻¹ HNO₃-0.5 mol L⁻¹ HF-0.4 mol L⁻¹ H₃PO₄. The ionization efficiency and stability did not change significantly when the Nb/Cr mass ratio was between 3 and 10. Thus, Nb/Cr was fixed at ~5 for routine measurement.

4.3.2. Sample Preparation

After weighing the powdered samples in the PFA vials (Savillex, USA), a 1:1 mixture of 2D HNO₃ and 2D HF was added with or without a DS. Ultramafic to andesitic samples were

first digested by agitating in an ultrasonic bath for 6 hours, then heated on a hot plate at 195 °C for 4 days. Felsic and sediment samples were digested by agitating in an ultrasonic bath for 4 days, then heated on a hotplate at 120°C for 6 hours. The reason for following a different digestion method for the felsic and sediment samples is to minimize the formation of insoluble Al-fluoride at high temperatures (Takei et al. 2001). The digested samples were evaporated to dryness at 120 °C, and subjected to repeated acid dissolution with 1 ml of 1D HCl. After drying, aqua regia was added to the sample, the mixture heated at 170°C for 2 days and subsequently evaporated to dryness.

For the JDo-1 (dolomite), Cr isotopic compositions were determined for both the bulk sample and the leachate solution after HCl dissolution. For the bulk measurement, the weighed sample in a 7 ml PFA vial was wetted with H₂O, and a DS was added. Then 6 mol L⁻¹ HCl was added, and the loosely capped vial was left at room temperature for 1 hour to enable degassing. Then the sample was digested at 120 °C for 2 days and then evaporated to dryness. Subsequently, to decompose the organic matter, 2 ml of 30% H₂O₂ was added to the sample and kept in the ultrasonic bath for 15 hours, before being evaporated to dryness. Aqua regia was then added to the sample and heated at 170 °C for 2 days and evaporated to dryness. The digestion method for the leachate of JDo-1 was similar to that performed elsewhere (Li et al. 2017). The sample was leached with 0.4 mol L⁻¹ HCl while agitating. Then the sample was centrifuged for 10 minutes at 4000 rpm. The DS was mixed with the supernatant solution, heated at 120°C for >6 hours, before being evaporated to dryness.

All the digested samples were diluted with 0.5 mol L⁻¹ HNO₃ and then an aliquot was taken and placed in another vial for Cr separation. For the unspiked samples, the DS was mixed with the aliquot of the sample solution, heated to equilibrium, and then slowly evaporated to dryness at 90 °C.

4.3.3. Chemical Separation

Chemical separation was carried out in a class 10 clean bench maintained at 24 ± 0.5 °C. A polypropylene column (ID ~ 5 mm h = 50 mm) filled with 1 ml of AG50W-X8 cation exchange resin was used for all the chromatographic separation. The separation procedure is summarized in *Table 13*.

Table 13 - Chromium Separation Procedure

Procedure	Reagent	Volume (mL)
Step 1: Removal of Ca and a majority of Fe		
Resin	AG50W-X8 (200-400 mesh)	1
Cleaning resin	3 mol L ⁻¹ HNO ₃	8
	6 mol L ⁻¹ HCl	8
	H ₂ O	8
Conditioning	10.5 mol L ⁻¹ HCl	1.5
Sample Loading	10.5 mol L ⁻¹ HCl	0.5
Cr Fraction	10.5 mol L ⁻¹ HCl	2.3
Ca Fraction	5 mol L ⁻¹ HNO ₃	4
Step 02: Removal of Al, V, Ti, and residual Fe		
Resin	AG50W-X8 (200-400 mesh)	1
Cleaning resin	3 mol L ⁻¹ HNO ₃	8
	6 mol L ⁻¹ HCl	8
	H ₂ O	8
Conditioning	0.5 mol L ⁻¹ HNO ₃	4
Sample Loading	0.1 mol L ⁻¹ HNO ₃	1
Fe, Al, V, Ti Fraction	1 mol L ⁻¹ HF	12
Cr fraction	10.5 mol L ⁻¹ HCl	4
	4 mol L ⁻¹ HCl	2
Step 03: Removal of Na, Mg, Al, Mn, K, and Ni		
Resin	AG50W-X8 (200-400 mesh)	1
Cleaning resin	3 mol L ⁻¹ HNO ₃	8
	6 mol L ⁻¹ HCl	8
	H ₂ O	16
Conditioning	0.05 mol L ⁻¹ Oxalic acid	1
<u>Sample Loading</u>	0.05 mol L ⁻¹ Oxalic acid	3
Remaining Cr fraction	0.5 mol L ⁻¹ HCl	2

The aim of the first ion exchange step (Step 1) was to separate Ca and Fe from Cr. A sample aliquot containing 100-300 ng of Cr in 0.5 ml of 10.5 mol L⁻¹ HCl was preheated at 120 °C for 30 minutes. After cooling down the sample solution to room temperature, it was loaded onto the resin. Chromium was immediately collected with an additional 2.3 ml of 10.5 mol L⁻¹ HCl, then dried at 120 °C. If it was necessary to collect Ca, then this undertaken by adding 4 ml of 5 mol L⁻¹ HNO₃.

The second ion exchange step (Step 2) aimed to separate Al, V, Ti, and residual Fe from Cr. The Cr fraction separated by Step 1 was dissolved in 1 ml of 0.1 mol L⁻¹ HNO₃, heated at 120 °C for 2 hours and then cooled to room temperature. After loading the sample solution onto the resin, V, Ti, and the residual Fe were washed out with 1 mol L⁻¹ HF. Note that care was taken to ensure that adding HF did not disturb the resin (see discussion). If it was difficult to introduce the whole sample to the column due to stickiness, then 0.2 ml of 0.5 mol L⁻¹ HF was added to the remaining sample and loaded onto the column (see discussion below). Subsequently, the Cr fraction was collected with 10.5 mol L⁻¹ and 4 mol L⁻¹ HCl, then evaporated to dryness at 120 °C.

The third ion exchange step (Step 3) aimed to separate Na, Mg, Al, Mn, K, and Ni from Cr. The Cr fraction separated by Step 2 was dissolved in 3 ml of 0.05 mol L⁻¹ H₂C₂O₄ solution and heated for 1 hour at 120 °C. The sample solution was immediately cooled down by immersing in a water bath for 15 minutes and then loaded onto the resin. Chromium was immediately collected with an additional 2 ml of 0.5 mol L⁻¹ HCl. The Cr fraction was evaporated to dryness at 80 °C and then the oxalates were oxidized using concentrated HNO₃ at 150 °C. To further decompose any organic matter, 300 μL of 30% H₂O₂ was added to the Cr fraction and the mixture was heated at 70 °C for 1 hour. The Cr fraction was then heated with 0.1 ml of 9 mol L⁻¹ HCl and evaporated to dryness at 120 °C. Finally, the Cr fraction was dissolved in 9 mol L⁻¹ HCl.

4.3.4. Mass Spectrometry

The measurement of Cr isotopes was performed by TIMS (Thermo TRITON Plus) using a single W filament geometry. Before sample loading, W filament (Nilaco, 0.0254 mm thickness × 0.762 mm width × 16 mm length) was degassed *in vacuo* for 30 minutes at 5.4 A. A polypropylene dam was applied to the filament before loading the sample. The Cr fraction dissolved in 9 mol L⁻¹ HCl was loaded onto the W filament with the activator and dried at 1.2 A. After drying, the filament was heated for 5 s, with the filament emitting a dull red glow

during this time. After installing the filaments in the TIMS, the filaments were preheated at 2.35 A for 10 min. The Cr isotope measurement was carried out in the static multicollection mode using seven Faraday cups equipped with $10^{11}\Omega$ feedback resistors: $^{49}\text{Ti}^+$ [L3], $^{50}\text{Cr}^+$ [L2], $^{51}\text{V}^+$ [L1], $^{52}\text{Cr}^+$ [C], $^{53}\text{Cr}^+$ [H1], $^{54}\text{Cr}^+$ [H2], and $^{56}\text{Fe}^+$ [H4]. The $^{49}\text{Ti}^+$, $^{51}\text{V}^+$, and $^{56}\text{Fe}^+$ intensities were monitored to calibrate the potential isobaric interferences of $^{50}\text{Ti}^+$ and $^{50}\text{V}^+$ on $^{50}\text{Cr}^+$ and $^{54}\text{Fe}^+$ on $^{54}\text{Cr}^+$. For the interference correction, the IUPAC values of $^{50}\text{Ti}/^{49}\text{Ti} = 0.95859$, $^{50}\text{V}/^{51}\text{V} = 0.002503$, and $^{54}\text{Fe}/^{56}\text{Fe} = 0.063703$ were used. The gain calibration was performed once a day at the beginning of each analytical session.

The Cr isotopic ratio was determined using two methods: the normal ionization mass spectrometry (normal-TIMS) method, operated at constant heating, and the total evaporation (TE-TIMS) method. For the normal TIMS method and TE-TIMS, 0.5 – 1 μg and 0.01 – 0.03 μg of Cr were loaded onto each filament, respectively.

The normal-TIMS method was performed as follows. The filament was first heated at 2.5 A for 5 minutes and then to 1285 $^{\circ}\text{C}$ at a rate of 10 mA min^{-1} . Typically, the beam intensities for $^{52}\text{Cr}^+$ in NIST SRM 979 were ~ 10 , 7, and 3 V for 1.0, 0.5, and 0.1 μg Cr, respectively. In contrast, the typical beam intensity of $^{52}\text{Cr}^+$, for 0.5-1 μg Cr extracted from geological samples, was 1 - 7 V. For each analysis, 20 blocks of 22 to 30 cycles were acquired with an integration time of 8 s, using amplifier rotation. In each block, a baseline measurement of 120 seconds was taken. Peak centering, filament focus, and lens focus were performed every seven blocks. Total acquisition time was ~ 2 hours. During the measurement, the inter-block filament current adjustment kept the $^{52}\text{Cr}^+$ signal between 80 - 200 % of the initial value. In general, inter-block operation was not performed for 0.5 to 1 μg Cr in NIST SRM 979 and 1 μg Cr in a given geological sample, but was operated for Cr abundances lower than these values.

The TE-TIMS method performed in this study was modified after (Van Kooten et al. 2016). The baseline measurement was performed for five minutes before each run. The current through the filament was increased to 2.35 A at a rate of 470 mA min^{-1} and then increased further until a temperature of 900 $^{\circ}\text{C}$ was reached at a rate of 40 mA min^{-1} and subsequently until a temperature of 1000 $^{\circ}\text{C}$ was achieved at a rate of 20 mA min^{-1} . Finally, the filament was heated through increasing the current at a rate of 50 mA min^{-1} and the acquisition of isotope measurements began when the ^{52}Cr beam current reached ~ 0.1 V. Isotope measurements were acquired through a heat slope of 8 mA s^{-1} , a maximum current of 10 V for $^{52}\text{Cr}^+$, an integration time of one second, with $^{52}\text{Cr}^+ > 2$ V as the threshold for data reduction. The interference

correction was performed for data obtained in each cycle. The total acquisition time was <15 minutes.

For the measurement of unspiked NIST SRM 979, the $^{53}\text{Cr}/^{52}\text{Cr}$ and $^{54}\text{Cr}/^{52}\text{Cr}$ during the measurements were corrected by a normalization value of $^{50}\text{Cr}/^{52}\text{Cr} = 0.051859$ (Shields et al. 1966) using the exponential law. The data reduction for the double spike methods was performed by the Newton-Raphson iteration method as described elsewhere (Albarède and Beard 2004). The mass-dependent fractionation that occurred in the natural system, during ion exchange chromatography and within the mass spectrometer was corrected using the exponential law. The mass-dependent Cr isotopic composition was expressed in the δ notation where the $^{53}\text{Cr}/^{52}\text{Cr}$ was made relative to the certified Cr isotope standard, NIST SRM 979 (Ball and Bassett 2000):

$$\delta^{53}\text{Cr} = \left[\frac{(^{53}\text{Cr}/^{52}\text{Cr})_{\text{sample}}}{(^{53}\text{Cr}/^{52}\text{Cr})_{\text{SRM 979}}} - 1 \right] \times 10^3.$$

4.4. Results and Discussion

4.4.1. Chemical Separation

Step 1 of the ion exchange separation procedure achieved the removal of Ca. It is important to remove Ca from the sample matrix in Step 1, because the presence of Ca can lead to the formation of fluoride and oxalate complexes in the subsequent steps and thus block the resin. However, the complete removal of Fe during Step 1 depends on the Fe concentration in the sample.

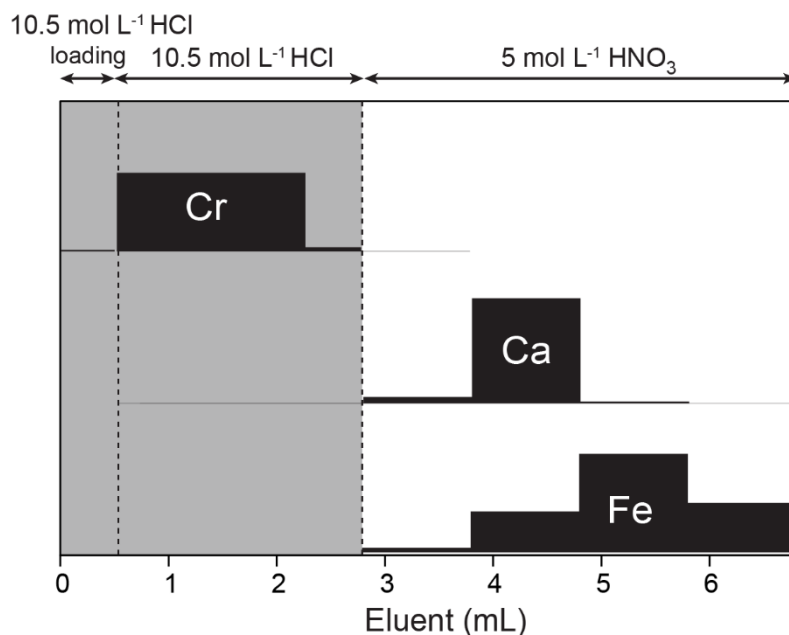


Figure 22 - Elution profile for Cr separation in step 1. All the elution curves were constructed using a multi-element standard solution having 1 $\mu\text{g g}^{-1}$ of each element. The Cr fraction collected is shown in gray.

It was necessary to use 10.5 mol L⁻¹ HCl as the loading solution solvent in Step 1, because of the low distribution coefficients (K_d) between AG50W-X8 and Cr(III) species in high-molarity HCl solutions (Nelson et al. 1964). Immediate elution of Cr soon after loading to the resin can be explained by the presence of neutral $\text{Cr}(\text{H}_2\text{O})_3\text{Cl}_3$ species (Collins et al. 1997) and/or the low K_d for the dechlorinated species (e.g. CrCl_2^+ , CrCl^{2+}) (Larsen et al. 2016). The Ca and a majority of the Fe will be retained in the resin due to the high K_d of the species formed from these elements in concentrated HCl (Nelson et al. 1964).

In Step 2 of the ion exchange separation procedure, the isobarically interfering elements, V, Ti, and the remaining Fe were removed from the Cr cut. Vanadium and Ti in the sample solution were in the +IV oxidation state prior to Step 2. It was noticed that the sample became partially insoluble in 0.1 mol L⁻¹ HNO₃, when it contained a considerable amount of Ti. Therefore, after carefully loading the supernatant sample solution onto the column, 0.2 ml of 0.5 mol L⁻¹ HF was added to the residue to produce Ti-fluoro-complex and these were then loaded onto the column, after the previously loaded solution had passed through the column.

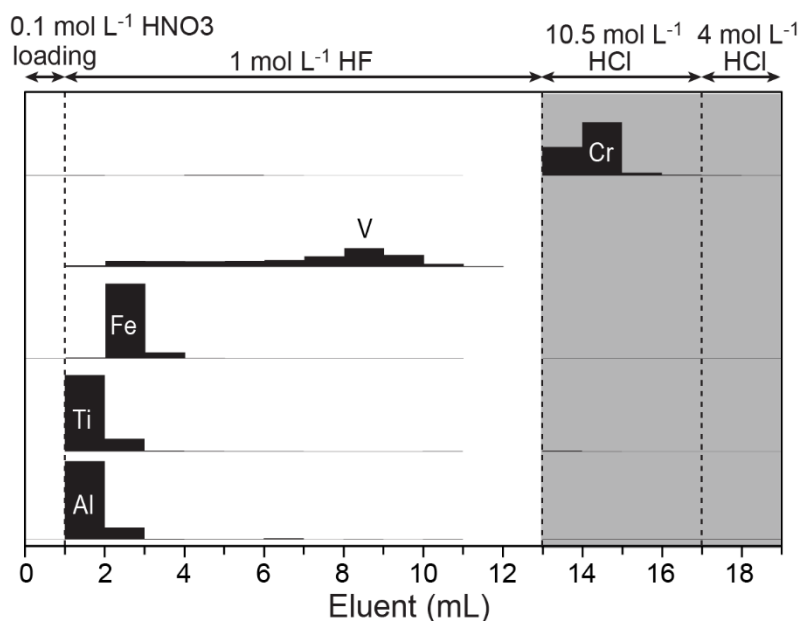


Figure 23 - Elution profile for step 2. The Cr fraction collected is shown in gray.

According to speciation modelling, HCrO_4^- and H_2CrO_4 should be the predominant species in diluted HNO_3 solutions at 120 °C (Larsen et al. 2016) and hence they should be eluted immediately after loading. However, Cr was not observed in the first elution fraction, implying that Cr was adsorbed onto the resin as $\text{Cr}(\text{H}_2\text{O})_6^{3+}$ owing to its' high K_d in cation exchange resin in HNO_3 media (Strelow et al. 1965). The Cr was left in the resin with the addition of HF, because Ti, V, Fe, and Al all have a high affinity to form fluorocomplexes (Brown 1964). This phenomenon is similar to that described during the first step of Ni separation reported by (Ratnayake et al. 2021). Here, with the addition of concentrated HCl, Cr was eluted along with the Na, Mg, K and Ni.

Meanwhile during Step 3, it was possible to separate Cr from group 1 and 2 elements and Ni. The oxalic acid used in Step 3 served as a reducing and chelating agent for Cr, promoting the formation of anionic Cr oxalate complexes (Krishnamurthy and Harris 1961). Heating the sample solution for 1 hour and immediately cooling it before loading was necessary to eliminate the formation of the $\text{Cr}(\text{C}_2\text{O}_4)^+$, which has a higher stability constant at lower temperatures (Krishnamurthy and Harris 1961). While the cationic oxalate complexes of the group 1 and group 2 elements remained adsorbed onto the resin, the anionic Cr oxalate complexes ($\text{Cr}(\text{C}_2\text{O}_4)_2^-$, $\text{Cr}(\text{C}_2\text{O}_4)_3^{3-}$, etc.) were eluted soon after loading. The addition of a further 2 ml of 0.5 mol L⁻¹ HCl enabled the recovery of any $\text{Cr}(\text{C}_2\text{O}_4)^+$ that may have formed.

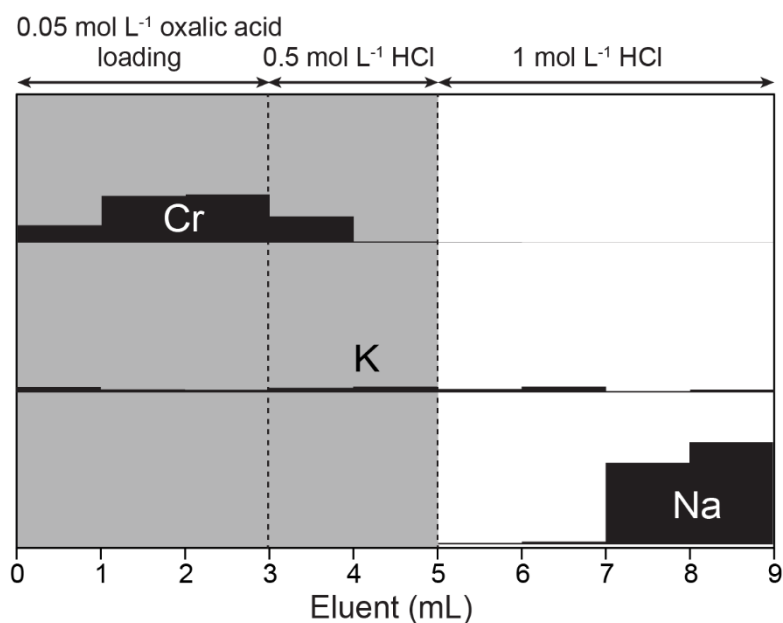


Figure 24 - Elution Profile for step 3. The Cr fraction collected is shown in gray.

4.4.2. Recovery yields and procedural blanks

The Cr recoveries for the analyzed reference materials were 90% for JP1 (peridotite), 90% for BCR-2 (basalt), 91% for AGV-2 (andesite), 99% for SCO-1 (shale), 90% for JSd-1 (sediment), 91% for STM-1 (syenite) and 99% for RGM-1 (rhyolite), with a mean value of $93 \pm 8 \%$ (2SD, $N = 7$). These results imply that the recovery is not dependent on the matrix composition. The total procedural blank for this method from sample decomposition to chemical separation was 0.17 ± 0.30 ng (2SD, $N = 3$). The blank contribution for the sample solution was $<0.2\%$ of the Cr in the sample, which is negligible for Cr isotope measurements.

4.4.3. The analytical precision of Cr isotope measurements of an un-spiked standard

The Cr isotopic compositions of the DS were determined by analyzing the NIST SRM 979, the DS, and mixtures of NIST SRM 979 and the DS. All analyses were performed by both the normal-TIMS and TE-TIMS methods, and the data was evaluated by comparing both datasets measured during the same analytical duration. The instrumental fractionation during the Cr isotope measurement followed a relationship that was in between the Rayleigh and exponential fractionation laws. When using the normal-TIMS method, the relationship was closer to the Rayleigh law, but when using the TE-TIMS method, it was closer to the exponential law (Figure 25) Since the analytical development of the TE-TIMS method is one of the main focuses of this study, the exponential law was used for the correction of instrumental fractionation for both methods. The measured $^{53}\text{Cr}/^{52}\text{Cr}$ and $^{54}\text{Cr}/^{52}\text{Cr}$ values of the NIST SRM 979 were 0.1134494 ± 0.0000023 and 0.0282068 ± 0.0000012 ($N=7$, 2SD),

respectively, by the normal-TIMS method and 0.1134502 ± 0.0000030 and 0.0282071 ± 0.0000015 ($N = 11$, 2SD), respectively, by the TE-TIMS method. The values obtained from both methods are within analytical uncertainty of each other. The average value, $^{53}\text{Cr}/^{52}\text{Cr} = 0.1134497$ and $^{54}\text{Cr}/^{52}\text{Cr} = 0.0282070$, were used for the determination of the $\delta^{53}\text{Cr}$ value of the spiked samples. The TE-TIMS method uses 20 ng of Cr for each analysis of NIST SRM 979 and the corresponding external precision of $^{53}\text{Cr}/^{52}\text{Cr}$ was six times better than that of the normal-TIMS method measured using the same amount of sample (Li et al. 2016).

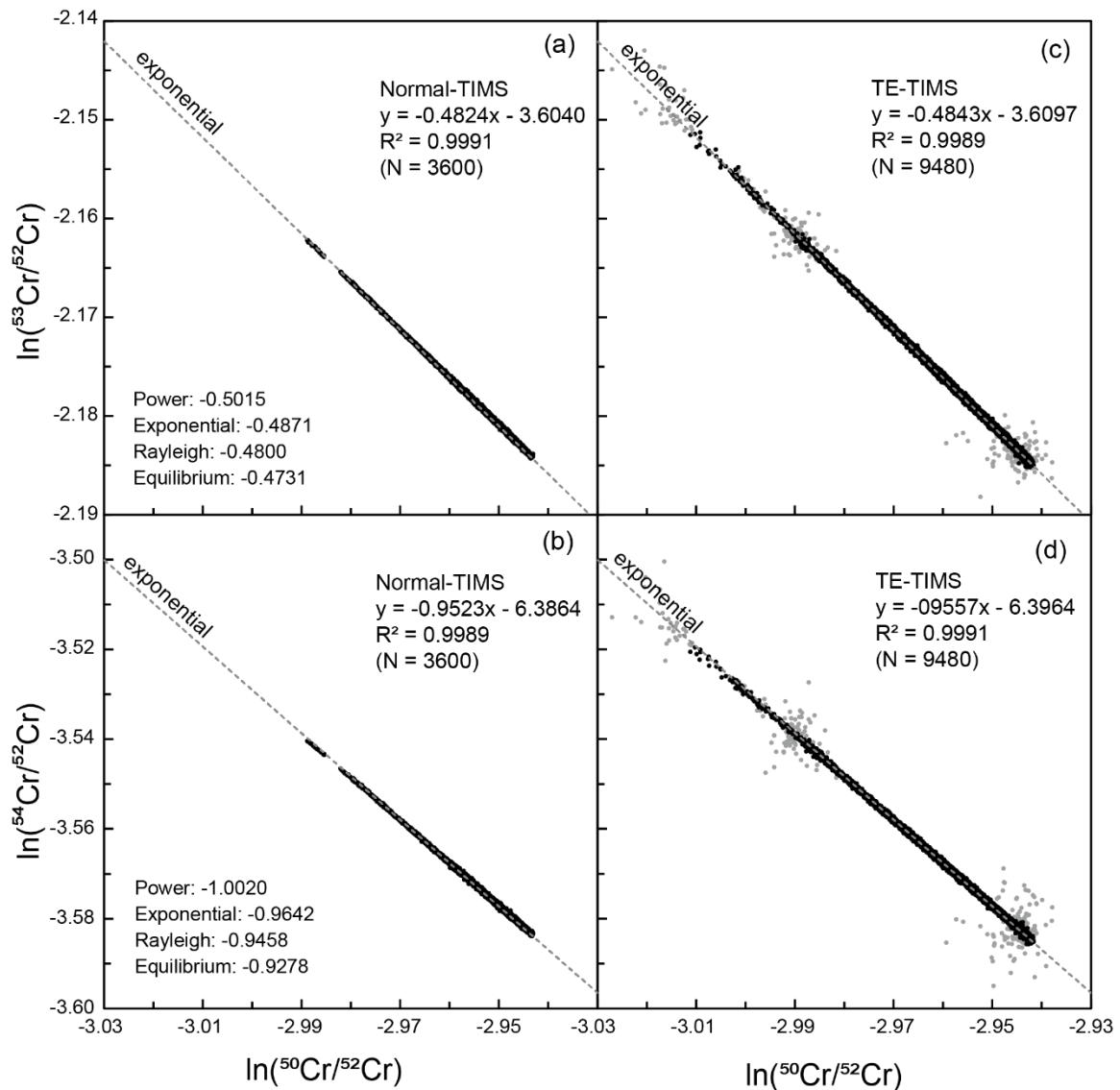


Figure 25 - Raw data of NIST SRM 979 measured by the normal-TIMS and TE-TIMS method. (a) $\ln(^{50}\text{Cr}/^{52}\text{Cr})$ vs. $\ln(^{53}\text{Cr}/^{52}\text{Cr})$ and (b) $\ln(^{50}\text{Cr}/^{52}\text{Cr})$ vs. $\ln(^{54}\text{Cr}/^{52}\text{Cr})$ of the raw data of NIST SRM 979 measured by the normal-TIMS method (6 fractions, $N = 3600$). (c) $\ln(^{50}\text{Cr}/^{52}\text{Cr})$ vs. $\ln(^{53}\text{Cr}/^{52}\text{Cr})$ and (d) $\ln(^{50}\text{Cr}/^{52}\text{Cr})$ vs. $\ln(^{54}\text{Cr}/^{52}\text{Cr})$ of the raw data of NIST SRM 979 measured by the TE-TIMS method (6 fractions, $N = 9480$). Black and gray circles in (c) and (d) are data with $^{52}\text{Cr} > 2 \times 10^{-11}$ and $^{52}\text{Cr} < 2 \times 10^{-11}$, respectively. All data were measured using $1 \mu\text{g}$ and $0.02 \mu\text{g}$ of Cr for normal-TIMS and TE-TIMS methods, respectively. The gray-colored broken lines represent the exponential fractionation lines, included for reference.

4.4.4. Double spike calibration

For the determination of the isotopic ratio of DS, the measured $^{50}\text{Cr}/^{52}\text{Cr}$, $^{53}\text{Cr}/^{52}\text{Cr}$, and $^{54}\text{Cr}/^{52}\text{Cr}$ of the DS was tentatively normalized to the $^{50}\text{Cr}/^{54}\text{Cr}$ value of the DS that was gravimetrically obtained. Then, the true $^{50}\text{Cr}/^{54}\text{Cr}$ for the DS was optimized by measuring the DS – NIST SRM 979 mixture prepared with the optimized mixing ratio. Note that the optimized proportion of the DS in the DS – NIST 979 mixture was 0.268, and the actual proportions for the experiment were between 0.245 and 0.301. The isotopic ratios of the DS were determined by both the normal-TIMS (N=13) and TE-TIMS (N=13) methods as $^{50}\text{Cr}/^{52}\text{Cr} = 42.0457 \pm 0.0015$, $^{53}\text{Cr}/^{52}\text{Cr} = 1.552452 \pm 0.000087$, and $^{54}\text{Cr}/^{52}\text{Cr} = 31.0256 \pm 0.0012$ (N = 26, 2SD), respectively.

To assess the reliability of the isotopic compositions of the DS, the $\delta^{53}\text{Cr}$ value of the NIST SRM 979 were measured by varying the mixing ratios of the DS – NIST SRM 979 mixture (Figure 26). The measured $\delta^{53}\text{Cr}$ values of the NIST SRM 979 were -0.002 ± 0.009 (N=26) and 0.000 ± 0.021 (N=36) for the normal-TIMS and TE-TIMS methods, respectively. The results confirmed that the DS was calibrated correctly. The 2SD external precision of 21 ppm for determining the $\delta^{53}\text{Cr}$ value, using a few tens of ng of Cr, obtained in this study is better than for any previous studies.

In addition, the $\delta^{53}\text{Cr}$ value of NIST SRM 3112a was measured by both the normal-TIMS and TE-TIMS methods, and resulted in values within the analytical uncertainty of each other: -0.106 ± 0.016 (1 μg Cr, N = 10, 2SD) and -0.103 ± 0.019 (20 ng Cr, N = 5, 2SD), respectively. The external precision of the $\delta^{53}\text{Cr}$ value of NIST SRM 3112a measured in this study is better than that measured in previous studies except for one study (-0.079 ± 0.018), which used 50 – 600 ng Cr (Scheiderich et al. 2015). The $\delta^{53}\text{Cr}$ values of NIST SRM 3112a measured in this study are within the 2SD analytical uncertainty of the previously reported values, but have the lowest mean values. The reason for our values being lower than other data is not apparent.

All of the $\delta^{53}\text{Cr}$ values obtained do not correlate with the proportion of the DS used in the analyzing fraction for both methods, and the difference of mean values among both methods is only 2 ppm, (figure 26). Thus, it was confirmed that the DS was precisely calibrated.

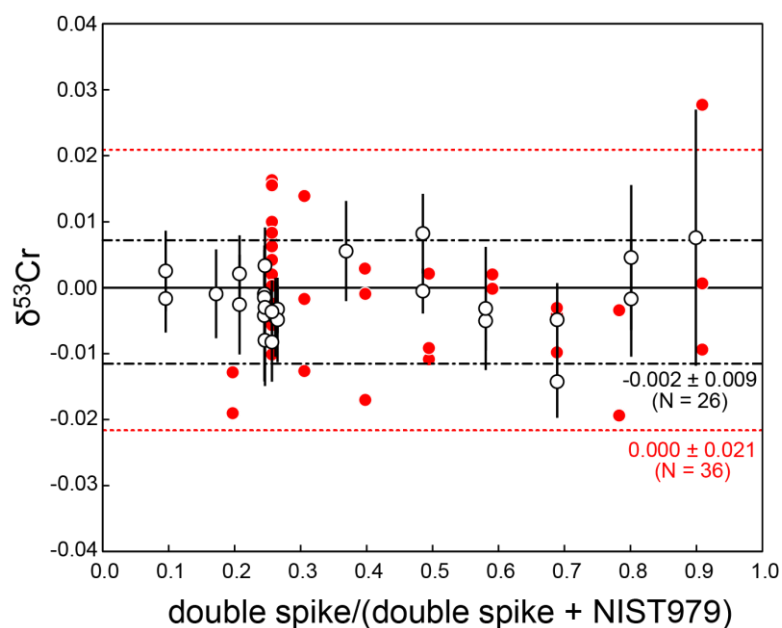


Figure 26 - The $\delta^{53}\text{Cr}$ of the DS – NIST 979 mixture with various ratios of DS and NIST 979. Filled and open circles are data determined by TE- and normal-TIMS methods, respectively. Error bars for the normal-TIMS methods are 2SE internal precision of each run. The 2SD of $\delta^{53}\text{Cr}$ determined by TE- and normal-TIMS methods are shown with red broken and black dash-dot-dash lines.

4.4.5. The effects of isobaric interferences and matrix elements on Cr isotope measurements

$^{50}\text{Ti}^+$, $^{50}\text{V}^+$, and $^{54}\text{Fe}^+$ can isobarically interfere with the measurement of $^{50}\text{Cr}^+$ and $^{54}\text{Cr}^+$ signals and can also inhibit the emission of Cr from the filament (C. Y. Liu et al. 2019a). Other matrix elements, such as K, Na, Ca, and Mg, were also reported to have the potential to suppress the Cr ionization from the filament (Liu et al. 2019). Therefore, the abundances of impurities in the purified Cr cuts from various matrices were analyzed by the triple quadrupole (TQ) ICP-MS (Table 14).

Table 14 - Impurities in the Cr fraction after column chromatography

Sample	Element/Cr after purification (mol ratio)							
	Na/Cr	Mg/Cr	K/Cr	Ca/Cr	Al/Cr	Fe/Cr	Ti/Cr	V/Cr
JP-1	0.8	0.1	0.7	0.4	0.1	0.6	0.1	0.0
BCR-2	1.9	0.1	1.0	0.8	0.0	0.1	1.5	0.1
JA-2	1.5	0.1	0.8	0.9	0.0	0.0	0.1	0.0
JSd-1	0.3	0.0	0.1	0.1	0.0	0.0	0.1	0.0
STM-1	2.3	0.2	0.7	0.8	0.0	0.2	0.1	0.2

The proportions of Fe/Cr, Ti/Cr and V/Cr in the Cr cut were nearly proportional to those ratios in the initial sample. Although 4 % of Fe remained in the Cr cut of the JP-1, >99.98% of Fe, >99.0% of Ti, and >98.5% of V were eliminated from the Cr cut for the other samples. The proportions of the interfering elements determined above have little effect on Cr isotope analysis, as shown below.

In the normal-TIMS method, the intensities of $^{50}\text{Ti}^+$ and $^{50}\text{V}^+$, which interfere with $^{50}\text{Cr}^+$, were not detected in all analyses. On the other hand, the interference of $^{54}\text{Fe}^+$ on $^{54}\text{Cr}^+$ was observed during the measurement of all geological samples. The proportion of $^{54}\text{Fe}^+$ contributing to the intensity of $m/z = 54$ was highest early in the data acquisition, ranging from 3 to 160 ppm in most of the samples. However, it decreased with time, reaching < 3 ppm within 100 to 200 scans (i.e., 5 to 10 blocks) and then maintained <2 ppm until the end. Exceptionally, one of the AGV-2 samples gave an extremely high intensity of $^{56}\text{Fe}^+$, which corresponded to a proportion of 4300 ppm $^{54}\text{Fe}^+$ contributing to the $m/z = 54$, and it took 11 blocks to reach < 3ppm (Figure 27). Such a high amount of Fe in the purified Cr cut was due to the excessive amount of sample loaded onto the column, which was resolved in later measurements by adjusting the amount of sample loaded. However, even under such a high interference of Fe, there was no difference in $\delta^{53}\text{Cr}$ values among the blocks, revealing that the $^{54}\text{Fe}^+$ isobaric correction was adequately applied (Figure 27)

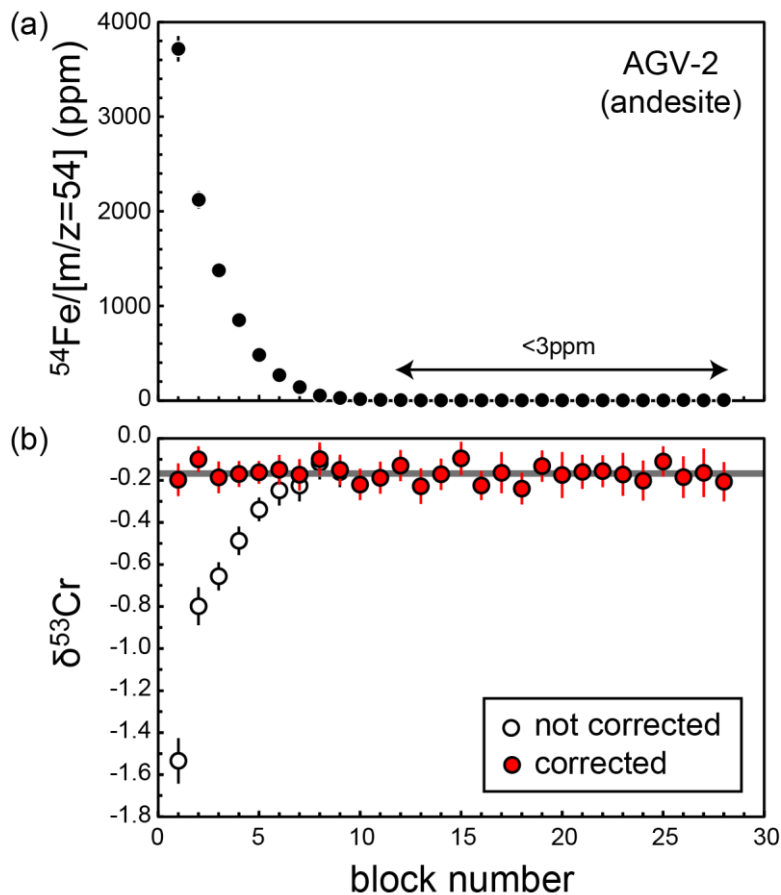


Figure 27 - (a) The proportion of ^{54}Fe in the $m/z=54$ during the measurement of the AGV-2, which has the highest degree of Fe interference in this study. (b) The $\delta^{53}\text{Cr}$ values of AGV-2 in each block. The gray line is the average value of all blocks. Error bars are 2SE of each block.

In the TE-TIMS method, the interference of $^{54}\text{Fe}^+$ on $^{54}\text{Cr}^+$ was observed for all geological samples. Ionization of Fe began to increase and reached to its maximum value at around 1270 to 1320 °C and then start to decrease (Figure 28). Above the threshold ($^{52}\text{Cr}^+ > 2\text{V}$), the proportion of the total $^{54}\text{Fe}^+$ intensity contributing to $m/z = 54$ was < 25 ppm for most of the samples. Exceptionally, the proportion in BCR-2 reached up to 40 ppm. This may be attributed to the fact that, among the samples measured, the highest amount of Fe present in the solution loaded onto the ion-exchange resin was in BCR-2. Based on Figure 28, the proportion of 40 ppm is small enough for the determination of Cr isotopic ratios, but in reality, the proportion varied during the measurement and reached the order of 10^3 ppm during the early cycles of the measurement (Figure 27). However, the corrected Cr isotope ratios did not deviate from the exponential law (Figure 28) even with this degree of Fe interference. Thus, the Cr isotope data was accurately determined even when the Fe interference was observed during the measurement by the TE-TIMS method.

In the TE-TIMS method, $^{51}\text{V}^+$ was not detected until the filament temperature reached around 1360 - 1420°C, after which the intensity increased with increasing filament temperature (Figure 28). In most samples, $^{49}\text{Ti}^+$ was not detected. In cases where it was detected, the ionization behavior of $^{49}\text{Ti}^+$ was similar to that of $^{51}\text{V}^+$. Above the threshold (i.e., $^{52}\text{Cr}^+ > 2\text{V}$) the proportion of the total $^{50}\text{V}^+ + ^{50}\text{Ti}^+$ contributing to the total intensity of $m/z = 50$ was 0.3 ± 0.9 ppm (2SD) and the highest value was 5 ppm observed in BCR-2. These values were negligible for the determination of precise Cr isotope compositions.

Consequently, the influence of the interfering elements for Cr isotope measurement by both the normal-TIMS and TE-TIMS methods was negligible after the Cr extraction method employed and the interference correction applied in this study. Li et al. (Li et al. 2016) mentioned that using the Nb-H₃PO₄ activator over the traditional silica-gel-based activator caused a quicker reduction of Fe ions during the Cr isotope measurement. Even though Li et al. (Li et al. 2016) insisted that this phenomenon was due to the effectiveness of the Nb-H₃PO₄-based activator to suppress the ionization of Fe during Cr ionization, this study reveals that ionization of Fe was not suppressed, but instead it was ionized more effectively at a lower temperature relative to Cr. As a result, most of the Fe on the filament was ionized a lower ionization temperature, leaving Cr behind to be ionized and measured later at a higher temperature.

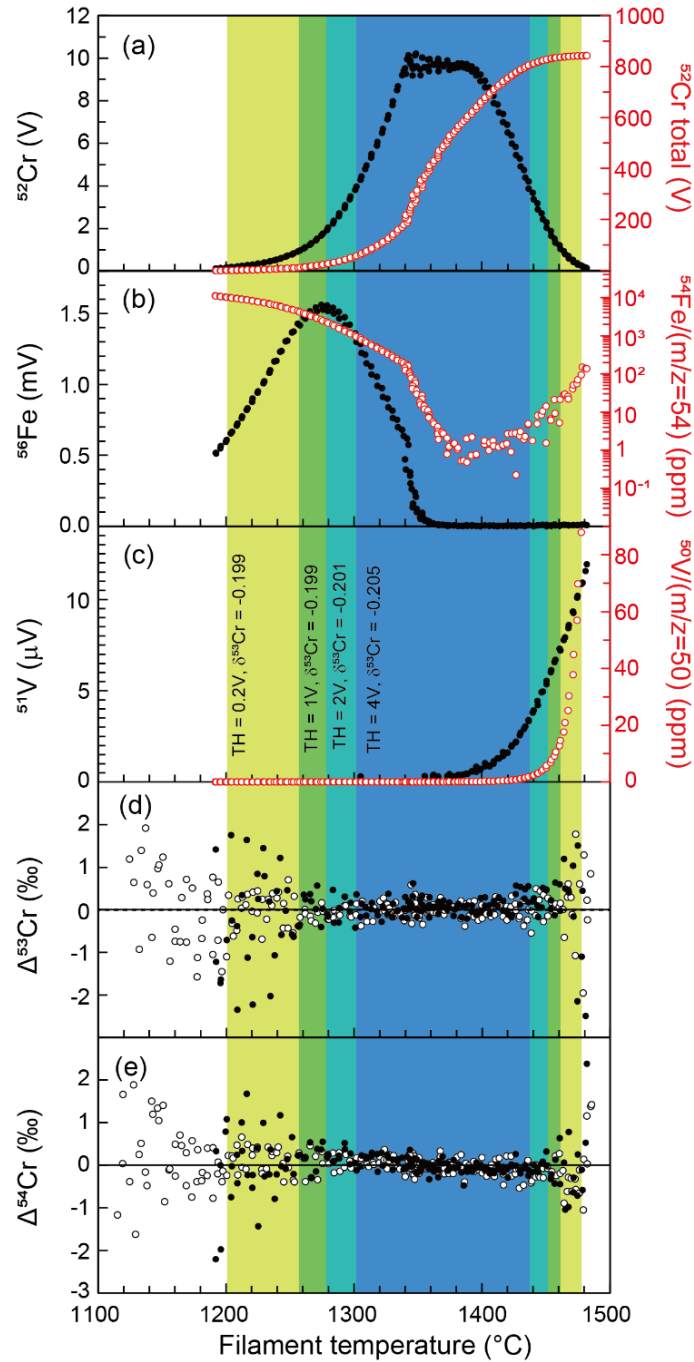


Figure 28 - An example of the data profile against the filament temperature during the measurement of geological sample measured by the TE-TIMS method. The selected sample is one of the BCR-2 which has the highest proportion both for Fe and V interference relative to Cr during this study. (a) the intensity of ^{52}Cr of each cycle (closed black) and total cycles (open red), (b) the intensity of ^{56}Fe (closed black) and the proportion of ^{54}Fe in the intensity of $m/z = 54$ for each cycle (open red), (c) the intensity of ^{51}V (closed black) and the proportion of ^{50}V in the intensity of $m/z = 50$ for each cycle (open red), (d) $\Delta^{53}\text{Cr}$ value [difference of $\ln(^{53}\text{Cr}/^{52}\text{Cr})$ value from the exponential fractionation line between $(^{50}\text{Cr}/^{52}\text{Cr})$ vs. $\ln(^{53}\text{Cr}/^{52}\text{Cr})$] (closed black), and (e) $\Delta^{54}\text{Cr}$ value [difference of $\ln(^{54}\text{Cr}/^{52}\text{Cr})$ value from the exponential fractionation line between $(^{50}\text{Cr}/^{52}\text{Cr})$ vs. $\ln(^{54}\text{Cr}/^{52}\text{Cr})$] (closed black). Open circles in (d) and (e) are $\Delta^{53}\text{Cr}$ and $\Delta^{54}\text{Cr}$ values of spiked NIST SRM 979 measured on the same day of the geological sample. The colored ranges indicate the different threshold (TH), $^{52}\text{Cr}=0.2, 1, 2,$ and 4 V, and the $\delta^{53}\text{Cr}$ values calculated in each TH were shown.

4.4.6. Blank contribution

The loading Cr blank was prepared for measurement by the DS-TE-TIMS method through mixing 4 ng of the DS with an activator containing 5 μg and 0.1 μg of Nb. This was equivalent to analyzing 1 μg and 0.02 μg of Cr during routine analysis. The loading blank yielded 16 ± 4 and 1.1 ± 0.6 pg, respectively. These values were < 55 ppm of the total amount of Cr loaded, which was negligible. The total procedural blank from the sample decomposition to the purification was 0.17 ± 0.30 ng (2SD, N = 3), which represented $< 0.2\%$ of Cr in the Cr cut in general, which was negligible.

4.4.7. Cr isotope variation in geological reference materials

The $\delta^{53}\text{Cr}$ value of geological samples were measured by both the normal-TIMS and TE-TIMS methods for six samples (JP1, UB-N, OKUM, BHVO-2, AGV-2, and JSd-1). The $\delta^{53}\text{Cr}$ values of these geological samples measured by both methods agree within 2SD uncertainty, as does NIST SRM 3112a (Figure 29). For the other eight samples, the $\delta^{53}\text{Cr}$ values were measured using the TE-TIMS method. Two or three individual sample batches were dissolved and measured for each sample. Except for JA-2, no heterogeneity in the $\delta^{53}\text{Cr}$ values, which exceeded the analytical uncertainty, was observed among the different fractions (heterogeneity of JA-2 will be discussed later). The $\delta^{53}\text{Cr}$ values for PCC-1, BHVO-2, BCR-2, and the JDo-1-leachate measured in this study were within the range of the previously reported values, although our values are relatively low compared to previous studies (Figure 29). However, for DTS-1, MUH-1, OKUM, and AGV-2, the $\delta^{53}\text{Cr}$ values in this study were lower than previous studies (Liu et al. 2019; Shi et al. 2021; Zhu et al. 2018; Zhu et al. 2021). Values from previous studies for the other samples (NIST SRM 3112a, JP-1, BHVO-2, BCR-2, and the JDo-1-leachate) measured simultaneously with DTS-1, MUH-1, OKUM, and/or AGV-2 (C. Y. Liu et al. 2019; Shi et al. 2021; Zhu et al. 2018; Zhu et al. 2021) agree with our data within the analytical uncertainty, although all but the JDo-1-leachate show systematically higher values compared to our values. Therefore, the distinct $\delta^{53}\text{Cr}$ values in DTS-1, MUH-1, OKUM, and AGV-2 in this study from those of previous datasets may be due to Cr isotopic heterogeneity among the sample bottles. However, as our data implies, there is no predominant heterogeneity within the same bottle.

The amounts of the JA-2 fraction digested were 119.3, 8.5, and 16.3 mg. There is a significant difference in $\delta^{53}\text{Cr}$ values, 0.12, between the latter two. Whereas, the values using larger sample volumes (119.3 mg) are intermediate between these values. Such an observation,

indicates that Cr isotopic heterogeneity exists among the minerals in JA-2. JA-2 is a Setouchi high-Mg andesite, and most of the Cr reservoirs in the Setouchi High-Mg andesite collected from areas close to the JA-2 collection site are Cr-rich spinel (Tatsumi and Ishizaka 1982). The Setouchi High-Mg andesite contains two types of spinels with different origins (Tatsumi et al. 2002), suggesting that these could have different $\delta^{53}\text{Cr}$ values. Further studies are necessary to verify this interpretation, but this method, which allows highly accurate Cr isotopic analysis with small amounts of Cr, is an effective tool for clarifying this hypothesis.

The $\delta^{53}\text{Cr}$ values show a systematic variation with their Cr mass fractions when comparing the ultramafic rocks, basalts, and andesites. The Cr content in these samples is positively correlated with Mg and indicates the degree of melt depletion and fractional crystallization in the case of peridotite and volcanic rocks, respectively. The more melt-depleted JP-1 and DTS-1 tend to show lower $\delta^{53}\text{Cr}$ values than the more fertile UB-N and MUH-1. From the fertile peridotite to komatiitic basalt, basalt, and andesite, the $\delta^{53}\text{Cr}$ values tend to decrease. During the partial melting of peridotite, the $\delta^{53}\text{Cr}$ values in the residue should get higher because lighter Cr is preferentially fractionated to the melt (Gall et al. 2017). By the crystal fractionation of the mantle-derived magma, the $\delta^{53}\text{Cr}$ values of residual melt should get lower because heavier Cr preferentially fractionates into the Cr^{3+} -rich phase (e.g. spinel and clinopyroxene) (Shen et al. 2020). Thus, the decreasing $\delta^{53}\text{Cr}$ values from lherzolite to andesite are consistent with the trend of partial melting of peridotite and fractional crystallization processes.

However, lower $\delta^{53}\text{Cr}$ values in the melt-depleted peridotite than the fertile peridotite cannot be explained simply by a partial melting process. The rare earth elements (REE) in these depleted peridotites (PCC-1, JP-1 and DTS-1) show light REE-enrichment relative to middle-REE (Makishima and Nakamura 1997), suggesting that these samples could have been metasomatized by a rock-melt interaction process. Thus, the Cr isotopic ratios of these depleted peridotites may have been affected not only by partial melting but also by metasomatism (Xia et al. 2017). The higher $\delta^{53}\text{Cr}$ values for felsic rocks (RGM-1 and STM-1) compared to basalts and andesites support the idea that these rocks were not simply formed by fractional crystallization of mantle-derived magma, but could have also been affected by partial melting of crustal materials.

For the JDo-1 sample, only the supernatant solution leached with hydrochloric acid was used to measure the Cr isotopic composition in previous studies (Figure 29). However, in this

study, both the bulk sample and the acid-leached supernatant solution were measured. The data reveals that carbonate minerals and silicate/oxide minerals in JDo-1 have different $\delta^{53}\text{Cr}$ values.

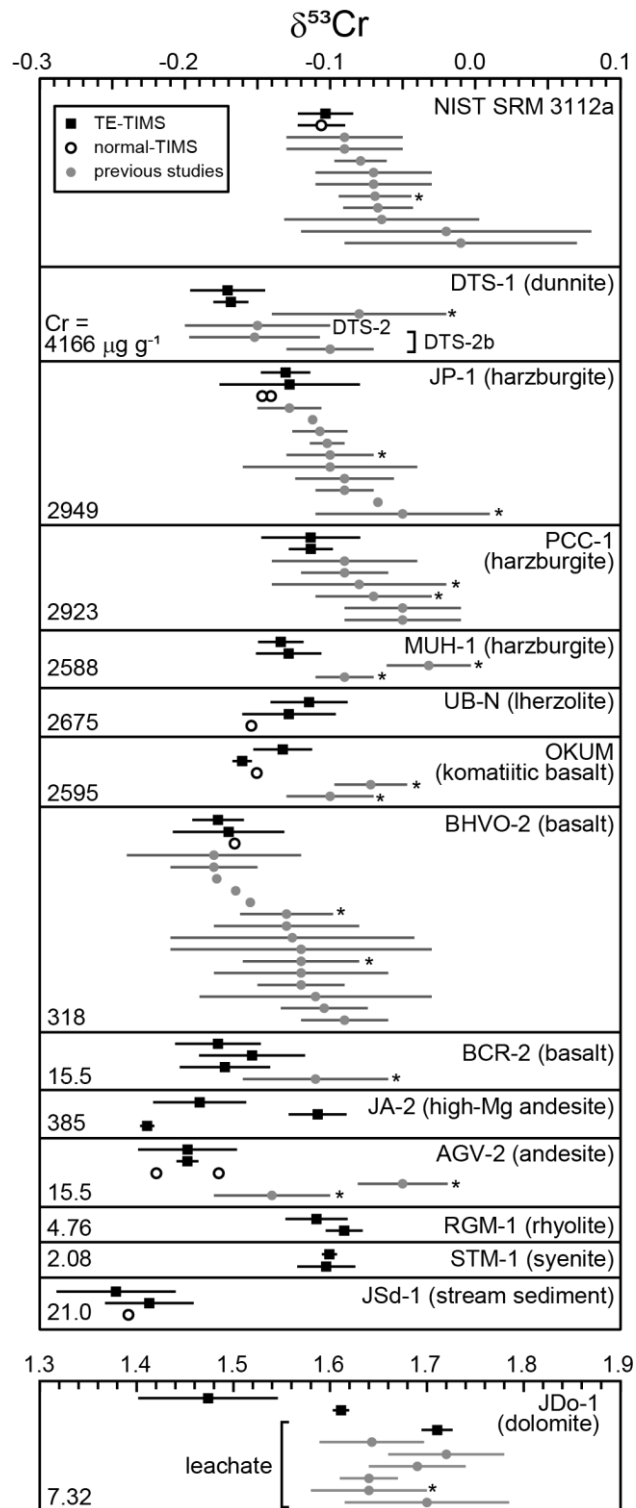


Figure 29 - The $\delta^{53}\text{Cr}$ values of the reference materials. Error bars are 2SD external precision when it is presented. The plot without error bar indicates the single data. The data with an asterisk for the reference values are from (C. Y. Liu et al. 2019b; Shi et al. 2021; J. M. Zhu et al. 2018b; K. Zhu et al. 2021) (see in detail in the main text).

Table 15 - The $\delta^{53}\text{Cr}$ values and mass fraction of Cr in reference materials

Sample name	Sample type ¹	TE-TIMS					Normal-TIMS	
		$\delta^{53}\text{Cr}$	2SD ²	N	Cr ($\mu\text{g g}^{-1}$)	2SD ²	$\delta^{53}\text{Cr}$	2SE ³
DTS-1	Dunite	-0.171	0.026	5	NA			
	[49.6]	-0.168	0.012	4	4166	14		
	mean	-0.169	(0.002)					
JP-1	Dunite	-0.131	0.017	5	NA		-0.144	(0.006)
	[44.7]	-0.128	0.048	3	2949	3.0	(-0.141 \pm 0.006,	
	mean	-0.129	(0.003)				-0.147 \pm 0.007)	
PCC-1	Harzburgite	-0.113	0.034	7	NA			
	[41.7]	-0.113	0.015	4	2923	4		
	mean	-0.113	(0.000)					
MUH-1	Harzburgite	-0.134	0.016	7	NA			
	[40.4]	-0.129	0.023	3	2588	6.2		
	mean	-0.131	(0.005)					
UB-N	lherzolite	-0.114	0.027	5	NA		-0.154	0.007
	[35.2]	-0.128	0.032	5	2675	24		
	mean	-0.121	(0.014)					
OKUM	Komatiitic basalt	-0.133	0.020	5	NA		-0.150	0.006
	[21.3]	-0.161	0.007	3	2595	6.8		
	mean	-0.147	(0.028)					
BHVO-2	Basalt	-0.177	0.018	5	NA		-0.166	0.007
	[7.3]	-0.170	0.038	3	318.0	1.0		
	mean	-0.174	(0.007)					
BCR-2	Basalt	-0.177	0.029	7	NA			
	[3.6]	-0.154	0.037	4	15.52	0.04		
		-0.172	0.031	3	15.52	0.10		
	mean	-0.168	0.025		15.52	(0.00)		
JA-2	High Mg andesite	-0.190	0.032	4	NA			
	[7.7]	-0.109	0.020	3	383.2	1.2		
		-0.226	0.005	3	386.9	0.5		
	mean	-0.175	0.120		385.0	(3.7)		
AGV-2	Andesite	-0.198	0.034	7	15.41	0.04	-0.198	(0.043)
	[1.8]	-0.198	0.008	3	15.61	0.10	(-0.220 \pm 0.013,	
	mean	-0.198	(0.000)		15.51	(0.20)	-0.177 \pm 0.018)	
RGM-1	Rhyolite	-0.109	0.021	3	4.720	0.010		
	[0.3]	-0.090	0.013	3	4.791	0.005		
	mean	-0.100	(0.019)		4.755			
STM-1	Syenite	-0.100	0.005	3	2.076	0.003		
	[0.1]	-0.103	(0.020)	2	2.249	0.002		
	mean	-0.102	0.002		2.163			

JSD-1	Stream sediment	-0.247	0.041	6	22.46	0.07	-0.239	0.008
		-0.225	0.031	3	19.60	0.04		
		-0.236	(0.023)		21.03	(2.87)		
JDo-1	Dolomite	1.474	0.072	4	7.877	0.017		
		1.611	0.009	3	6.759	0.006		
		mean	1.543	(0.138)		7.32	1.12	
JDo-1 (leachate)	Dolomite leachate	1.711	(0.016)	2	NA			
NIST NBS3112a	Standard solution	-0.103	0.019	5	NA		-0.106	0.016*
								(*2SD, N=10)

1: Numbers in brackets are mass fraction of MgO in wt.%. 2: data in parentheses are difference of the duplicated data. 3: 2 standard error of internal precision. Data in parentheses are difference of the duplicated data. NA: not analyzed.

4.5. Conclusions

A three step Cr separation procedure, which is applicable for a wide array of sample matrices ranging from ultramafic to felsic lithologies, was developed in this study. The method is devoid of extensive sample pretreatment procedures, including the use of oxidizing and reducing reagents, which are time-consuming and adversely affect isotope measurements. To measure the Cr isotopes, we have developed the DS-TE-TIMS procedure. This method reduced the amount of Cr required for the analysis to ~20 ng per an analysis and shortened the acquisition time to <15 minutes, while maintaining the same analytical precision as conventionally applied TIMS methods. Thus, the methods developed in this study enabled high-precision Cr isotope analysis in geological samples with various matrix and Cr compositions using relatively small sample volumes.

Credit author statement –

- Dilan M. Ratnayake (*Conceptualization, Methodology, Investigation, Writing original Draft*)
- Ryoji Tanaka (*Methodology, Investigation, Writing original Draft, Writing – Review & Editing, Supervision, Resources*)
- Eizo Nakamura (*Supervision*)

4.6. References

Ball, J. W., & Bassett, R. L. (2000). Ion exchange separation of chromium from natural water matrix for stable isotope mass spectrometric analysis. *Chemical Geology*, 168(1–2), 123–134. [https://doi.org/10.1016/S0009-2541\(00\)00189-3](https://doi.org/10.1016/S0009-2541(00)00189-3)

- Brown, R. B. (1964). *The effect of hydrofluoric acid on the cation exchange behavior of metal ions*.
- Collins, C. H., Pezzin, S. H., Rivera, J. F. L., Bonato, P. S., Windmüller, C. C., Archundia, C., & Collins, K. E. (1997). Liquid chromatographic separation of aqueous species of Cr(VI) and Cr(III). *Journal of Chromatography A*, 789(1–2), 469–478.
[https://doi.org/10.1016/S0021-9673\(97\)00676-6](https://doi.org/10.1016/S0021-9673(97)00676-6)
- De Laeter, J. R., Böhlke, J. K., De Bièvre, P., Hidaka, H., Peiser, H. S., Rosman, K. J. R., & Taylor, P. D. P. (2003). Atomic weights of the elements: Review 2000 (IUPAC Technical Report). *Pure and Applied Chemistry*, 75(6), 683–800.
<https://doi.org/10.1351/pac200375060683>
- Ellis, A. S., Johnson, T. M., & Bullen, T. D. (2002). Chromium isotopes and the fate of hexavalent chromium in the environment. *Science*, 295(5562), 2060–2062.
<https://doi.org/10.1126/science.1068368>
- Frei, R., Gaucher, C., Poulton, S. W., & Canfield, D. E. (2009). Fluctuations in Precambrian atmospheric oxygenation recorded by chromium isotopes. *Nature*, 461(7261), 250–253. <https://doi.org/10.1038/nature08266>
- Gall, L., Williams, H. M., Halliday, A. N., & Kerr, A. C. (2017). Nickel isotopic composition of the mantle. *Geochimica et Cosmochimica Acta*, 199, 196–209.
<https://doi.org/10.1016/j.gca.2016.11.016>
- Halicz, L., Yang, L., Teplyakov, N., Burg, A., Sturgeon, R., & Kolodny, Y. (2008). High precision determination of chromium isotope ratios in geological samples by MC-ICP-MS. *Journal of Analytical Atomic Spectrometry*, 23(12), 1622–1627.
<https://doi.org/10.1039/b808351g>
- Hibiya, Y., Iizuka, T., Yamashita, K., Yoneda, S., & Yamakawa, A. (2019). Sequential Chemical Separation of Cr and Ti from a Single Digest for High-Precision Isotope Measurements of Planetary Materials. *Geostandards and Geoanalytical Research*, 43(1), 133–145. <https://doi.org/10.1111/ggr.12249>
- Isotopes, N., Albarède, F., & Beard, B. (2004). *Analytical Methods for Non-Traditional Isotopes*. 55, 113–152.
- Krishnamurty, K. V., & Harris, G. M. (1961). The chemistry of the metal oxalato complexes.

Chemical Reviews, 61(3), 213–246. <https://doi.org/10.1021/cr60211a001>

- Larsen, K. K., Wielandt, D., Schiller, M., & Bizzarro, M. (2016). Chromatographic speciation of Cr(III)-species, inter-species equilibrium isotope fractionation and improved chemical purification strategies for high-precision isotope analysis. *Journal of Chromatography A*, 1443, 162–174. <https://doi.org/10.1016/j.chroma.2016.03.040>
- Li, C. F., Feng, L. J., Wang, X. C., Chu, Z. Y., Guo, J. H., & Wilde, S. A. (2016). Precise measurement of Cr isotope ratios using a highly sensitive Nb₂O₅ emitter by thermal ionization mass spectrometry and an improved procedure for separating Cr from geological materials. *Journal of Analytical Atomic Spectrometry*, 31(12), 2375–2383. <https://doi.org/10.1039/c6ja00265j>
- Li, C. F., Feng, L. J., Wang, X. C., Wilde, S. A., Chu, Z. Y., & Guo, J. H. (2017). A low-blank two-column chromatography separation strategy based on a KMnO₄ oxidizing reagent for Cr isotope determination in micro-silicate samples by thermal ionization mass spectrometry. *Journal of Analytical Atomic Spectrometry*, 32(10), 1938–1945. <https://doi.org/10.1039/c7ja00225d>
- Liu, C. Y., Xu, L. J., Liu, C. T., Liu, J., Qin, L. P., Zhang, Z. Da, ... Li, S. G. (2019). High-Precision Measurement of Stable Cr Isotopes in Geological Reference Materials by a Double-Spike TIMS Method. *Geostandards and Geoanalytical Research*, 43(4), 647–661. <https://doi.org/10.1111/ggr.12283>
- Lugmair, G. W., & Shukolyukov, A. (1998). Early solar system timescales according to ⁵³Mn-⁵³Cr systematics. *Geochimica et Cosmochimica Acta*, 62(16), 2863–2886. [https://doi.org/10.1016/S0016-7037\(98\)00189-6](https://doi.org/10.1016/S0016-7037(98)00189-6)
- Makishima, A., & Nakamura, E. (1997). Suppression of matrix effects in ICP-MS by high power operation of ICP: Application to precise determination of Rb, Sr, Y, Cs, Ba, REE, Pb, Th and U at ng g⁻¹ levels in milligram silicate samples. *Geostandards Newsletter*, 21(2), 307–319. <https://doi.org/10.1111/j.1751-908X.1997.tb00678.x>
- Nakamura, E., Kobayashi, K., Tanaka, R., Kunihiro, T., Kitagawa, H., Potiszil, C., ... Tsuda, Y. (2022). On the origin and evolution of the asteroid Ryugu: A comprehensive geochemical perspective. *Proceedings of the Japan Academy Series B: Physical and Biological Sciences*, 98(6), 227–282. <https://doi.org/10.2183/PJAB.98.015>

- Nakamura, E., Makishima, A., Moriguti, T., Kobayashi, K., Sakaguchi, C., Yokoyama, T., ... Takei, H. (2003). Comprehensive geochemical analyses of small amounts (< 100 mg) of extraterrestrial samples for the analytical competition related to the sample return mission MUSES-C. *The Institute of Space and Astronautical Science Report. S.P. : The First Open Competition for the MUSES-C Asteroidal Sample Preliminary Examination Team*, (16), 49–101. Retrieved from <http://ci.nii.ac.jp/naid/120006834538/en/>
- Nelson, F., Murase, T., & Kraus, K. A. (1964). Ion exchange procedures. I. Cation exchange in concentration HCl and HClO₄ solutions. *Journal of Chromatography A*, 13(C), 503–535. [https://doi.org/10.1016/s0021-9673\(01\)95146-5](https://doi.org/10.1016/s0021-9673(01)95146-5)
- Qin, L., Rumble, D., Alexander, C. M. O. D., Carlson, R. W., Jenniskens, P., & Shaddad, M. H. (2010). The chromium isotopic composition of Almahata Sitta. *Meteoritics and Planetary Science*, 45(10–11), 1771–1777. <https://doi.org/10.1111/j.1945-5100.2010.01109.x>
- Qin, L., & Wang, X. (2017). Chromium isotope geochemistry. *Non-Traditional Stable Isotopes*, 82(Vi), 379–414. <https://doi.org/10.2138/rmg.2017.82.10>
- Ratnayake, D. M., Tanaka, R., & Nakamura, E. (2021). Novel nickel isolation procedure for a wide range of sample matrices without using dimethylglyoxime for isotope measurements using MC-ICP-MS. *Analytica Chimica Acta*, 1181. <https://doi.org/10.1016/j.aca.2021.338934>
- Rosman, K. J. R., & Taylor, P. D. P. (1998). Isotopic compositions of the elements 1997 (Technical Report). *Pure and Applied Chemistry*, 70(1), 217–235. <https://doi.org/10.1351/pac199870010217>
- Rudge, J. F., Reynolds, B. C., & Bourdon, B. (2009). The double spike toolbox. *Chemical Geology*, 265(3–4), 420–431. <https://doi.org/10.1016/j.chemgeo.2009.05.010>
- Scheiderich, K., Amini, M., Holmden, C., & Francois, R. (2015). Global variability of chromium isotopes in seawater demonstrated by Pacific, Atlantic, and Arctic Ocean samples. *Earth and Planetary Science Letters*, 423(2015), 87–97. <https://doi.org/10.1016/j.epsl.2015.04.030>
- Schiller, M., Van Kooten, E., Holst, J. C., Olsen, M. B., & Bizzarro, M. (2014). Precise

- measurement of chromium isotopes by MC-ICPMS. *Journal of Analytical Atomic Spectrometry*, 29(8), 1406–1416. <https://doi.org/10.1039/c4ja00018h>
- Shen, J., Xia, J., Qin, L., Carlson, R. W., Huang, S., Helz, R. T., & Mock, T. D. (2020). Stable chromium isotope fractionation during magmatic differentiation: Insights from Hawaiian basalts and implications for planetary redox conditions. *Geochimica et Cosmochimica Acta*, 278, 289–304. <https://doi.org/10.1016/j.gca.2019.10.003>
- Shi, K., Wu, G., Zhu, J. M., & Wang, X. (2021). Accurate measurement of chromium isotopic compositions in geological reference materials by double-spike mc-icp-ms. *Atomic Spectroscopy*, 42(3), 128–133. <https://doi.org/10.46770/AS.2021.008>
- Shields, W. R., Murphy, T. J., Catanzaro, E. J., & Garner, E. L. (1966). Absolute isotopic abundance ratios and the atomic weight of a reference sample of chromium. *Journal of Research of the National Bureau of Standards Section A: Physics and Chemistry*, 70A(2), 193. <https://doi.org/10.6028/jres.070a.016>
- Sossi, P. A., Moynier, F., & Van Zuilen, K. (2018). Volatile loss following cooling and accretion of the Moon revealed by chromium isotopes. *Proceedings of the National Academy of Sciences of the United States of America*, 115(43), 10920–10925. <https://doi.org/10.1073/pnas.1809060115>
- Strelow, F. W. E., Rethemeyer, R., & Bothma, C. J. C. (1965). Ion Exchange Selectivity Scales for Cations in Nitric Acid and Sulfuric Acid Media with a Sulfonated Polystyrene Resin. *Analytical Chemistry*, 37(1), 106–111. <https://doi.org/10.1021/ac60220a027>
- Takei, H., Yokoyama, T., Makishima, A., & Nakamura, E. (2001). Formation and suppression of AlF₃ during HF digestion of rock samples in Teflon bomb for precise trace element analyses by ICP-MS and ID-TIMS. *Proceedings of the Japan Academy Series B: Physical and Biological Sciences*, 77(1), 13–17. <https://doi.org/10.2183/pjab.77.13>
- Tatsumi, Y., Nakashima, T., & Tamura, Y. (2002). The petrology and geochemistry of calc-alkaline andesites on Shodo-Shima Island, SW Japan. *Journal of Petrology*, 43(1), 3–16. <https://doi.org/10.1093/petrology/43.1.3>
- Tatsumi, Yoshiyuki, & Ishizaka, K. (1982). Origin of high-magnesian andesites in the

- Setouchi volcanic belt, southwest Japan, I. Petrographical and chemical characteristics. *Earth and Planetary Science Letters*, 60(2), 293–304.
[https://doi.org/10.1016/0012-821X\(82\)90008-5](https://doi.org/10.1016/0012-821X(82)90008-5)
- Trinquier, A., Birck, J. L., Allègre, C. J., Göpel, C., & Ulfbeck, D. (2008). ^{53}Mn - ^{53}Cr systematics of the early Solar System revisited. *Geochimica et Cosmochimica Acta*, 72(20), 5146–5163. <https://doi.org/10.1016/j.gca.2008.03.023>
- Van Kooten, E. M. M. E., Wielandt, D., Schiller, M., Nagashima, K., Thomen, A., Larsen, K. K., ... Bizzarro, M. (2016). Isotopic evidence for primordial molecular cloud material in metal-rich carbonaceous chondrites. *Proceedings of the National Academy of Sciences of the United States of America*, 113(8), 2011–2016.
<https://doi.org/10.1073/pnas.1518183113>
- Wang, X., & Johnson, T. M. (2021). Factors Affecting the Robustness of Data Inversion for Stable Isotope Measurement Using the Double Spike Method: Insights from Chromium Isotope Analysis. *Analytical Chemistry*, 93(20), 7449–7455.
<https://doi.org/10.1021/acs.analchem.1c00434>
- Wei, W., Frei, R., Chen, T. Y., Kläbe, R., Liu, H., Li, D., ... Ling, H. F. (2018). Marine ferromanganese oxide: A potentially important sink of light chromium isotopes? *Chemical Geology*, 495(July), 90–103.
<https://doi.org/10.1016/j.chemgeo.2018.08.006>
- Xia, J., Qin, L., Shen, J., Carlson, R. W., Ionov, D. A., & Mock, T. D. (2017). Chromium isotope heterogeneity in the mantle. *Earth and Planetary Science Letters*, 464, 103–115. <https://doi.org/10.1016/j.epsl.2017.01.045>
- Yamakawa, A., Yamashita, K., Makishima, A., & Nakamura, E. (2010). Chromium isotope systematics of achondrites: Chronology and isotopic heterogeneity of the inner solar system bodies. *Astrophysical Journal*, 720(1), 150–154. <https://doi.org/10.1088/0004-637X/720/1/150>
- Zhang, Q., Amor, K., Galer, S. J. G., Thompson, I., & Porcelli, D. (2018). Variations of stable isotope fractionation during bacterial chromium reduction processes and their implications. *Chemical Geology*, 481(January), 155–164.
<https://doi.org/10.1016/j.chemgeo.2018.02.004>

- Zhu (朱柯), K., Moynier, F., Schiller, M., Alexander, C. M. O. D., Barrat, J. A., Bischoff, A., & Bizzarro, M. (2021). Mass-independent and mass-dependent Cr isotopic composition of the Rumuruti (R) chondrites: Implications for their origin and planet formation. *Geochimica et Cosmochimica Acta*, 293, 598–609.
<https://doi.org/10.1016/j.gca.2020.10.007>
- Zhu, J. M., Wu, G., Wang, X., Han, G., & Zhang, L. (2018). An improved method of Cr purification for high precision measurement of Cr isotopes by double spike MC-ICP-MS. *Journal of Analytical Atomic Spectrometry*, 33(5), 809–821.
<https://doi.org/10.1039/c8ja00033f>
- Zhu, K., Moynier, F., Alexander, C. M. O., Davidson, J., Schrader, D. L., Zhu, J.-M., ... Becker, H. (2021). Chromium Stable Isotope Panorama of Chondrites and Implications for Earth Early Accretion. *The Astrophysical Journal*, 923(1), 94.
<https://doi.org/10.3847/1538-4357/ac2570>

Chapter 5: Obtaining accurate isotopic fractionation data from cells: the basics

5.1. Introduction

The cyanobacterial population in the marine photic zone is contributing 17% of the net marine primary productivity (Flombaum et al. 2013) and it has been estimated that their population in the photic zone varies from $10^4 - 10^5$ cells mL^{-1} (Bishop et al. 2019 and references therein). Therefore, cyanobacteria play a major role regarding trace metal cycling in their habitats through various biogeochemical processes, such as (see (Bishop et al. 2019 for a review) :

1. Generating reactive organic ligands on cell walls that adsorb metal/nonmetal ions from growth media.
2. Generating extra-cellular ligands to alter trace metal bio-availability.
3. Assimilating for enzymatic use.
4. Producing dissolved organic matter upon cell lysis which adsorbs trace elements.

Bacterial surfaces have many kinds of ligands such as carboxyl, hydroxyl, phosphoryl and amino groups, and these can protonate and deprotonate depending on pH conditions in the growth medium (Liu et al. 2015). These ligands are capable of binding metals when they are deprotonated and they also serve as sites for nucleation of authigenic mineral phases (Konhauser et al. 1998). Therefore, precipitation of secondary minerals (e.g. iron oxyhydroxides, sulfides) on bacterial surfaces is a common process in nature as well as in laboratory grown bacterial cultures. Precipitation of these minerals on cells can create additional adsorption surfaces, such that trace metals can adsorb onto and coprecipitate with these phases (Bishop et al. 2019; Tang and Morel 2006; Tovar-Sanchez et al. 2003). These processes may alter the bio-availability of trace metals in the experimental growth medium and therefore erroneous interpretation can be drawn for the metal utilization and their isotope fractionation in the bacterial cultures.

Trace metals can also isotopically fractionate during the above processes owing to the differences in bond energies associated with bacterial surfaces, ligands and mineral phases (Fujii et al. 2011; Fujii et al. 2011; Kafantaris and Borrok 2014; Lacan et al. 2006; Wasylenki et al. 2015). There is no clear understanding about the fate of these adsorbed elemental fractions and some may eventually release and return to the medium upon bacterial degradation, while some of them may remain. However, in some instances (e.g. rapid silicification, rapid sedimentation) there is a possibility of preserving the adsorbed trace metal component for

longer periods of time. Therefore, variations in isotope compositions and elemental abundance patterns that are observed in samples collected from the preserved bacterial habitats may have resulted from a combination of isotopic and elemental fractionation associated with biotic processes, such as cellular uptake, and abiotic processes like adsorption and mineral precipitation. Thus, determination of biogenicity of such samples is challenging due to the large uncertainty associated with interpretations derived from elemental and isotopic fractionations.

Even though there are experimental studies that have focused on elemental fractionation upon cellular adsorption (Pokrovsky et al. 2008) there is only a limited understanding of the isotope fractionation associated with these processes due to experimental difficulties in differentiating them (Komárek et al. 2022) from the isotope fractionation resulting from intracellular incorporation. Therefore, it is necessary to understand the importance of these abiotic processes by clarifying the direction and magnitude of isotope fractionation associated with each process. This will eventually be helpful for evaluating the isotope signatures used as tracers for paleo-environmental reconstruction and to explore the possibility of using them as a tool for the detection of bio-signatures in the future.

5.1.1. Removal of adsorbed elements from cell surfaces

The majority of ligands affixed to bacterial surfaces deprotonate at higher pH levels and thus protonating those ligands back at low pH may release the adsorbed metals. Therefore, experimental studies have been carried out to remove adsorbed elements from cell surfaces using reagents with low pH (Liu et al., 2015, Bishop et al., 2019). However, the binding constants for the adsorption sites can change depending upon both environmental parameters and the competing metal ion (Borrok et al. 2004). Thus, it is an a priori requirement to determine the magnitude and direction of the isotope fractionation associated with the adsorption of each element of interest. The reagents that are currently being used to wash out adsorbed elements from cultured cells are summarized in Table 16.

Broadly these reagents can be categorized into 4 groups as follows.

1. Solutions having chelation ability
 - a. EDTA
(ethylenediaminetetraacetic acid) or DTPA (diethylenetriaminepentaacetic acid)
 - b. Oxalate solution
2. Solutions with reducing capabilities

- a. Ti(III) citrate
 - b. Stannous solution
3. Solutions capable of donating protons (acids)
 - a. Nitric acid
 - b. Hydrochloric acid
 4. Solutions with mixed properties

Oxalate / EDTA / citrate mixtures

Table 16 - Techniques used for remove the adsorbed components from bacterial cells

Element	Microorganism	Treatment to remove residual media	Assessment of the media removal	Reference
Zn	Bacteria	Washing cells with UV treated Seawater	-	(Köbberich and Vance 2019)
Ni, Cu, Co, Zn	Bacteria	0.56 M NaCl Followed by pH adjustments with HCl	Yes	(Bishop et al. 2019)
Zn	Diatoms	Lowering Fe in growth media to reduce precipitation of Fe hydroxides	-	(Köbberich and Vance 2017)
Zn	Bacteria	0.01 M NaClO ₄ (5 times)	Yes	(Kafantaris and Borrok 2014)
Cu	Bacteria		-	(Navarrete et al. 2011)
Zn	Diatoms	Acetic acid, Hydroxylamine Hydrochloride	-	(Andersen et al. 2011)
Ni	Bacteria	PBS solution	-	(Cameron et al. 2009b)

		Consisted of NaCl, Na ₂ HPO ₄ , KH ₂ PO ₄ , ± KCl		
Cu	Bacteria and diatoms	0.01-0.1 M NaNO ₃	-	(Pokrovsky et al. 2008)

Previous studies have shown that oxalate and EDTA solutions alone, or when used as mixtures, were not effective in removing extracellular iron oxyhydroxides (FeO_x) in the marine diatom *Thalassiosira weissflogii* (Tang and Morel 2006). The use of Ti (III) and stannous (Sn²⁺) containing solutions is hampered by their short shelf life because of their reactivity with oxygen (Tovar-Sanchez et al. 2003). Additionally, there is evidence that Ti (III) citrate solutions could produce cell lysis in phytoplankton (Sunda and Huntsman 1995). Therefore, in this study, Ti (III) and/or citrate containing solutions were not used. The use of HNO₃ acid as a reagent was omitted since a part of this study was carried out for the determination of nitrogen isotope compositions under urea uptake (chapter 6).

Therefore, as a preliminary study, the removal of the adsorbed elements from laboratory grown cyanobacterial cultures were evaluated using HCl and Sn²⁺ solutions. The adsorption onto the precipitated FeO_x was the main focus because of its ubiquitous availability in oxidized environments. The removal of adsorbed elements and their isotopic variation was evaluated by studying the Zn isotopic variation of the treated and untreated cell fractions and results are presented.

5.2. Materials and Reagents

Water used in the experiments were prepared using a Milli-Q system (Merck Millipore, France) and had a conductivity of 18.2 MΩ cm⁻¹. Electronic (EL) grade 36% HCl (Kanto Chemical Co., Inc.) and 70% HNO₃ (Kanto Chemical Co., Inc.) were distilled by PFA sub-boiling distillation apparatus. The distilled reagents are referred as 1D (distillation once) or 2D (distillation twice) prefix before the acid name. Guaranteed grade oxalic acid dihydrate (Fujifilm Wako Pure Chemical Co.) was diluted in water to make the 0.05 mol L⁻¹ oxalic acid solution. The 30 % H₂O₂ (Kanto Chemical Co. Inc.) and HClO₄ (Kanto Chemical Co. Inc.) was used as it is for digesting the cells. Guaranteed grade silicon dioxide (Quartz, Fujifilm Wako Pure Chemical Co.) were used for the preliminary adsorption experiments. Acids used for

removing the adsorbed elements and elution in the ion exchange chromatography were prepared by diluting non-distilled acids with water.

Synechococcus sp. PCC 7002 was purchased from Laboratoire Collection des Cyanobactéries, Institut Pasteur, France. The recipe of culture media used for cell growth is shown in Table 222 in chapter 6. Glassware used for cell growth was pre-cleaned by soaking in a diluted high-purity alkaline detergent (TMSC, Tama Chemicals), 0.5 mol L⁻¹ HNO₃ and 4 mol L⁻¹ HCl for >12h each. After each soaking step, the glassware was rinsed five times with water. Finally, the cleaned glassware was autoclaved.

5.3. Methodology

5.3.1. Experiments for the removal of adsorbed elements on SiO₂ particles

To determine the most effective reagent to wash out the adsorbed metals from the cultured cyanobacterium *Synechococcus sp.* PCC 7002, a preliminary study was carried out by treating the SiO₂ particles that were equilibrated with the growth medium used for cell culture with different reagents. SiO₂ was selected because it does not react with the media and therefore the surface adsorption process can be isolated.

First, SiO₂ particles were added to A+ growth medium and kept in a thermostatic water bath at 38 °C which was shaking at 70 rpm. These conditions were similar to cyanobacterial cell culturing conditions. After 10 days of equilibration, the SiO₂ particles were removed from the medium by centrifugation at 4000 rpm for 10 minutes in a fixed angle centrifuge using Nanosep[®] centrifugal devices (300 K, Pall Co., USA). Then, an aliquot of the filtrate was sampled to analyze the medium composition. The SiO₂ particles retained on the filter were treated with the reagents listed in Table 17 to remove FeO_x precipitated on their surfaces.

The treatment procedure was carried out as follows. First the particles were equilibrated with 0.5 ml of the corresponding reagent for 5 minutes, and then centrifuged at 4000 rpm for 5 minutes to separate and recover the particles again. This treatment was carried out 3 times (indicated as W1, W2, W3) for each of reagent used. Each time an aliquot of the filtrate was sampled for analysis of the trace elements that were removed by desorption from the SiO₂ particles. Finally, the SiO₂ particles were heated with 2D HF at 150 °C, dried and dissolved in 0.5 mol L⁻¹ HNO₃, and the elemental composition was analyzed using a sector field inductive coupled plasma mass spectrometer (ICP-MS).

Table 17 – Reagents used to treat cells and SiO₂ in the experiments carried out in this study

	Experiment A	Experiment B	Experiment C	Experiment D
Reagents	0.5 mmol L ⁻¹ HCl	0.9 mmol L ⁻¹ SnCl ₂	0.5 mmol L ⁻¹ HCl + 0.9 mmol L ⁻¹ SnCl ₂	Water (only for cells)

5.3.2. Experiments for the removal of adsorbed elements on cyanobacterial cells

Subsequently the same experiments were performed using cyanobacterial cells grown in A⁺ liquid media with a U₅N₉₅ (see Table 22 in chapter 6) composition, in order to understand whether the morphological and physical differences between cells and the SiO₂ particles changes the effectiveness of the removal of the adsorbed component.

The Nanosep[®] centrifugal devices (300K, Pall Co. USA) were used to separate the cells from the growth media and from the solutions used for treatments during the experiments (A-C) conducted with the cyanobacterial cells. First an aliquot of the growth medium including cells was centrifuged at 2500 rpm in a fixed angle centrifuge for 10 minutes, and then a 0.2 ml of aliquot of the filtrate was taken into a 7 ml PFA vial (Savillex, USA). The rest of the filtrate was discarded. Then 0.5 ml of appropriate reagent was added to the cells that were retained on the filter unit, gently mixed and kept still for 5 minutes and centrifuged again at 2500 rpm for 10 minutes. This step was repeated twice and each time a 0.2 ml fraction was collected from the filtrate. Finally, cells were transferred to a 7ml PFA vial using water as a carrier, dried at 130 °C for 12 hours and weighed again to obtain the dry weight. Dry weight was calculated as the difference between the weight of the vial with dried cells and the weight of empty vial. The same procedure was followed for different aliquots of cells, replacing the 0.05 mmol L⁻¹ HCl with SnCl₂ and HCl-SnCl₂ mixtures. The collected aliquots from the filtrate in each experiment were dried at 130 °C and dissolved in 0.5 mol L⁻¹ HNO₃. After obtaining the dry weight, the cell fractions were decomposed by heating with 1D HNO₃ at 170 °C for 12 hours. Next, they were evaporated to dryness, heated with HClO₄ at 196 °C, dried, and then dissolved in 0.5 mol L⁻¹ HNO₃.

Similar set of experiments were carried out using cells grown on the same growth media, except that they were not digested in order to observe morphological changes upon the treatment. After each treatment procedure, an aliquot of cells was diluted 10⁶ times with water

and air dried at room temperature for 48 hours. The dried cells were observed through scanning electron microscopy (SEM) to check whether cells were damaged upon the treatment.

Since low pH and oxidizing reactions can damage cyanobacterial cells (David et al. 2005), an additional experiment (D) was carried out to explore whether excess water could be utilized to wash out the adsorbed component. Two cell aliquots from the same growth media (U₅N₅₀) were used in experiment D and they were collected into a pre-cleaned vertical twin membrane centrifugal concentrators (300K, Vivaspin 20, Sartorius, UK). One aliquot was repeatedly (4 times) treated with 5 ml water and the other with 0.5 mmol L⁻¹ HCl. In between the treatment, cells were left still for 5 minutes after mixing with the corresponding reagent, similar to the previous set of experiments. Finally, the cells were collected into a pre-weighed 7 ml PFA vial, dried at 130 °C for 12 hours and weighed again to obtain the dry weight. Then the cells were digested using a similar procedure as mentioned above and element concentrations were measured.

5.3.3. Evaluation of the changes in isotopic composition of cyanobacterial cells upon different treatment procedures.

Cell fractions that were grown on urea- and Ni-containing media were separately treated with 0.5 mmol L⁻¹ HCl and water, three times each, to determine the contribution of the extracellular Zn fraction to the isotopic composition of whole cells, and also to evaluate the varied treatment procedures. The filtrate consisting of desorbed elements was collected into a single container for each reagent. Zn concentration and isotopic composition of the treated cells and filtrate were measured using isotope dilution and the double spike techniques respectively. Removal of matrix elements from Zn was undertaken using ion exchange chromatography described in chapter 2, and isotope measurements were carried out using multi-collector inductively coupled plasma mass spectrometer (Neptune plus, Thermo-Scientific). The conditions used for isotope measurements are listed in Table 18.

Table 18 - Instrument settings used for Zn isotope measurement

Parameter		Setting					
RF Power		1200 W					
Sample Cone		Normal Ni					
Skimmer Cone		X Ni					
Desolvator		Apex IR (Elemental Scientific, USA)					
APEX IR Temperature Configuration		100 °C Heating and -3 °C Cooling					
Nebulizer		Self-Aspirating PFA microflow (Elemental Scientific, USA)					
Aspiration Rate		50 $\mu\text{L min}^{-1}$					
Mass Resolution Power		4000					
Analyte Concentration		100 ng g^{-1}					
Analyte Base		0.5 mol L^{-1} HNO_3					
Number of Blocks		1					
Number of cycles per block		25					
Integration Time		4.194 s					
Idle Time		3.000 s					
Cup	L3	L2	L1	C	H1	H2	H3
Main Configuration	^{63}Cu	^{64}Zn	^{65}Cu	^{66}Zn	^{67}Zn	^{68}Zn	^{70}Zn
Sub Configuration				^{62}Ni			
				^{72}Ge			

5.4. Results

The results for the treatments carried out for SiO₂ particles and cyanobacteria are shown in

Figure 30. Among the metals adsorbed onto SiO₂ particles, Zn and Fe were measured because of their high abundance in phytoplankton including cyanobacteria (Morel et al. 2013) and also in the A+ growth medium. All tested reagents effectively removed the majority of Zn associated with the SiO₂ particles, resulting in only <5% of the Zn remaining after the entire treatment. However, none of the solutions could effectively remove Fe adsorbed/precipitated on the SiO₂ particles, leaving $\geq 56\%$ of Fe retained on the particles. The use of SnCl₂ solution alone removed a maximum amount of Fe (44 %) from the SiO₂ particles whereas only 27% of Fe was removed when the HCl-SnCl₂ solution was used.

Removal of Zn from the cyanobacterial cells using HCl was gradual, as has been observed for SiO₂. However, when using Sn²⁺ solutions, a sudden release of 60 % of the total Zn fraction (i.e. both extracellular and intracellular Zn components) occurred during the second treatment step (W2). This was observed in both instances where Sn was used alone, and in combination with HCl, and thus it cannot be considered as an error associated with the experimental procedure. In addition to the sudden release of Zn, it was observed that the cells were clumped together and turned a yellowish brown colour upon the addition of SnCl₂. Contrastingly, the addition of 0.5 mmol L⁻¹ HCl only resulted in cell clumps without a change of color (Figure 32).

Figure 31 shows the recovery of elements in the digested cell fractions relative to the dry weight of the sample after completion of the treatment procedure with 5 ml water and 0.5 mmol L⁻¹ HCl. Both cell fractions that were utilized were sampled on the same day from the same growth medium, and the intra-cellular metal quota can be considered as constant in both fractions. It was observed that the cells clumped together when 0.5 mmol L⁻¹ HCl was used for the treatment. Once cells were clumped they were strongly attached onto the filter unit and were hard to remove completely. Therefore, recovery of cells was lower in the HCl treated fractions. Despite cell clumping, the metal fraction associated with cells was depleted in the cells treated with 0.5 mmol L⁻¹ HCl compared to the cells that were treated with water (Figure 31).

Table 19 - Removal of Fe and Zn from SiO₂ and Cells upon the use of different reagents to wash out adsorbed components.

Reagent	Element	% of Element fraction			
		Treatment step 1 (W1)	Treatment step 2 (W2)	Treatment step 3 (W3)	SiO ₂
0.5 mmol L ⁻¹ HCl	Fe	4.0	1.0	0.0	94.9
	Zn	64.4	27.4	7.4	64.7
0.9 mmol L ⁻¹ SnCl ₂	Fe	28.5	13.2	2.8	55.6
	Zn	69.9	23.8	4.6	1.6
0.9 mmol L ⁻¹ SnCl ₂ + 0.5 mmol L ⁻¹ HCl	Fe	21.7	3.3	2.2	72.8
	Zn	77.9	13.5	6.3	2.4

Reagent	Element	% of Element fraction			
		Treatment step 1 (W1)	Treatment step 2 (W2)	Treatment step 3 (W3)	Cells
0.5 mmol L ⁻¹ HCl	Fe	1.7	2.3	1.4	94.7
	Zn	24.1	20.0	8.5	47.4
0.9 mmol L ⁻¹ SnCl ₂	Fe	38.5	15.7	2.5	43.3
	Zn	4.3	63.3	10.0	22.4
0.9 mmol L ⁻¹ SnCl ₂ + 0.5 mmol L ⁻¹ HCl	Fe	30.6	13.4	3.7	52.3
	Zn	1.1	55.3	16.2	27.4

% of Elements washed out in each treatment step and % elements retained in the final SiO₂ or cell fraction

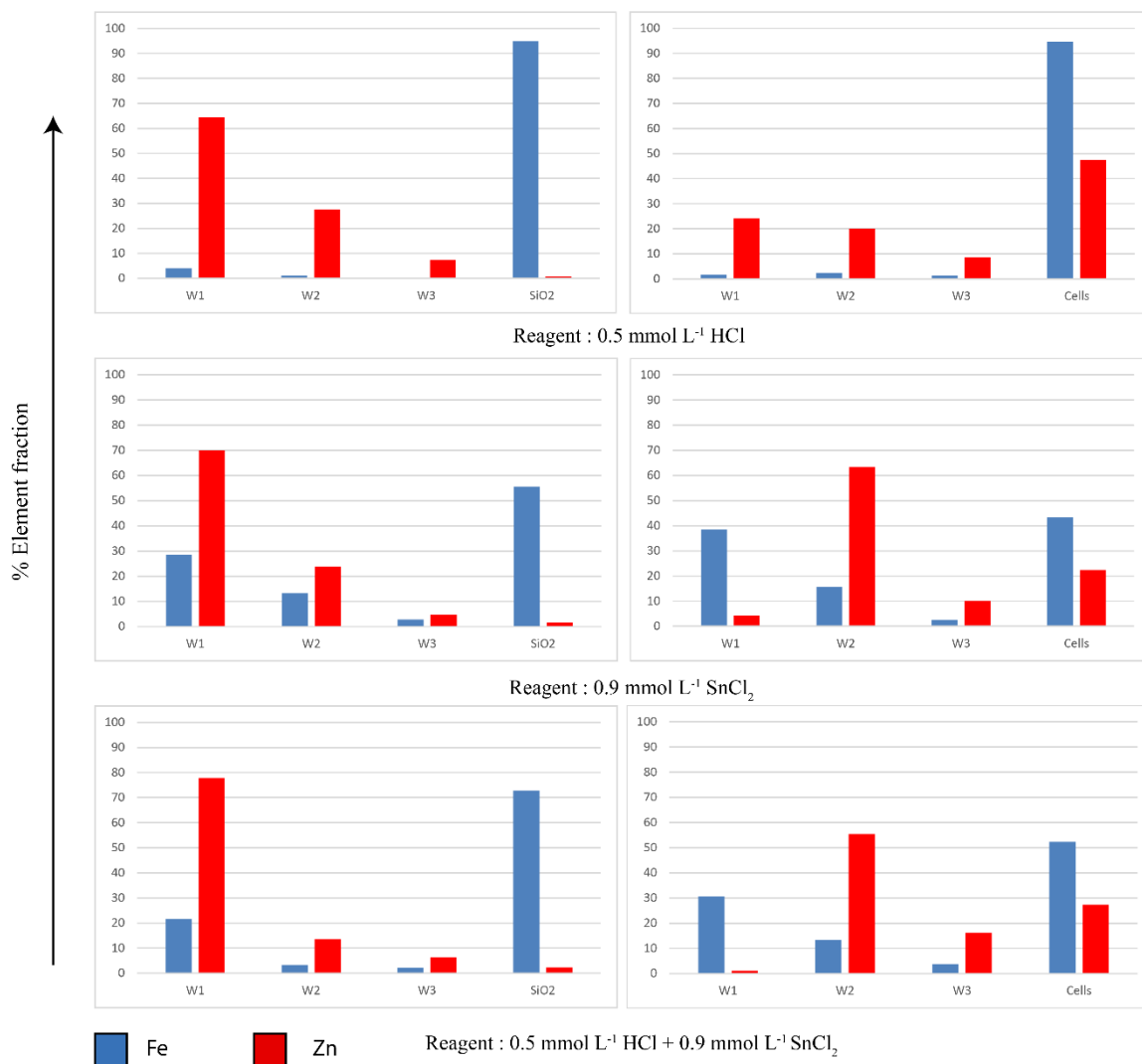


Figure 30 - Desorbed element fractions from SiO₂ and cell surfaces. In each graph W1,W2,W3 represents the filtrate after treatment of the corresponding reagent. SiO₂ and Cells represent the digested SiO₂ particles and cells after the treatment respectively. Y axis represents the percentage of elements washed out in each step and percentage of elements retained in the final SiO₂ or Cells fraction.

Table 20 - Yield of elements in treated cell fractions normalized to dry weight of cells

Element	H ₂ O treated cells	0.5 mmol L ⁻¹ HCl treated cells
Na	3.51 x 10 ¹	3.23 x 10 ⁰
Mg	1.53 x 10 ²	6.99 x 10 ¹
Ca	1.92 x 10 ¹	9.24 x 10 ⁰
Mn	1.06 x 10 ⁰	5.47 x 10 ⁻¹
Fe	1.13 x 10 ¹	6.46 x 10 ⁰
Co	1.66 x 10 ⁻²	9.04 x 10 ⁻³
Ni	2.38 x 10 ⁻²	1.10 x 10 ⁻²
Cu	7.86 x 10 ⁻²	4.55 x 10 ⁻²
Zn	3.84 x 10 ⁰	2.09 x 10 ⁰
Mo	1.39 x 10 ⁻²	6.58 x 10 ⁻³

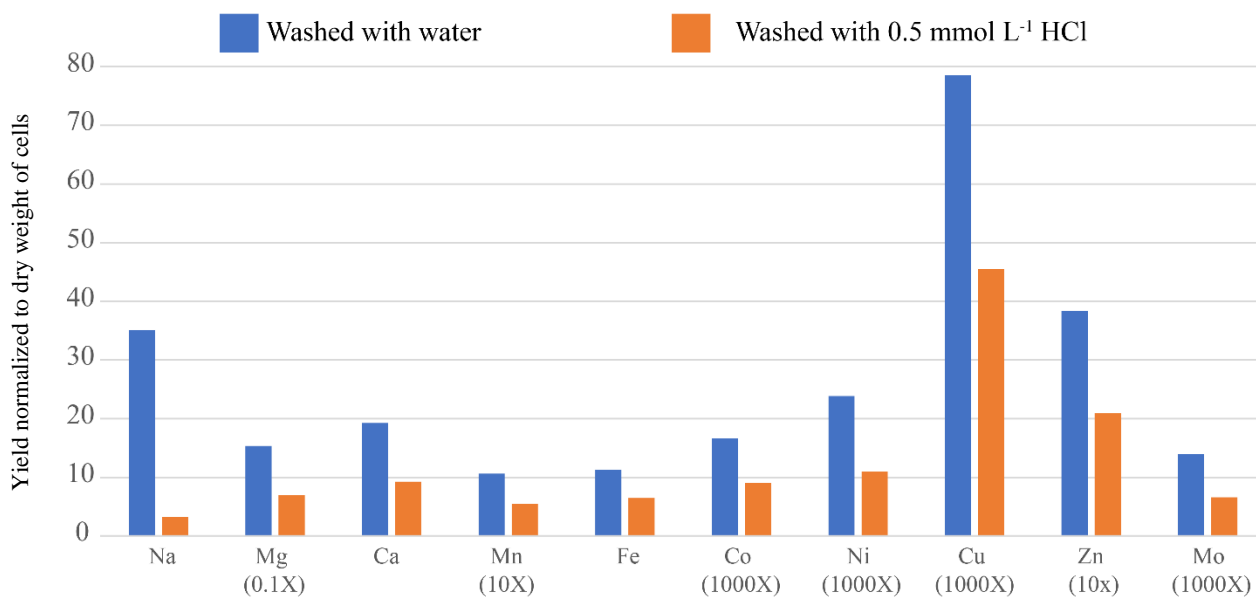


Figure 31 - Yields of elements in treated cell fractions normalized to dry weight of cells

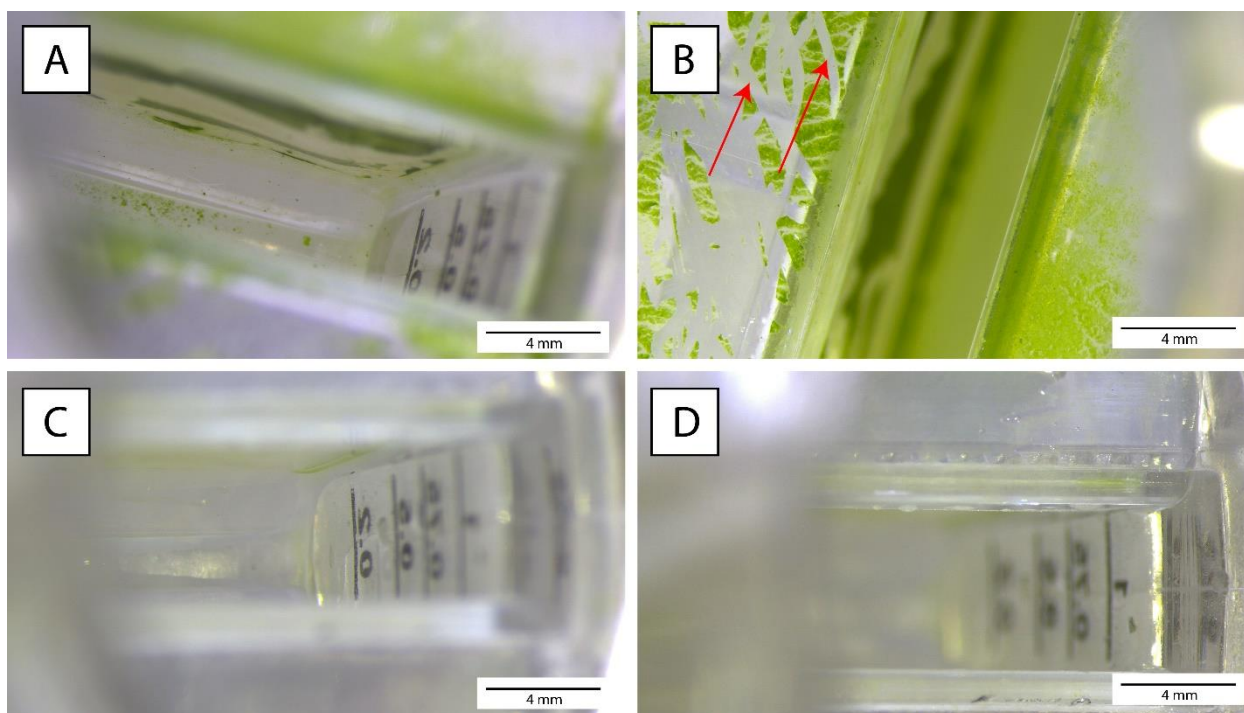


Figure 32 - Images of the filter unit after treating cells with $0.5 \text{ mmol L}^{-1} \text{ HCl}$ (A,B) and water (C,D). The red arrows indicate the lines created by the pipette tip on strongly attached cells to the filter unit. Note that the filter unit that was treated with water do not have any cells attached (C,D).

SEM images (Figure 33) obtained from the treated cell fractions do not show any visible cell breakage in the cell fractions treated with $0.5 \text{ mmol L}^{-1} \text{ HCl}$ and water. However, some of the cells were broken in the fractions treated with SnCl_2 (Figure 33 C arrow). Cell clumps consisting of a maximum of 3 cells were observed in water-treated fractions whereas larger cell clumps were observed in the fractions treated with $0.5 \text{ mmol L}^{-1} \text{ HCl}$. The debris surrounding the cells, irrespective of the treatment procedure, were either caused by the incomplete removal of adsorbed elements or by the production of exopolysaccharides (EPS) upon dehydration (Rossi and De Philippis 2015).

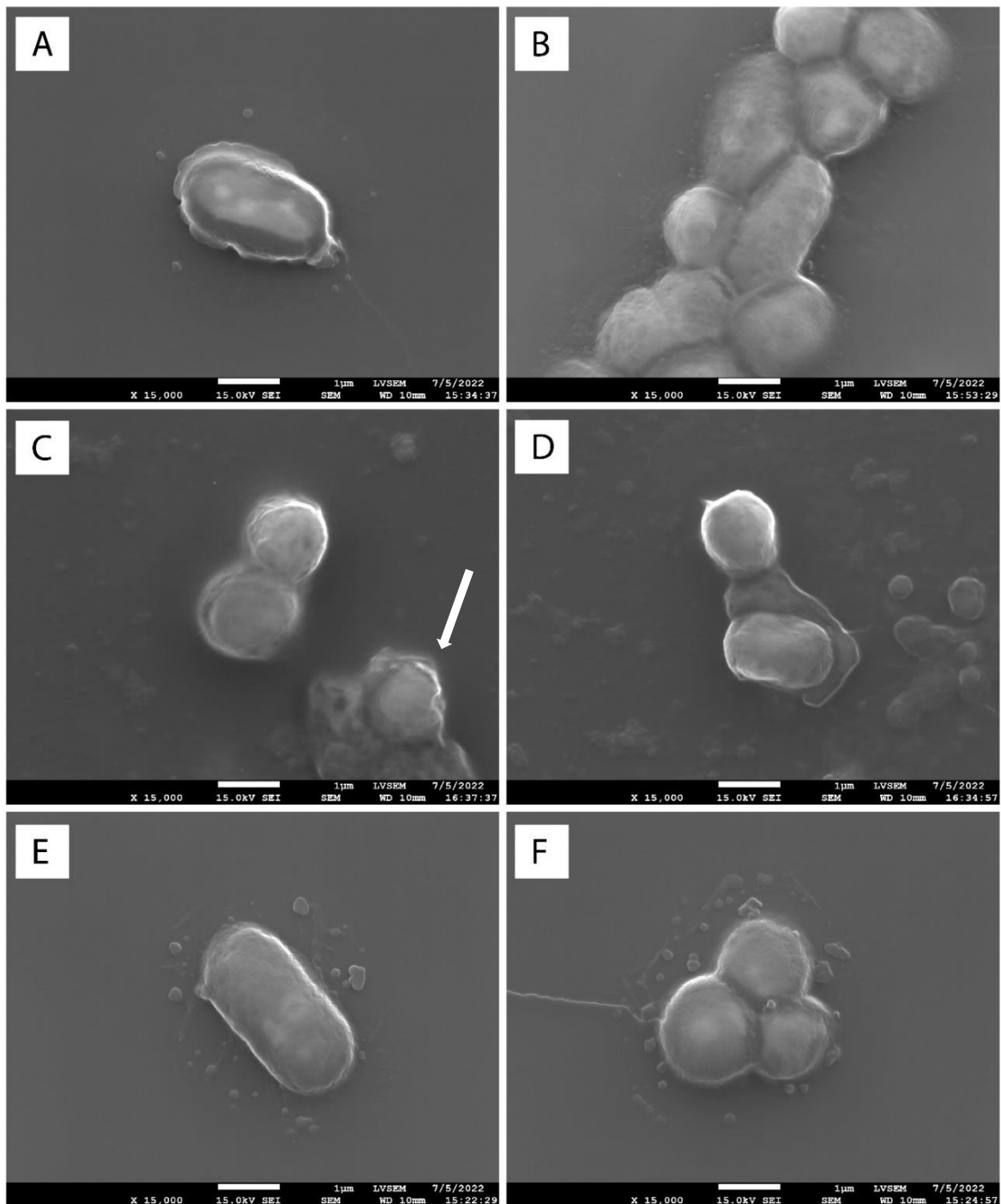


Figure 33 - SEM images of cells treated with HCl (A,B), SnCl₂ (C,D) and water (E,F). Note the damaged cell in the lower right corner of the SnCl₂ treated cells in C. The arrow indicates deformed/membrane damaged cells.

The Zn isotopic composition of the water- and HCl-treated cells and the corresponding filtrates, together with the growth medium composition, are shown in Figure 34. The filtrate after water treatment did not contain sufficient Zn for isotope measurement, indicating insufficient removal of Zn from the adsorbed pool. The water treated cells were enriched with ^{66}Zn compared to the growth media but the measured values are within the analytical uncertainty. On the other hand, $\delta^{66}\text{Zn}$ of the filtrate after HCl treatment is enriched with heavier Zn isotopes and the value is within the uncertainty of that of H₂O treated cells.

Table 21 - Zn isotopic composition of the cells treated with different reagents and associated medium.

Sample	$\delta^{66}\text{Zn}_{(\text{IRMM } 3702)}$	2SE
Cells treated with water	0.32	0.04
Cells Treated with HCl	0.02	0.04
HCl filtrate after treatment	0.27	0.04
Growth medium	-0.02	0.04

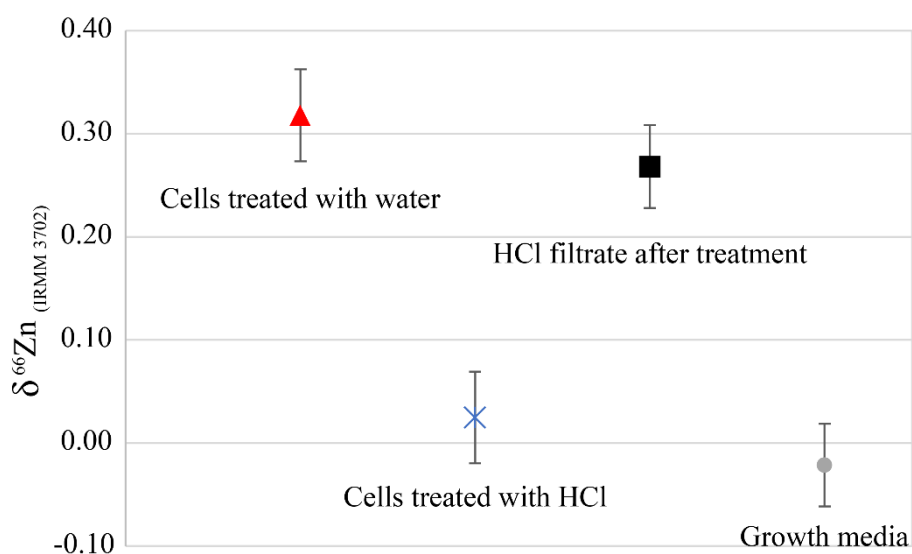


Figure 34 - Zn isotopic variation in water and HCl treated cells and the HCl filtrate after treating cells. Please note that the cells were grown in a same media and harvested on same time.

5.5. Discussion

Since quartz (SiO_2) is resistant to acid dissolution and since the cations in the solution could not diffuse into the SiO_2 under the performed experimental conditions, all the cations measured for SiO_2 were adsorbed ones. However, SiO_2 has the capability to act as nucleation sites for authigenic minerals, which is similar to cells acting as nucleation sites for the formation of minerals. Thus, SiO_2 particles are good proxies to use in evaluating the adsorption behavior onto cells. However, these particles are not representative for adsorption resulted by metal binding on to the reactive ligands on bacterial cells. Thus, in the following discussion on the experiments carried out with SiO_2 , the word “adsorption” only implies adsorption onto precipitated mineral surfaces.

Near-complete removal of Zn and incomplete removal of Fe from the SiO_2 particles indicate that the majority of Zn must have been adsorbed on to the precipitated iron phases and the remaining Zn fraction (~5%) was structurally incorporated into the iron phases. It has been experimentally proven that Zn can incorporate into Fe-oxyhydroxides over a wide range of pH conditions (Juillot et al., 2008).

On the other hand, the variable degrees of Fe removal from the SiO_2 particles indicate that the adsorbed Fe cannot be removed either by dissolution or oxidation. The higher degree of Fe removal in the W1 fraction of Sn solutions relative to those with HCl may be caused by the oxidation of Fe phase. The oxidization of chloride in HCl by Sn oxidation may reduce the effectiveness of the SnCl_2 solution where used in a SnCl_2 -HCl mixture. Therefore, using the SnCl_2 reagent alone is comparatively a better option for the removal of FeO_x that precipitated at a pH of 8.2. On the other hand, use of HCl is not effective for the removal of Fe from SiO_2 particles, and only 5% of Fe was removed upon the treatment.

The sudden removal of Zn from the cells upon treatment with Sn^{2+} solutions in the W2 fraction indicates either the delayed removal of adsorbed Zn or the release of Zn intracellular Zn pool, probably initiated by cellular damage. Subsequent SEM observations have confirmed the cellular damage and therefore use of Sn solutions should be undertaken with caution. Since Sn^{2+} solutions are effective in removing the majority of Fe from surfaces as observed in SiO_2 experiments, reducing the equilibration time between the cells and Sn reagent and/or reducing the concentration of the reagent may be alternative options to prevent cell damage.

The aggregation of cells on the surface of the filter unit after treatment with HCl may possibly be due to the acid tolerance mechanisms adapted by cyanobacteria such as excretion of exopolysaccharides (EPS) (Cruz et al. 2020). Even though visible damage of the cells was not observed under SEM, the potential damage to cells caused by pH imbalance between the inside and outside of the cell membrane should be further studied because external environmental pH changes affects cell membrane properties (Guan and Liu 2020 and references therein). Additionally, cell aggregation reduces the surface area where proton exchanges occur in subsequent treatments. Therefore, this behavior can result incomplete removal of adsorbed elements. Additionally, the efficiency of removing adsorbed elements, including mineral precipitates, will be varied depending upon the type of bacterial cells, interaction period with the reagent and the concentration of the reagent used (e.g Pokrovsky et al. 2005). Therefore, it is necessary to perform preliminary inspections for effective removal of adsorbed components and at the same time any potential cell damage should also be evaluated.

Assuming HCl treatment does not harm the cell membrane, Zn isotopic data indicate that the Zn adsorbed on the cells has positive $\delta^{66}\text{Zn}$ values and that most of this adsorbed Zn could be removed by HCl treatment. The result also revealed that little fractionation occurred in measured Zn isotopes between the cells and medium.

The results of this study clearly indicate that clarification of the abiotic elemental and isotopic fractionation process is needed before evaluation of the biogenicity of a particular sample using isotope and elemental fractionation signatures. Only the adsorption-related isotope fractionation was focused on in this study, but in nature a number of post-depositional alteration processes can mask the actual biotic signature. Thus, discrimination of biotic and abiotic signatures from an ancient sample should only be carried out when the following conditions are met.

Conditions that should be fulfilled by the sample:

1. Signs of rapid sedimentation/silicification.
2. Morphological resemblance to modern biogenic samples (not always required but preferred).
3. Little post-depositional alteration.

Procedures that should be followed to use transition metal isotope signatures to determine biogenicity:

1. Determining mineral phases associated with the sample and their potential primary mineral phases (prior to diagenesis and alteration).
2. Determining the element enrichment patterns in the sample and their correlation to observed textural features.
3. Understanding the use of transition metals in modern biology and understanding their bioavailability with the environmental conditions and evolutionary use of them.
4. Comparison with data obtained from modern analogs to evaluate the preservation potential of the sample, and the elemental and isotope fractionation trends over geological history.
5. Understanding the isotope and elemental fractionation of the desired element with the associated mineral phases.
6. Evaluating post-depositional alteration and corresponding changes that are associated with elemental and isotopic fractionation.
7. Confining the magnitude and direction of biological fractionation of metal isotopes using plate culture. (using same or a similar organism)
8. Confining isotope fractionation from adsorption and co-precipitation on cell surfaces using culturing in liquid media.
9. Measurement of the isotope signature of the sample.

Considering all of the above factors, determination of biogenicity of a sample only using transition metal isotope signatures can be considered as an extremely difficult or an impossible task. Thus, the transition metal isotope fractionation trends observed in the environment may not always represent actual biogenic signature, and most probably they are mixed signatures from abiotic and biotic processes. Therefore, even if such samples do display unprecedented fractionation values, one cannot simply assign them as biogenic or abiogenic as we still do not fully understand the processes which can alter/mask the isotope signatures.

5.6. Conclusions

Comparison of $0.5 \text{ mmol L}^{-1} \text{ HCl}$, $0.9 \text{ mmol L}^{-1} \text{ SnCl}_2$, and $0.5 \text{ mmol L}^{-1} \text{ HCl} + 0.9 \text{ mmol L}^{-1} \text{ SnCl}_2$ to remove FeO_x adsorbed on quartz and cell surfaces revealed that SnCl_2 was the most effective. However, it is not suitable to use for the treatment of cyanobacterial cells as it may damage the cell wall. Even though the effectiveness of $0.5 \text{ mmol L}^{-1} \text{ HCl}$ is greater

than that of using water to remove adsorbed fractions from cell surfaces, the potential cell membrane damage from acid induced stress from HCl treatment should be further evaluated. Even if there is no cell damage associated with HCl treatment, the loss of cells upon aggregation and attachment on filter unit can lower the expected metal yields. Thus, larger batch cultures may be necessary for confining transition metal isotope fractionation by biological processes, especially when using HCl as a reagent to remove the adsorbed elemental fraction.

Application of isotope signatures to natural samples should be carried out with extreme caution and a procedure was introduced in this work to understand more accurately the origin of a particular isotope signature. Considering the uncertainty and complexity associated with the suggested procedure it can be concluded that it is extremely difficult if not impossible to determine biogenicity only by the use of transition metal isotope fractionation. Use of transition metal isotope signatures in combination with traditional stable isotope systems and parallel in detail textural analysis may helpful for better understanding of the isotope signatures preserved in natural samples.

5.7. References

- Andersen, Morten B. et al. 2011. “The Zn Abundance and Isotopic Composition of Diatom Frustules, a Proxy for Zn Availability in Ocean Surface Seawater.” *Earth and Planetary Science Letters* 301(1–2): 137–45.
- Bishop, Brendan A. et al. 2019. “Adsorption of Biologically Critical Trace Elements to the Marine Cyanobacterium *Synechococcus* Sp. PCC 7002: Implications for Marine Trace Metal Cycling.” *Chemical Geology* 525(May): 28–36.
<https://doi.org/10.1016/j.chemgeo.2019.05.021>.
- Borrok, D. et al. 2004. “The Effect of Acidic Solutions and Growth Conditions on the Adsorptive Properties of Bacterial Surfaces.” *Chemical Geology* 209(1–2): 107–19.
- Borrok, David, Benjamin F. Turner, and Jeremy B. Fein. 2005. “A Universal Surface Complexation Framework for Modeling Proton Binding onto Bacterial Surfaces in Geologic Settings.” *American Journal of Science* 305(6-8 SPEC. ISS.): 826–53.
- Cameron, Vyllinniskii, Derek Vance, Corey Archer, and Christopher H. House. 2009. “A Biomarker Based on the Stable Isotopes of Nickel.” *Proceedings of the National Academy of Sciences of the United States of America* 106(27): 10944–48.

- Cruz, Diogo et al. 2020. “Exopolysaccharides from Cyanobacteria: Strategies for Bioprocess Development.” *Applied Sciences (Switzerland)* 10(11).
- Flombaum, Pedro et al. 2013. “Present and Future Global Distributions of the Marine Cyanobacteria *Prochlorococcus* and *Synechococcus*.” *Proceedings of the National Academy of Sciences of the United States of America* 110(24): 9824–29.
- Fujii, Toshiyuki, Frédéric Moynier, Nicolas Dauphas, and Minori Abe. 2011. “Theoretical and Experimental Investigation of Nickel Isotopic Fractionation in Species Relevant to Modern and Ancient Oceans.” *Geochimica et Cosmochimica Acta* 75(2): 469–82.
- Fujii, Toshiyuki, Frédéric Moynier, Marie Laure Pons, and Francis Albarède. 2011. “The Origin of Zn Isotope Fractionation in Sulfides.” *Geochimica et Cosmochimica Acta* 75(23): 7632–43.
- Guan, Ningzi, and Long Liu. 2020. “Microbial Response to Acid Stress: Mechanisms and Applications.” *Applied Microbiology and Biotechnology* 104(1): 51–65.
- Juillot, F., Maréchal, C., Ponthieu, M., Cacaly, S., Morin, G., Benedetti, M., Hazemann, J. L., Proux, O., & Guyot, F. (2008). Zn isotopic fractionation caused by sorption on goethite and 2-Line ferrihydrite. *Geochimica et Cosmochimica Acta*, 72(19), 4886–4900. <https://doi.org/10.1016/j.gca.2008.07.007>
- Kafantaris, Fotios Christos A., and David M. Borrok. 2014. “Zinc Isotope Fractionation during Surface Adsorption and Intracellular Incorporation by Bacteria.” *Chemical Geology* 366: 42–51. <http://dx.doi.org/10.1016/j.chemgeo.2013.12.007>.
- Köbberich, Michael, and Derek Vance. 2017. “Kinetic Control on Zn Isotope Signatures Recorded in Marine Diatoms.” *Geochimica et Cosmochimica Acta* 210: 97–113. <http://dx.doi.org/10.1016/j.gca.2017.04.014>.
- . 2019. “Zn Isotope Fractionation during Uptake into Marine Phytoplankton: Implications for Oceanic Zinc Isotopes.” *Chemical Geology* 523(March): 154–61. <https://doi.org/10.1016/j.chemgeo.2019.04.004>.
- Komárek, Michael et al. 2022. “Metal Isotope Complexation with Environmentally Relevant Surfaces: Opening the Isotope Fractionation Black Box.” *Critical Reviews in Environmental Science and Technology* 52(20): 3573–3603.

- Konhauser, K. O., Fisher, Q. J., Fyfe, W. S., Longstaffe, F. J., & Powell, M. A. (1998). Authigenic mineralization and detrital clay binding by freshwater biofilms: The brahmani river, India. *Geomicrobiology Journal*, 15(3), 209–222.
<https://doi.org/10.1080/01490459809378077>
- Lacan, Francois, Roger Francois, Yongcheng Ji, and Robert M. Sherrell. 2006. “Cadmium Isotopic Composition in the Ocean.” *Geochimica et Cosmochimica Acta* 70(20): 5104–18.
- Liu, Yuxia et al. 2015. “Cell Surface Reactivity of *Synechococcus* Sp. PCC 7002: Implications for Metal Sorption from Seawater.” *Geochimica et Cosmochimica Acta* 169: 30–44.
- Morel, F. M.M., A. J. Milligan, and M. A. Saito. 2013. 8 Treatise on Geochemistry: Second Edition *Marine Bioinorganic Chemistry: The Role of Trace Metals in the Oceanic Cycles of Major Nutrients*. 2nd ed. Elsevier Ltd. <http://dx.doi.org/10.1016/B978-0-08-095975-7.00605-7>.
- Navarrete, Jesica U., David M. Borrok, Marian Viveros, and Joanne T. Ellzey. 2011. “Copper Isotope Fractionation during Surface Adsorption and Intracellular Incorporation by Bacteria.” *Geochimica et Cosmochimica Acta* 75(3): 784–99.
<http://dx.doi.org/10.1016/j.gca.2010.11.011>.
- Pokrovsky, O. S. et al. 2008. “Copper Isotope Fractionation during Its Interaction with Soil and Aquatic Microorganisms and Metal Oxy(Hydr)Oxides: Possible Structural Control.” *Geochimica et Cosmochimica Acta* 72(7): 1742–57.
- Pokrovsky, O. S., J. Viers, and R. Freydier. 2005. “Zinc Stable Isotope Fractionation during Its Adsorption on Oxides and Hydroxides.” *Journal of Colloid and Interface Science* 291(1): 192–200.
- Rossi, Federico, and Roberto De Philippis. 2015. “Role of Cyanobacterial Exopolysaccharides in Phototrophic Biofilms and in Complex Microbial Mats.” *Life* 5(2): 1218–38.
- Sunda, William G., and Susan A. Huntsman. 1995. “Iron Uptake and Growth Limitation in Oceanic and Coastal Phytoplankton.” *Marine Chemistry* 50(1–4): 189–206.

- Tang, Degui, and François M.M. Morel. 2006. “Distinguishing between Cellular and Fe-Oxide-Associated Trace Elements in Phytoplankton.” *Marine Chemistry* 98(1): 18–30.
- Tovar-Sanchez, Antonio et al. 2003. “A Trace Metal Clean Reagent to Remove Surface-Bound Iron from Marine Phytoplankton.” *Marine Chemistry* 82(1–2): 91–99.
- Wasylenki, Laura E., Haleigh D. Howe, Lev J. Spivak-Birndorf, and David L. Bish. 2015. “Ni Isotope Fractionation during Sorption to Ferrihydrite: Implications for Ni in Banded Iron Formations.” *Chemical Geology* 400: 56–64.

Chapter 6: Was the Great Oxidation Event controlled by the bioavailability of urea and Ni?

6.1. Introduction

The rise of atmospheric oxygen for the first time in Earth's history, sometime in between 2.4-2.1 Ga (reviewed in Lyons et al. 2014), had significantly changed its biogeochemical cycles. Oxidative reactions can change the nutrient availability in the water column qualitatively as well as quantitatively, and force the biosphere to adapt to the new environmental conditions. However, the timing, cause, and dynamics of this event, called the Great Oxidation Event (GOE), is currently under debate.

Cyanobacteria played a major role in the GOE as the primary source of production of molecular oxygen accumulating in the atmosphere. Therefore, if the expansion of cyanobacterial oxygen production alone permanently changed the Earth's atmospheric composition, there must have been favorable environmental conditions and ample nutrients for the proliferation of cyanobacteria before onset of the GOE.

Among these nutrients, nitrogen played a major part because it comprises ~10% of the dry weight of cyanobacteria (Bradley and Nichols 1918; Flores and Herrero 1994) and it can alter the growth of cyanobacterial stains (Kramer et al. 2022). The nitrogen isotopic record of ancient sediments suggested that biological nitrogen fixation (BNF, conversion of atmospheric N_2 into NH_4^+) had begun by 3.2 Ga (Stüeken et al. 2015). Additionally, the abiotic conversion of atmospheric N_2 into the forms of NH_4^+ , HCN or NO_x species (termed as fixed nitrogen) could also have produced bioavailable nitrogen during Archean. Despite the nitrogen isotopic evidences for an early origin of BNF, Kasting and Siefert 2001 postulated that the deficit or excess of abiotically produced NO or HCN, respectively, may have triggered the evolution of BNF or as a protective mechanism (Fani et al. 2000) from harmful HCN.

Apart from these geochemical perspectives, it is unclear how the ancient cyanobacteria had the biological capability to produce nitrogenase enzymes necessary for BNF. Nitrogen fixation is an energetically expensive process and nitrogenase requires either Mo, V, or Fe to function (Rucker and Kacar, 2023). Experimental studies have confirmed that nitrogen fixation capacity is significantly dependent on the abundance of Mo (Glass et al. 2010; Zerkle et al. 2006). However, the presence of the Mo isoform in the Archean is enigmatic due to the limited availability of Mo during anoxic weathering (Frank et al. 2003). Furthermore, the structural

and phylogenetic analyses have shown that the Mo isoform predates the V and Fe-dependent nitrogenase enzyme isoforms (Boyd et al. 2011).

On the other hand, nitrogenase is extremely sensitive to oxygen, and all known nitrogenases are inactivated by oxygen (Allen et al. 2019 and references therein; Fay 1992). Therefore, if early evolution of nitrogenase is correct, cyanobacteria that produced it must have had a way to protect it from the oxygen that they produce by themselves.

Having heterocysts, specialized nitrogen fixing cells, is one of the nitrogenase protective mechanisms utilized by cyanobacteria. However, fossil evidence for the first appearance of heterocysts is from early Devonian period (Butterfield 2015; Schirrmeister et al. 2015). Hence, the earliest unicellular cyanobacteria in morphological section I (unicellular-dividing by binary fission) (Rippka, Deruelles et al. 1979) might only have had the circadian expression (temporal separation of nitrogen fixation during dark and photosynthesis during daytime) to fix nitrogen, and therefore would have been unable to fix copious amounts of nitrogen (Stal 2006). Thus, from the origin of cyanobacteria until the evolution of heterocysts, oxygen inhibition of nitrogenase (Allen et al. 2019) could have prevailed, resulting in delayed atmospheric oxygen accumulation. However, it was proposed that oxygen levels dropped back after the GOE (figure 1) coinciding with the end of the positive carbon isotope excursion observed in marine carbonates (Bekker and Holland 2012). Thus, it is unclear how cyanobacteria could have increased atmospheric oxygen levels while fixing copious amounts of nitrogen by the end of the Archean and why they were unable to maintain the oxygen production after the GOE.

In spite of having nitrogenase and its protective mechanisms, cyanobacteria can rely on alternative nitrogen sources such as urea (H_2NCONH_2). It is a simple organic molecule that may have present as concentrated pools on early Earth (Salván et al. 2020), and it is also energetically cheaper than fixing atmospheric nitrogen (Erratt et al. 2018) for microorganisms including cyanobacteria. Therefore, if urea was available in the Archaean biosphere it may have affected the biogeochemical nitrogen cycle. However, experimental growth on urea can trigger mortality in some cyanobacterial species, and it is assumed that pH imbalance in the cells that triggered by excess urea consumption cause this growth limitation (Sakamoto et al., 1998). While experimental studies have shown that this growth limitation depends on urea concentration, there is no agreement as to the optimum urea levels that can support cyanobacterial growth (Erratt et al. 2018; Sakamoto et al. 1998). It is well known that urease

enzyme which hydrolyses urea needs Ni in its active center, and therefore it is necessary to consider the effect of Ni concentration in the medium when evaluating the growth of cyanobacteria in the presence of urea. This is particularly important for understanding the evolution of cyanobacteria because Ni flux in the Precambrian ocean changed significantly over time (Konhauser et al. 2009). However, no systematic study has been carried out to understand the effect of Ni on the growth of cyanobacteria in the presence of urea.

To experimentally identify the capability of cyanobacteria in using urea as an effective nitrogen source and to evaluate whether there is a connection between the evolution of the biological nitrogen cycle and the GOE, in this study we conducted culture experiments of a non-heterocystous unicellular cyanobacterium, *Synechococcus sp.* PCC 7002 (herein after PCC 7002) under various urea and Ni concentrations in the media to assess the importance of urea in the metabolic activities of cyanobacteria in the Archaean biosphere. Based on these experimental results, theoretical considerations that may have led to atmospheric oxidation are discussed, linking the Lomagundi events (LE) and Snowball Earth events (SE). Furthermore, for the first time we measured for the first time the isotopic fractionation factors of nitrogen and Ni during urea uptake by cyanobacteria.

6.2. Experimental Method

6.2.1. Reagents and Materials

Water used in the experiments was prepared using a Milli-Q system (Merck Millipore, France) and with a conductivity of $>18.2 \text{ M}\Omega \text{ cm}^{-1}$. Guaranteed grade 46% HF (Fujifilm Wako Pure Chemical Co., Inc.), electronic (EL) grade 36% HCl (Kanto Chemical Co., Inc.) and EL grade 70% HNO₃ (Kanto Chemical Co., Inc.) were distilled by a PFA sub-boiling distillation apparatus. The distilled reagents are referred to with an 1D (distillation once) or 2D (distillation twice) prefix before the acid name. Guaranteed grade oxalic acid dihydrate (Fujifilm Wako Pure Chemical Co.) was diluted in water to make the 0.05 mol L^{-1} oxalic acid solution. 30 % H₂O₂ (Kanto Chemical Co. Inc.) was used as is. Acids used for elution in ion exchange chromatography were prepared by diluting non-distilled acids with water. The recipe of the culture medium is shown in Table 222. Glassware used for cell growth was pre-cleaned by soaking in a diluted, high-purity alkaline detergent (TMSC, Tama Chemicals), 0.5 mol L^{-1} HNO₃ and 4 mol L^{-1} HCl for $>12\text{h}$ each. After each soaking step, the glassware was rinsed five times with water. Finally, they were autoclaved.

6.2.2. Cell Growth Conditions

Synechococcus sp. PCC 7002 was purchased from Laboratoire Collection des Cyanobactéries, Institut Pasteur, France. They were grown photoautotrophically in modified medium A of (Stevens et al. 1973) as shown in Table 22. The medium was modified with a 10-fold increase in Fe, Mn, Cu and Co to obtain faster growth rates. Additionally, the growth medium used in this study did not include any synthetic chelators (such as aminopolycarboxylates e.g. EDTA) in order to more precisely assess the growth limiting metal concentrations and to obtain an isotopically homogenous growth medium for a given instance. Urea and trace metals were added to the autoclaved growth media using syringe filters (0.2 μm , Advantec, Japan).

Pre-cultures were grown on agar plates of modified medium A+ composition (table 22) under a 12:12 h light: dark photoperiod ($250 \mu\text{E m}^{-2} \text{s}^{-1}$), and single colonies were inoculated in 3 ml of liquid medium of modified medium A+ to undertake preliminary growth experiments. The liquid medium was also kept under a 12:12 h light: dark photoperiod ($250 \mu\text{E m}^{-2} \text{s}^{-1}$) in a thermostatic water bath (Thomas Kagaku Co., Japan) at $38 \pm 0.1 \text{ }^\circ\text{C}$ with 70 rpm shaking.

Afterwards cells were cultured in 100 ml liquid media while varying Ni and urea concentrations, to compare their growth rates and to construct growth curves. Cell growth was monitored for ~20 days by measuring the optical density daily at 730 nm with a spectrophotometer (AS ONE, Japan).

Table 22 - Composition of modified A+ medium

Component	Manufacturer	Concentration in growth media (mmol L^{-1})
NaCl	Fujifilm Wako Pure Chemical Corporation	3.08×10^2
$\text{MgSO}_4 \cdot 7\text{H}_2\text{O}$		2.00×10^1
$\text{CaCl}_2 \cdot 2\text{H}_2\text{O}$		2.52×10^0
Triz Base (ph 8.2)		8.26×10^0
$\text{Na}_2\text{S}_2\text{O}_3 \cdot 5\text{H}_2\text{O}$		1.21×10^1
$\text{H}_2\text{NCONH}_2^*$	MP Biomedicals, France	varied
KCl	Kanto Chemical Co., INC.	8.05×10^0
KH_2PO_4	Kanto Chemical Co., INC.	3.70×10^{-1}
Trace Elements		

H ₃ BO ₃	Fujifilm Wako Pure Chemical Corporation	5.5×10 ⁻¹
ZnCl ₂		2.3×10 ⁻³
FeCl ₃ .6H ₂ O		1.4×10 ⁻²
MnCl ₂ .4H ₂ O		2.2×10 ⁻²
CuSO ₄ .5H ₂ O		1.2×10 ⁻⁵
CoCl ₂ .6H ₂ O		5.0×10 ⁻⁶
Vitamin B ₁₂	Sigma Aldrich.co USA	3.0×10 ⁻⁵
MoO ₃	Kanto Chemical Co. Inc.	2.1×10 ⁻⁴
NiCl ₂ .6H ₂ O	Kanto Chemical Co., INC.	varied
*Added upon the requirement (see text)		

Table 23 - Growth Conditions

Name	Ni concentration (nmol L ⁻¹)	Urea Concentration (mmol L ⁻¹)	Medium Type
U ₁ N ₄₅	45	1	Liquid
U ₁ N ₉₅	95		
U ₁ N ₄₄₅	445		
U ₃ N ₄₅	45	3	
U ₃ N ₉₅	95		
U ₃ N ₁₄₅	145		
U ₃ N ₄₄₅	445		
U ₅ N ₄₅	45	5	
U ₅ N ₉₅	95		
U ₅ N ₄₄₅	445		
U ₁₀ N ₄₅	45	10	
U ₁₀ N ₉₅	95		
U ₁₀ N ₄₄₅	445		
U ₅₀ N ₄₅	45	50	
U ₅₀ N ₉₅	95		
U ₅₀ N ₄₄₅	445		
U _{0.001} Ni ₁₀₀₀ A	1000	0.001	Agar
U ₁ N ₁₀₀₀ A	1000	1	

U ₅ N ₁₀₀₀ A	1000	5	
U ₁₀ N ₁₀₀₀ A	1000	10	
U ₅₀ N ₁₀₀₀ A	1000	50	
U ₅₀ N ₅₀ A	50	50	
When cells were grown in liquid media the temperature of the water bath was maintained at 38 ± 0.1 °C at all times and a 12:12 light: dark photoperiod was applied using $250 \mu\text{E m}^{-2} \text{s}^{-1}$. The stage was shaken at 70 rpm throughout the experiments.			

Cells growing at the end of the exponential phase were harvested for isotope measurements using pre-cleaned vertical twin membrane centrifugal concentrators (300K, Vivaspin 20, Sartorius, UK).

Residual weakly adsorbed metals on cell surfaces were washed by adding 10 ml of water to the centrifugal concentrator filter unit, followed by gently mixing the cell suspension with a pipette, then centrifuging at 2500 rpm in a swinging bucket centrifuging device. This treatment was repeated two more times using 5 ml of water in each step. Finally, the biomass collected on the filter was pipetted out with the addition of water (if necessary) into a pre-cleaned 7 ml PFA vial (Savillex, USA).

6.2.3. Elemental and Stable isotope analysis

For elemental abundance and Ni isotope analyses, the biomass obtained was evaporated, then digested with 30 drops of 70% 1D HNO₃ at 170 °C for 12 h. Then, the sample was evaporated at 120 °C and heated at 196°C for 12 h after adding 20 drops of HClO₄ acid. After drying down the sample, it was dissolved in 0.5 mol L⁻¹ HNO₃.

The trace element and Ni isotopic analysis procedures follow (Ratnayake et al. 2021). In brief, elemental analysis was conducted using an inductively coupled plasma mass spectrometer (Thermo-Scientific Element XR ICP-MS) with medium and high-mass resolving power modes. The isotope dilution technique was applied to determine the mass fractions of elements in samples and procedural blanks. Ni isotope measurements were undertaken using a multi-collector ICP-MS (Thermo-Scientific Neptune Plus). The double-spike method was used to correct the mass fractionation occurring during sample preparation and measurement.

Biomass used for nitrogen isotope composition measurements was loaded into pre-cleaned Sn capsules (Ludi Swiss, Switzerland) and sealed and kept frozen until analysis.

Nitrogen isotope composition of the cyanobacteria and medium were determined by an elemental-analysis isotope ratio mass spectrometry (EA-IRMS) system consisting of an autosampler (Costech ZeroBlank), a flash combustion EA (Thermo Fisher Scientific Flash 2000), a universal continuous flow interface (Thermo Fisher Scientific ConFlo VI), and an IRMS (Thermo Fisher Scientific MAT253). The total procedural blank of nitrogen measured by combusting the Sn foils and capsules were 20-80 ng. International working standards, IAEA-N-2 and IVA-urea, were used to calibrate the $\delta^{15}\text{N}$ values ($\delta^{15}\text{N} = [^{15}\text{N}/^{14}\text{N}]_{\text{sample}} / [^{15}\text{N}/^{14}\text{N}]_{\text{air}} - 1$) of unknown samples.

6.3. Results

6.3.1. Preliminary experiments

Initially, the growth of PCC 7002 was examined on an agar medium with varying urea concentrations, from 0.001 to 50 mmol L⁻¹, and fixed Ni concentration at 1000 nmol L⁻¹, a value above the upper limit of that in Precambrian seawater (400 nmol L⁻¹) (Konhauser et al. 2009) (Table 23). Cells grew in the agar medium containing 1 to 10 mmol L⁻¹ urea. When the urea concentration was low at 0.001 mmol L⁻¹, cell growth was not observed. When the urea concentration was high at 50 mmol L⁻¹, cells grew for several days but were bleached after that. To examine the Ni dependence of cell bleaching, the Ni concentration was reduced to 50 nmol L⁻¹ while keeping the urea concentration at 50 mmol L⁻¹ in the agar medium, resulting in cell growth for several days and then bleaching. Thus, it was found that PCC 7002 can grow on Ni-bearing agar medium with optimized urea concentration, i.e. ~1 to ~10 mmol L⁻¹, and growth was inhibited when urea in the medium was deficient or excessive.

The absorbance in the preliminary cultures was measured on day 15 of growth, after cells had been grown in 3 ml liquid media under various Ni and urea concentrations (Fig. 1). Peaks of absorbance corresponding to each Ni concentration were obtained in media containing 3 and 5 mmol L⁻¹ urea, while the lowest absorbances were obtained at 10 and 50 mmol L⁻¹ urea, irrespective of Ni concentration.

The growth curves of cells under various conditions are presented in Fig. 2. When urea concentrations were fixed at 1 and 3 mmol L⁻¹, the lowest growth rates were observed at higher Ni concentration (445 nmol L⁻¹) in the media. The growth rates decreased with increasing Ni levels in the 3 mmol L⁻¹ urea cultures, but this relationship was inverted at 1 mmol L⁻¹ urea, where the growth rate was slightly higher in U₁N₉₅ than U₁N₄₅. The maximum absorbance exhibited by U₃N_i cultures were in a similar range (~0.3 – 0.4) irrespective of the Ni levels. However, the maximum absorbance of cells grown at 1 mmol L⁻¹ urea was < 0.3 at all Ni levels. In both U₁N_i and U₃N_i, the cultures turned yellow-green after 4-5 days of growth in their stationary phase (Fig. 2C inset) irrespective of the Ni levels contained, indicating nitrogen limitation.

Table 24 – Absorbances (730nm) of 3 ml liquid cultures on the 15th day after inoculation

Urea (mmol L ⁻¹) Ni (nmol L ⁻¹)	1	3	5	10	50
45	0.172	0.31	0.325	0.12	0.102
95	0.295	0.324	0.306	0.093	0.105
445	0.33	0.339	0.261	0.112	0.101

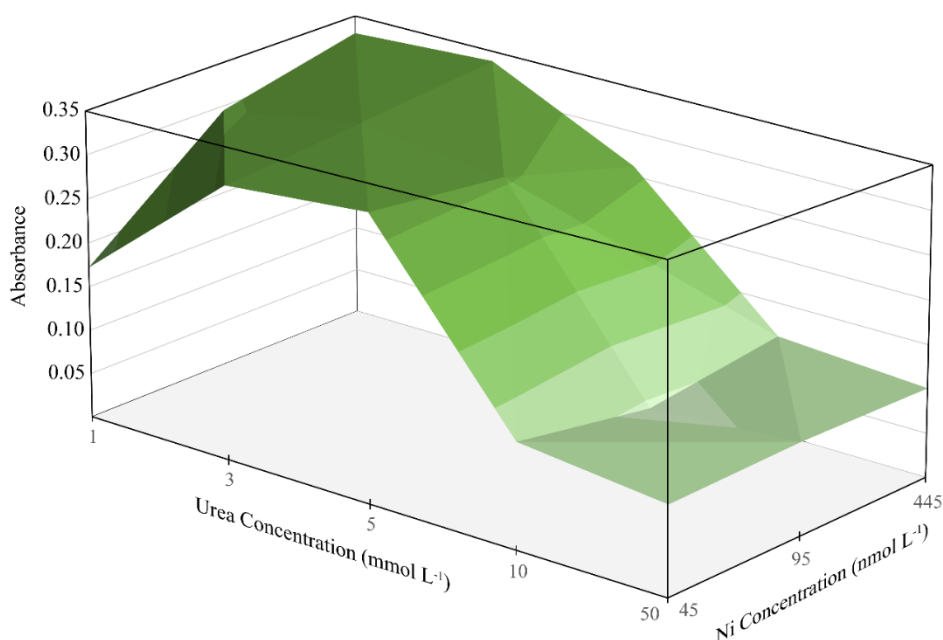


Figure 35 - Absorbance values of cyanobacteria grown in 3 ml liquid media at different conditions on the 15th day after inoculation

At a constant Ni concentration level of 445 nmol L⁻¹, high growth rates were observed in cultures grown in 5 mmol L⁻¹ urea, followed by 3 mmol L⁻¹ urea cultures. Growth rates of cultures grown in 10 and 50 mmol L⁻¹ urea were significantly lower, the latter being the lowest among all experiments. At 10 and 50 mmol L⁻¹ urea levels, the absorbance at the stationary phase was 2-3 times lower than that observed for 3 and 5 mmol L⁻¹ urea.

The cells grown in these settings (10 and 50 mmol L⁻¹ urea) were bleached (Fig. 2B inset a and b) once they reached the stationary phase. Here, a gradual change from green to yellow-green was not observed, and cells were bleached within a day. Growth characteristics

in the 50 mmol L⁻¹ urea were similar to those observed in the agar medium, but they were different for 10 mmol L⁻¹ urea supplemented cultures, where a prolonged growth without bleaching was observed (~30 days) in agar.

6.3.2. Nitrogen and Ni isotope fractionation by *Synechococcus* sp. PCC 7002

Table 25 - Ni and nitrogen isotope fractionation by *Synechococcus* PCC 7002

	$\Delta^{15}\text{N}_{(\text{Biomass} - \text{Medium})}$ (‰)	2SD	n	Growth medium composition	Growth Phase	Number of days after inoculation
N	-5.44	0.05	2	U ₃ N ₉₅	End of exponential	11 and 13
Ni	-0.09	0.03	2	U ₃ N ₄₄₅	End of exponential	12
	-0.02	0.03	2		End of stationary	16

Table 26 Absorbance values of bacterial cultures grown in different growth media

Cumulative time (Hours)	Absorbance (730 nm)	
	U ₁₀ N ₄₄₅	U ₅₀ N ₄₄₅
24.00	0.054	0.055
44.50	0.057	0.054
72.00	0.055	0.056
96.50	0.057	0.056
120.50	0.058	0.057
145.50	0.062	0.058
167.50	0.066	0.061
190.00	0.073	0.064
216.00	0.080	0.066
238.75	0.083	0.067
287.25	0.093	0.076
315.50	0.105	0.078
339.00	0.116	0.078
364.00	0.130	0.084
388.75	0.142	0.084
409.25	0.143	0.084
432.75	0.141	0.082
454.25	0.146	0.084

Cumulative time (Hours)	Absorbance (730 nm)	Cumulative time (Hours)	Absorbance (730 nm)	
	U ₃ N ₄₅		U ₃ N ₄₄₅	U ₃ N ₁₄₅
24.00	0.057	24.00	0.052	0.052
44.75	0.061	90.00	0.055	0.055
70.25	0.065	117.50	0.065	0.064
93.00	0.075	141.00	0.075	0.081
141.50	0.133	162.50	0.085	0.099
169.00	0.230	186.50	0.107	0.135
192.50	0.302	210.50	0.139	0.199
217.50	0.357	234.50	0.183	0.262
242.25	0.360	258.00	0.226	0.287
262.75	0.352	285.75	0.313	0.309
286.25	0.348	330.25	0.330	0.329
307.50	0.343	354.25	0.331	0.353
332.00	0.334	378.75	0.330	0.348
		427.00	0.313	0.328
		454.50	0.298	0.321
		479.00	0.283	0.317

Cumulative time (Hours)	Absorbance (730 nm)		
	U ₁ N ₄₅	U ₁ N ₉₅	U ₁ N ₄₄₅
24.00	0.066	0.063	0.063
48.00	0.067	0.065	0.060
72.25	0.075	0.071	0.061
95.75	0.096	0.076	0.063
136.25	0.122	0.108	0.066
160.75	0.139	0.138	0.077
187.25	0.173	0.210	0.092
211.25	0.214	0.277	0.103
256.25	0.215	0.269	0.113
282.25	0.212	0.264	0.129
304.75	0.213	0.269	0.141
333.25	0.210	0.269	0.178
356.75	0.209	0.276	0.197
381.75	0.209	0.270	0.213
406.75	0.202	0.273	0.218
430.25	0.205	0.276	0.220
454.75	0.203	0.278	0.230

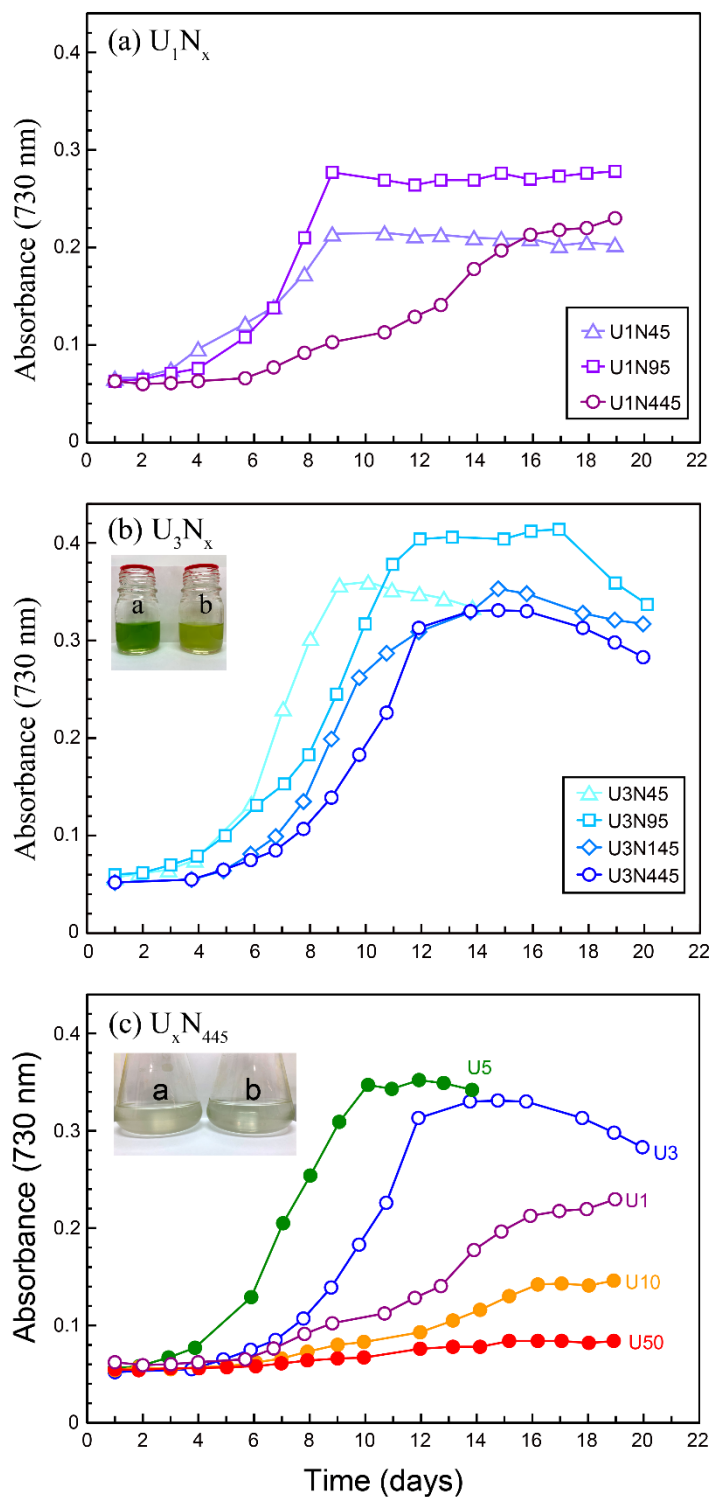


Figure 36 - Growth curves of bacterial cultures grown in (A) 1 mmol L⁻¹ urea at variable [Ni], (B) 445 nmol L⁻¹ Ni at variable [urea], (C) 3 mmol L⁻¹ urea at variable [Ni]. Inset figure in B shows the bleached cells in (a) U₁₀N₄₄₅ (b) U₅₀N₄₄₅. Inset figure in C shows the (a) Cells growing in exponential phase (b) color change after growing several days in the stationary phase.

6.4. Discussion

6.4.1. Urea as a potential nitrogen source

Signs of chlorosis (inset figure 36b) observed during the stationary growth phase of the cyanobacterial cultures may have been caused by nitrogen limitation and it indicates a rapid uptake of urea at the exponential growth phase. However, slower growth rates and cell bleaching at higher concentration levels of urea (10 and 50 mmol L⁻¹) indicate severe toxic effects involving urea uptake similar to result reported in Sakamoto et al. (1998). The same study also reported cyanobacterial growth at 50 mmol L⁻¹ urea, but a proper comparison is hindered by the differences in experimental setups such as their use of EDTA chelators. The ability of EDTA to reduce urease activity (Svane et al. 2020) may have lowered the bio-consumption of urea and thus toxicity may have not occurred in the experiments carried out by Sakamoto et al. 1998.

Nevertheless, the prolonged growth observed in agar plates containing 10 mmol L⁻¹ urea indicate that the growth inhibitory effects of urea can be mitigated by reducing its bio-availability even when it is present at moderate levels. Therefore, we propose that the different growth patterns observed in similar levels of urea present in agar and liquid media were caused by differences in bioavailable urea levels and its diffusion rates. If correct, it can be assumed that favorable growth conditions in moderately high urea concentrations could have prevailed, especially in mat forming cyanobacterial habitats which are continuously inundated by nutrient rich water.

In summary, the observed discrepancies in cyanobacterial growth upon urea uptake suggests that severe growth inhibitory effects are expressed whenever urea is present in high bioavailable levels, but it can also act as an effective nitrogen source upon prolonged availability at a low concentration level.

6.4.2. Effect of Ni for the growth of cyanobacteria.

Ni is important for consuming urea as a nitrogen source because the urease enzyme which catalyzes the hydrolysis of urea has two Ni atoms in its active center (reviewed in Kappaun et al. 2018). The presence of Ni in the growth media can increase the urease activity of *Synechococcus sp.* PCC 7002 by 15-fold compared to a Ni free media (Sakamoto and Bryant 2001). Therefore, the rate of urea hydrolysis may also increase accordingly. Thus, urea consumption can be elevated by the presence of high Ni levels and therefore the growth inhibitory effects of urea can be more pronounced at the presence of Ni. On the other hand, the

growth rate can be increased at low urea levels (1 mmol L⁻¹) by the addition of Ni due to the expression urease enzyme. However, the growth rate limitation at the highest Ni level tested, irrespective of urea levels, indicate that the maximum favorable Ni levels are below 445 nmol L⁻¹. Yet the observed similar maximum absorbance levels (in U₃N_i and U₁N_i) indicate that excess Ni only effects for the rate of growth but not the final biomass. Thus, we propose the growth inhibitory effects from Ni observed in this study are related to urea hydrolysis. Therefore, the proposed Ni level in Archean ocean (~400 nmol L⁻¹, (Konhauser et al. 2009)) alone could not have inhibited the growth of non-diazotrophic unicellular cyanobacteria, especially under the presence of chelating agents.

The minimum growth favorable Ni level observed in this study (45 nmol L⁻¹) is significantly lower than previously proposed level of 5 μmol L⁻¹ (Sakamoto and Bryant 2001). This difference may have been caused by the use of EDTA in the growth medium in the experiments reported by Sakamoto and Bryant 2001. Use of EDTA may have limited the net bio-available Ni by forming Ni-EDTA complex (log K_f = 18.4 Harris et al., 2016). Therefore, the results obtained in this study represent more accurate effects of Ni for the utilization of urea in the absence of EDTA.

Finding the exact mechanism of urea and Ni induced growth limitation of *Synechococcus* sp. PCC 7002 is beyond the scope of this study. But it can be concluded that the presence of high urea levels together with Ni elevate urea consumption and limit the growth.

6.4.3. Nitrogen and Ni isotope fractionation

The only available previous study regarding nitrogen isotope fractionation associated with urea uptake is confined to a marine diatom species where cells were depleted in ¹⁵N compared to the medium, by a δ¹⁵N value of 0.8 ± 0.6 ‰ (Waser et al. 1998b). In contrast, the results obtained in this study show a significant depletion of ¹⁵N in the cyanobacterial biomass. The differences in the enrichment factors obtained between the two studies may be the result of unique pathways to assimilate nitrogen in diatoms and cyanobacteria (Rogato et al. 2015; Veaudor et al. 2019). Nevertheless, the obtained isotope fractionation is in between the fractionation resulting from Fe-V (δ¹⁵N -8 to -6 ‰) and Mo (δ¹⁵N -4 to +1‰) nitrogenase related to N₂ fixation, and it falls in the upper limit of the fractionation caused by NH₄⁺ assimilation (δ¹⁵N -4 to -27 ‰) (reviewed in Stüeken et al. 2016).

The obtained enrichment factor may change upon the passive diffusion of urea into the cells and passive loss of NH₃ from the cells at the post exponential phase (Sakamoto et al.

1998). But the data obtained in this study were collected from bacteria growing at the end of the exponential phase and therefore the above affects should be negligible.

The direct comparison of the obtained enrichment factors with the paleo-nitrogen isotope record is impossible because of the:

6. Unavailability of the nitrogen isotopic composition of urea produced in the Archean.
7. Lack of experimental nitrogen isotope enrichment factors for the utilization of urea and other nitrogen sources by methanogens.
8. Lack of understanding about the evolutionary history of the urease enzyme.
9. Ambiguities of the nitrogen isotope record itself (see Ader et al. 2016 for a review)

The nitrogen source for urea in the Archean could be atmospherically derived HCN, formed from the reaction of photo dissociated N_2 and CH_4 (Zahnle 1986). In the absence of a self-shielding effect from N_2 , experimental studies have shown that organic aerosols may deplete ^{15}N by a $\delta^{15}N$ value of ~ 15 - 26 ‰ (Kuga et al. 2014). Even though these experiments not represent the photo dissociation of N_2 in thin Earth's Archean atmosphere, it was found that aerosols progressively become enriched in ^{15}N with increasing CH_4 fraction in the experimented gas mixtures. Therefore, it is reasonable to assume that aerosols and their derived organic compounds (like urea) produced in the Archean may have been neither extremely depleted nor enriched in ^{15}N . Thus, we propose urea assimilation as a possible candidate to explain the depleted $\delta^{15}N$ signals from 3.7 Ga meta-turbidites (-1 to -10 ‰) (Stüeken et al. 2021).

Comparing the observed $\delta^{15}N$ trends in the sedimentary record to the changes in the biological nitrogen cycle over time is complicated due to metamorphic alteration (Ader et al. 2016). Yet if the observed trends were exclusively produced by fractionating atmospherically fixed nitrogen (by biological N_2 fixation), either the proposed urea source was negligible or it should have been diminished with time. Given that the difficulty in protecting nitrogenase from oxygen in non-diazotrophic cyanobacteria and the nitrogen control (Flores and Herrero 2005) acting on cyanobacteria upon the availability of reduced nitrogen sources, a hypothesis is developed to explain the evolution of cyanobacteria supported by abiotically produced urea as a nitrogen source.

The observed Ni isotope fractionation factor in this study is smaller than the experimentally obtained fractionation factors for Ni adsorption onto ferrihydrite and goethite

(-0.77 and -0.35 ‰ respectively) (Gueguen et al., 2018, Wasylenki et al., 2015), thus, it may represent the fraction that is associated with cyanobacterial cells. However, differentiation of the extracellular adsorbed fraction and the intracellular fraction is not possible as explained in previous chapter (see Chapter 5 of this thesis). However, the variation of the fractionation factor between the two analyse can be explained by the abiotic adoption related isotope fractionation during the two different growth stages.

During exponential growth, bacteria rapidly expand by binary fission and therefore more and more adsorption surfaces will be generated. Thus, isotopes will be kinetically fractionated during this stage. Once the bacterial culture reaches the stationary phase in a batch culture, the net bacterial growth stops, and upon initiation of the death phase the culture is dominated by dying cells rather than newly formed cells. Thus, the majority of cells in a sample collected upon the initiation of death phase contains dead/ or cells that are reaching the death phase. Therefore, once the growth has stopped and all the adsorption sites are filled, the metal isotopes may equilibrate with the medium and thus eventually isotopically homogenize with the medium. Hence, this example also reconfirms the difficulty in using transition metal isotope signatures to determining biogenicity of a sample based on enzyme specific isotope fractionation trends.

6.4.4. Hypothesis on the events that lead to the GOE

i. Was there significant abiotic production of urea in the Archean?

In the primitive ocean, urea can be produced from cyanogen (CN)₂ hydrolysis in the presence of NH₄⁺ (Lohrmann 1972). According to this mechanism, cyanogen would be derived from the photodissociation products of ferrocyanide ([Fe(CN)₆]⁴⁻). Therefore, a continuous CN⁻ flux (probably as HCN) would have been necessary to produce urea in the primitive oceans where abundant Fe was present.

Production pathways for HCN in Earth's primitive atmosphere includes shock heating (generated by impacts and lightning) and reactions of CH₄ with photo-dissociated nitrogen atoms (see Kasting 1990 for a review). Thus, during the late heavy bombardment period (LHB) significant flux of HCN could have prevailed. However, decreasing impact rates (Grieve 1980) may have slowed the HCN production eventually, and lightning alone could not have produced sufficient fixed nitrogen for an evolving biomass (reviewed in Stüeken et al. 2016). Therefore, availability of CH₄ is necessary to sustain HCN production and hence urea formation after the emergence of life. CH₄ may have either formed abiotically in the pre-biotic world from the

photolysis of H₂O in the presence of CO or from methanogenesis (Kasting 1990 and references therein) after life evolved. Geochemical evidence for methanogenesis dates back to >3.4 Ga (Ueno et al. 2006) and it is calculated that, at a CH₄ mixing ratio of 1000 ppmv in post biotic atmospheres a minimum HCN production rate of 30 Tg/yr could be achieved (Tian et al., 2011, Zahnle, 1986). Thus, according to the Lohrmann mechanism, formation of 1 mmol L⁻¹ urea in the post biotic Archean ocean would have only taken 15 million years (Table 27) in the presence of lower limit of NH₄⁺ (Bada and Miller 1968).

It is argued that the stability of atmospheric NH₃ was limited in the Archean due to photochemical destruction (Kasting 1982). However, atmospheric rainout and hydrolysis of HCN in the presence of sulfides (Marsh and Martin 1957) indicates a small, yet vital supply of NH₄⁺ to the Archean oceans. Therefore NH₄⁺ replete conditions could have been commonly observed during the meso-Archean (Yang et al. 2019). Therefore, the production of urea could have continued until these ingredients were depleted. The concentration of urea must have increased gradually as it began to form, owing to its remarkable stability when subjected to harmful irradiation such as UV and γ rays (Gan et al. 2023; González et al. 1989).

ii. Why did not cyanobacteria expand during the Archean?

If urea was available throughout the Archean, cyanobacteria could have utilized it and expanded while oxygenating the atmosphere. But multiple lines of evidences such as the presence of detrital pyrite and uraninite grains, mass independent S isotope fractionation etc. support for a delayed oxygenation of the atmosphere until the onset of the Proterozoic (Lyons et al. 2014).

Our data suggest that this delay could be attributed to the presence of high urea concentration (> 10 mmol L⁻¹) in cyanobacterial habitats, limiting the expansion and growth of cyanobacteria. However, growth limitation by moderate urea concentrations (~10 mmol L⁻¹) may not have occurred if primitive cyanobacteria were capable of adhering to and growing on liquid-air interfaces by forming microbial mats (e.g. stromatolites). This model supports the hypothesis that ancestral cyanobacteria could have lived as attached organisms rather than as a free-floating one (Hammerschmidt et al. 2021)

In addition to cyanobacterial growth inhibition, growth of methanogens can also be inhibited by high urea levels. However, the evolutionary oldest hydrogenotrophic methanogens (Muñoz-Velasco et al. 2018) have a high urea tolerance as compared to other methanogenic species (Tian et al. 2018), explaining their potential for ecological success in habitats

containing high urea concentration. Thus, CH₄ production may not have been disrupted owing to toxic effects related to urea metabolism.

High levels of Ni concentration in the Archean ocean (~400 nmol L⁻¹) (Konhauser et al. 2009) may also have had a negative impact on the growth rate of cyanobacteria as observed in (figure 36). However, it is possible that the presence of natural chelators may have reduced the bio-available Ni concentration. Therefore, the presence of 400 nmol L⁻¹ Ni and its declination to 200 nmol L⁻¹ in primitive oceans towards the Proterozoic (Konhauser et al. 2009) may not have significantly disrupted cyanobacterial growth, as evidenced in this study (figure 36).

iii. Expansion of cyanobacteria

The inhibition of methanogenesis due to reduced Ni flux to the oceans (Konhauser et al. 2009) may have indirectly lowered urea production by limiting CH₄ flux to the Archean atmosphere. The lowering of urea-related toxicity due to decreasing urea production and decreasing Ni flux may have created favorable growth conditions for cyanobacteria.

Increasing oxygen concentration in sea water may have facilitated the oxidation of NH₄⁺ and CN⁻, further removing the ingredients for urea production. Furthermore, gradual formation of the ozone layer may have blocked the UV irradiation that promoted photodissociation of CH₄ and probably N₂. As a result, eventually the urea concentration could have decreased to < 5 mmol L⁻¹, promoting a rapid expansion of cyanobacteria and finally leading to the GOE (figure 37).

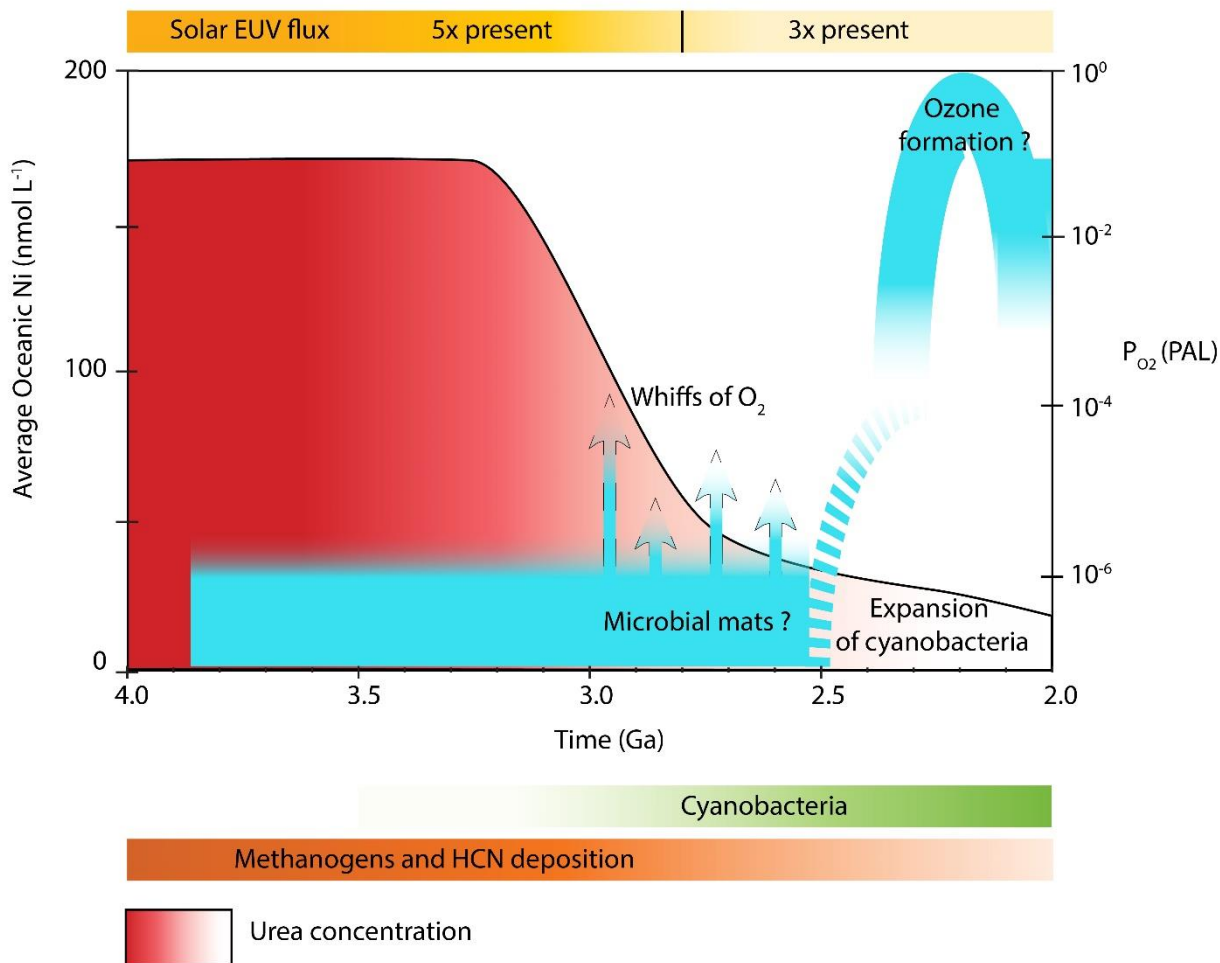


Figure 37 - Urea and Ni controlled GOE. The average oceanic Ni concentration plotted is from Konhauser et al., (2009) and the Oxygen evolution curve is from Lyons et al., 2014. Solar EUV flux is from Ribas et al., 2005.

iv. Biological implications

The reduction in net CH₄ accumulation due to oxidative conversion to CO₂ could have drastically reduced urea production and eventually it become insufficient to supply nitrogen to a larger biomass. This evolutionary pressure for supplementation of nitrogen could have resulted in the invention of nitrogen fixing nitrogenase or refinement of the substrate specificity of readily available nitrogenase/detoxoyase (Fani et al. 2000). Oxidative weathering initiated after the GOE can deliver Mo for the functioning of nitrogenase. Even if N₂ fixation was initiated, the nitrogenase activity may have been inhibited by O₂ itself until heterocyst development (Allen et al. 2019).

On the other hand, even if nitrogenase and cyanase (that catalyzes cyanate (NCO⁻¹) decomposition) were present in primitive cyanobacteria before the GOE, the function of those

enzymes would have been repressed until fixed nitrogen sources (urea and NH_4^+) got depleted (termed as “nitrogen control”) (Harano et al. 1997; Herrero et al. 2001). Repressed nitrogenase will also limit the uptake of CN^- as its degradation is also controlled by nitrogenase (Fani et al. 2000). However, the presence of constitutive urease activity in phylogenetically distant cyanobacteria PCC 7002 (Veaudor et al. 2019) supports an early evolution of urease genes.

NH_4^+ could have been used by cyanobacteria along with urea assimilation as urease synthesis is not repressed upon NH_4^+ uptake (Ge et al. 1990). However, assimilation of NH_4^+ is capable of reducing the urea in primitive oceans as it is required for urea production. But experimental studies have shown that urea is preferentially take up by cyanobacteria relative to inorganic nitrogen sources (Erratt et al. 2020). Therefore, urea production may not have been significantly affected by NH_4^+ uptake. However, future work is necessary to understand the rate of urea production from the Lohrmann mechanism so that the effect of NH_4^+ depletion can be evaluated.

v. Snow ball Earth and the Lomagundi event

Limited production and accumulation of CH_4 caused by reduction of methanogenesis (Konhauser et al. 2009) and oxidative destruction, respectively, could reduce the CH_4 -induced greenhouse effect. Therefore, the Earth may have suffered from a prolonged glaciation (known as the Snow Ball Earth event (SE)) once the GOE occurred. In previous conceptual models, it was hypothesized that this glaciation preceded the GOE. This study, however, suggests that SE should have occurred after the GOE, which supports more recent studies (Warke et al. 2020 and references therein).

Additionally, the rapid expansion of cyanobacterial biomass driven by rapid urea uptake during or at the onset of the GOE may explain the increased $^{13}\text{C}/^{12}\text{C}$ ratios of marine carbonates (known as the Lomagundi event (LE)), thus supporting the conventional explanation that ^{12}C removal from organic burial was accelerated (Karhu and Holland 1996). Therefore, if the events followed the order explained above, the LE, SE and GOE can be considered not as discrete events but instead may have been interconnected, resulting from an interplay among cyanobacteria, Ni and urea in Earth’s atmosphere, geosphere, hydrosphere and biosphere.

Table 27 - Urea production yield in Archean oceans

	Minimum	Maximum
HCN production rate (Tg/year)	30	
NH ₄ ⁺ (mmol L ⁻¹)	1	
Accumulation time (years)	1.50E+07	
Archaean Water Mass (kg)	1.21E+21	2.1E+21
Urea yield %	13	30
Reaction (Lohrmann 1972)	$[Fe(CN)_6]^{4-} + h\mu \rightarrow [Fe(CN)_6]^{3-} + h\mu \rightarrow [Fe(CN)_5H_2O]^{3-} + CN^*$ $(CN)_2 + H_2O \rightarrow HCN + HCNO$ $HCNO + NH_3 \rightarrow NH_4OCN \leftrightarrow H_2NCONH_2$	
Urea conc. Archean Ocean after accumulation (mol/L)	1.03E-03	4.13E-03

6.5. Conclusions

We conclude that urea can serve as an efficient nitrogen source for cyanobacteria, which have the ability to hydrolyze urea. However, too much bioavailable urea inhibits cyanobacterial growth and those inhibitory effects are enhanced by the presence of high Ni in growth media. Therefore, the variable presence of Ni and urea in Earth's early history may have controlled the expansion of cyanobacteria and hence the oxidation of the Earth's atmosphere.

6.6. References

- Ader, M. et al. 2016. 'Interpretation of the Nitrogen Isotopic Composition of Precambrian Sedimentary Rocks: Assumptions and Perspectives'. *Chemical Geology* 429: 93–110.
- Allen, John F., Brenda Thake, and William F. Martin. 2019. 'Nitrogenase Inhibition Limited Oxygenation of Earth's Proterozoic Atmosphere'. *Trends in Plant Science* 24(11): 1022–31.
- Bada, Jeffrey L., and Stanley L. Miller. 1968. 'Ammonium Ion Concentration in the Primitive Ocean'. *Science* 159(3814): 423–25. <https://www.science.org>.
- Bekker, A., and H. D. Holland. "Oxygen Overshoot and Recovery during the Early Paleoproterozoic." *Earth and Planetary Science Letters*, vol. 317–318, Feb. 2012, pp. 295–304, doi:10.1016/j.epsl.2011.12.012.
- Berman-Frank, Ilana, Pernilla Lundgren, and Paul Falkowski. 2003. 'Nitrogen Fixation and Photosynthetic Oxygen Evolution in Cyanobacteria'. *Research in Microbiology* 154(3): 157–64.

- Boyd, Eric S., Trinity L. Hamilton, and John W. Peters. 2011. 'An Alternative Path for the Evolution of Biological Nitrogen Fixation'. *Frontiers in Microbiology* 2(OCT): 1–11.
- Bradley, Harold C., and M. Starr Nichols. 1918. 'NITROGEN CONTENT OF BACTERIAL CELLS'. *Journal of Biological Chemistry* 33(3): 525–29.
- Erratt, Kevin J., Irena F. Creed, and Charles G. Trick. 2018. 'Comparative Effects of Ammonium, Nitrate and Urea on Growth and Photosynthetic Efficiency of Three Bloom-Forming Cyanobacteria'. *Freshwater Biology* 63(7): 626–38.
- . 2020. 'Differential Drawdown of Ammonium, Nitrate, and Urea by Freshwater Chlorophytes and Cyanobacteria¹'. *Journal of Phycology* 56(2): 458–68.
- Fani, Renato, Romina Gallo, and Pietro Liò. 2000. 'Molecular Evolution of Nitrogen Fixation: The Evolutionary History of the NifD, NifK, NifE, and NifN Genes'. *Journal of Molecular Evolution* 51(1): 1–11.
- Fay, P. 1992. 'Oxygen Relations of Nitrogen Fixation in Cyanobacteria'. *Microbiological Reviews* 56(2): 340–73.
- Flores, E, and A Herrero. 2005. 'Nitrogen Assimilation and Nitrogen Control in Cyanobacteria'. In *Biochemical Society Transactions*, , 164–67.
- Flores, Enrique, and Antonia Herrero. 1994. 'Assimilatory Nitrogen Metabolism and Its Regulation'. In *The Molecular Biology of Cyanobacteria*, , 487–517.
- Gan, Dingwei et al. 2023. 'Urea-Mediated Warm Ponds: Prebiotic Formation of Carbamoyl Amino Acids on the Primordial Earth'. *Earth and Planetary Science Letters* 607.
- Ge, X., K. Cain, and R. Hirschberg. 1990. 'Urea Metabolism and Urease Regulation in the Cyanobacterium *Anabaena Variabilis*'. *Canadian Journal of Microbiology* 36(3): 218–22.
www.nrcresearchpress.com.
- Grieve, Richard. 1980. 'Impact Bombardment and Its Role in Proto-Continental Growth on the Early Earth'. 10(818): 1–22.
- Gueguen, B., Sorensen, J. V., Lalonde, S. V., Peña, J., Toner, B. M., & Rouxel, O. (2018). Variable Ni isotope fractionation between Fe-oxyhydroxides and implications for the use of Ni isotopes as geochemical tracers. *Chemical Geology*, 481(January), 38–52.
<https://doi.org/10.1016/j.chemgeo.2018.01.023>

- Hammerschmidt, Katrin et al. 2021. ‘The Order of Trait Emergence in the Evolution of Cyanobacterial Multicellularity’. *Genome Biology and Evolution* 13(2): 1–10.
- Harano, Yoshimi et al. 1997. ‘Identification and Nitrogen Regulation of the Cyanase Gene from the Cyanobacteria *Synechocystis* Sp. Strain PCC 6803 and *Synechococcus* Sp. Strain PCC 7942’. *Journal of Bacteriology* 179(18): 5744–50.
- Herrero, A., A. M. Muro-Pastor, and E. Flores. 2001. ‘Nitrogen Control in Cyanobacteria’. *Journal of Bacteriology* 183(2): 411–25.
- Kappaun, Karine, Angela Regina Piovesan, Celia Regina Carlini, and Rodrigo Ligabue-Braun. 2018. ‘Ureases: Historical Aspects, Catalytic, and Non-Catalytic Properties – A Review’. *Journal of Advanced Research* 13: 3–17.
- Karhu, Juha A., and Heinrich D. Holland. 1996. ‘Carbon Isotopes and the Rise of Atmospheric Oxygen’. *Geology* 24(10): 867–70.
- Kasting, James F. 1982. ‘Stability of Ammonia in the Primitive Terrestrial Atmosphere’. *Journal of Geophysical Research: Oceans* 87(C4): 3091–98.
- Kasting, James F. 1990. ‘Bolidic Impacts and the Oxidation State of Carbon in the Earth’s Early Atmosphere’. *Origins of Life and Evolution of the Biosphere* 20(3–4): 199–231.
- Kasting, James F., and Janet L. Siefert. 2001. ‘The Nitrogen Fix’. *Nature* 412(6842): 26–27.
- Konhauser, Kurt O. et al. 2009a. ‘Oceanic Nickel Depletion and a Methanogen Famine before the Great Oxidation Event’. *Nature* 458(7239): 750–53.
- . 2009b. ‘Oceanic Nickel Depletion and a Methanogen Famine before the Great Oxidation Event’. *Nature* 458(7239): 750–53.
- Kramer, Benjamin J., et al. “Nitrogen and Phosphorus Significantly Alter Growth, Nitrogen Fixation, Anatoxin-a Content, and the Transcriptome of the Bloom-Forming Cyanobacterium, *Dolichospermum*.” *Frontiers in Microbiology*, vol. 13, no. September, 2022, pp. 1–22, doi:10.3389/fmicb.2022.955032.
- Kuga, Maïa et al. 2014. ‘Nitrogen Isotopic Fractionation during Abiotic Synthesis of Organic Solid Particles’. *Earth and Planetary Science Letters* 393: 2–13.

- Lohrmann, R. 1972. 'Formation of Urea and Guanidine by Irradiation of Ammonium Cyanide'. *Journal of Molecular Evolution* 1(3): 263–69.
- Lyons, Timothy W., Christopher T. Reinhard, and Noah J. Planavsky. 2014. 'The Rise of Oxygen in Earth's Early Ocean and Atmosphere'. *Nature* 506(7488): 307–15.
- Marsh, J. D. F., and Margaret J. Martin. 1957. 'The Hydrolysis and Polymerization of Hydrogen Cyanide in Alkaline Solutions'. *Journal of Applied Chemistry* 7(4): 205–9.
- Menor Salván, C. et al. 2020. 'Prebiotic Origin of Pre-RNA Building Blocks in a Urea "Warm Little Pond" Scenario'. *ChemBioChem* 21(24): 3504–10.
- Muñoz-Velasco, Israel et al. 2018. 'Methanogenesis on Early Stages of Life: Ancient but Not Primordial'. *Origins of Life and Evolution of Biospheres* 48(4): 407–20.
- Navarro-González, Rafael, Christopher P. McKay, and Delphine Nna Mvondo. 2001. 'A Possible Nitrogen Crisis for Archaean Life Due to Reduced Nitrogen Fixation by Lightning'. *Nature* 412(6842): 61–64.
- Navarro-González, R., A. Negrón-Mendoza, and E. Chacón. 1989. 'The γ -Irradiation of Aqueous Solutions of Urea. Implications for Chemical Evolution'. *Origins of Life and Evolution of the Biosphere* 19(2): 109–18.
- Rippka, R., J. Deruelles, and J. B. Waterbury. 1979. 'Generic Assignments, Strain Histories and Properties of Pure Cultures of Cyanobacteria'. *Journal of General Microbiology* 111(1): 1–61.
- Rogato, Alessandra et al. 2015. 'The Diatom Molecular Toolkit to Handle Nitrogen Uptake'. *Marine Genomics* 24: 95–108. <http://dx.doi.org/10.1016/j.margen.2015.05.018>.
- Sakamoto, Toshio, and Donald A Bryant. 2001. 'Requirement of Nickel as an Essential Micronutrient for the Utilization of Urea in the Marine Cyanobacterium *Synechococcus* Sp. PCC 7002'. *Microbes and Environments* 16(3): 177–84.
- Sakamoto, Toshio, Victoria B Delgaizo, and Donald A Bryant. 1998. 'Growth on Urea Can Trigger Death and Peroxidation of the Cyanobacterium *Synechococcus* Sp. Strain PCC 7002'. *Applied and Environmental Microbiology* 64(7): 2361–66. <https://journals.asm.org/journal/aem>.

- Schirrmeister, Bettina E., Patricia Sanchez-Baracaldo, and David Wacey. 2016. 'Cyanobacterial Evolution during the Precambrian'. *International Journal of Astrobiology* 15(3): 187–204.
- Stal, Lucas J. 2006. 'Cyanobacterial Mats and Stromatolites'. *The Ecology of Cyanobacteria*: 61–120.
- Stevens, S. E., C. O. Pat Patterson, and Jack Myers. 1973. 'The Production of Hydrogen Peroxide By Blue-Green Algae: A Survey'. *Journal of Phycology* 9(4): 427–30.
- Stüeken, Eva E. et al. 2021. 'Reconstructing Nitrogen Sources to Earth's Earliest Biosphere at 3.7 Ga'. *Frontiers in Earth Science* 9(April).
- Stüeken, Eva E., Roger Buick, Bradley M. Guy, and Matthew C. Koehler. 2015. 'Isotopic Evidence for Biological Nitrogen Fixation by Molybdenum-Nitrogenase from 3.2 Gyr'. *Nature* 520(7549): 666–69.
- Stüeken, Eva E., Michael A. Kipp, Matthew C. Koehler, and Roger Buick. 2016. 'The Evolution of Earth's Biogeochemical Nitrogen Cycle'. *Earth-Science Reviews* 160: 220–39.
<http://dx.doi.org/10.1016/j.earscirev.2016.07.007>.
- Svane, Simon et al. 2020. 'Inhibition of Urease Activity by Different Compounds Provides Insight into the Modulation and Association of Bacterial Nickel Import and Ureolysis'. *Scientific Reports* 10(1).
- Tian, Hailin, Ioannis A. Fotidis, Konstantinos Kissas, and Irimi Angelidaki. 2018. 'Effect of Different Ammonia Sources on Aceticlastic and Hydrogenotrophic Methanogens'. *Bioresource Technology* 250(November 2017): 390–97.
- Ueno, Yuichiro et al. 2006. 'Evidence from Fluid Inclusions for Microbial Methanogenesis in the Early Archaean Era'. *Nature* 440(7083): 516–19.
- Veaudor, Théo, Corinne Cassier-Chauvat, and Franck Chauvat. 2019. 'Genomics of Urea Transport and Catabolism in Cyanobacteria: Biotechnological Implications'. *Frontiers in Microbiology* 10.
- Warke, Matthew R. et al. 2020. 'The Great Oxidation Event Preceded a Paleoproterozoic "Snowball Earth"'. *Proceedings of the National Academy of Sciences of the United States of America* 117(24): 13314–20.

- Waser, N. A.D. et al. 1998. 'Nitrogen Isotope Fractionation during the Uptake and Assimilation of Nitrate, Nitrite, Ammonium, and Urea by a Marine Diatom'. *Limnology and Oceanography* 43(2): 215–24.
- Wasylenki, L. E., Howe, H. D., Spivak-Birndorf, L. J., & Bish, D. L. (2015). Ni isotope fractionation during sorption to ferrihydrite: Implications for Ni in banded iron formations. *Chemical Geology*, 400, 56–64. <https://doi.org/10.1016/j.chemgeo.2015.02.007>
- Yang, J. et al. 2019. 'Ammonium Availability in the Late Archaean Nitrogen Cycle'. *Nature Geoscience* 12(7): 553–57.
- Zahnle, K. J. 1986. 'Photochemistry of Methane and the Formation of Hydrocyanic Acid (HCN) in the Earth's Early Atmosphere.' *Journal of Geophysical Research* 91(D2): 2819–34.

7. Conclusions

It was proposed long ago that the transition metal isotope signatures derived from biological activity can also be used as evidence for life. Therefore, in this study, ion exchange techniques were developed to sequentially separate transition elements from geological samples which enables measuring multiple transition metal isotopic signatures from a single sample. However, the lack of knowledge about the abiotic isotope fractionation processes can make it difficult to apply these signatures to natural samples. For example, cellular adsorption, diagenesis etc. can mask/alter the enzyme-specific transition metal isotope signatures. Therefore, in this study the effects of adsorption on isotopic composition was evaluated by comparing the techniques that are being used to get rid of adsorbed element components from cell surfaces. In addition, the isotopic composition of the treated cells and desorbed component upon different treatment procedures was checked. It was found that available techniques are incapable of completely removing the adsorbed component and some even cause cellular damage in studied cyanobacterium, *Synechococcus sp.* PCC 7002. Moreover, it was observed that cellular adsorption-related isotope fractionation masks the intracellular Zn isotope signature and the observed Ni isotope fractionation factor for cells and its adsorbed component in laboratory cyanobacterial cultures of cyanobacteria (*Synechococcus sp.* PCC 7002) is varied upon the sampling stage. Thus, it is essential to evaluate these processes in advance before determining enzyme-specific isotope fractionation factors using laboratory cultures.

Considering the experimental difficulties in differentiation of enzyme specific isotope fractionation factors, it is not recommended to solely depend on isotope signatures when determining biogenicity of a sample. When analyzing chemical signatures from ancient geological samples, it is crucial to consider the formation settings of these samples and subsequent changes that may have occurred before drawing any conclusions. Therefore, it is recommended to combine textural/morphological observations and geochemical signatures, including multiple transition elemental isotope signatures together with traditional C,N and O isotope systems when determining the biogenicity of a particular sample.

On the other hand, understanding the presence of bio-available nutrients in a particular environment indirectly provides evidence for the habitability of a particular life form in that environment. In addition to the major nutrients (C, N, O, P), transition metals are important micro-nutrients to many species. Considering the limited availability of Mo in the Precambrian environment and the extreme sensitivity of nitrogenase towards oxygen, it is enigmatic how

primitive cyanobacteria were capable of fixing atmospheric N₂. Laboratory cultures of unicellular cyanobacteria (*Synechococcus* sp. PCC 7002) grown in urea-containing A+ medium have demonstrated that it can utilize urea (1-5 mmol L⁻¹) as a nitrogen source and can survive under maximum Ni concentrations inferred (~400 nmol L⁻¹) for Archean oceans. However, cyanobacteria were growth limited at high urea concentrations (>10 mmol L⁻¹). Therefore, this thesis proposes that cyanobacteria may have utilized urea as an alternative nitrogen source during the Archean. However, the observed toxic effects of urea at high concentrations may have limited the expansion of cyanobacteria, delaying the GOE until the onset of Proterozoic. Furthermore, it is proposed that expansion of primitive cyanobacteria may not have been limited by the availability of Mo, which is essential for the functioning of nitrogenase enzyme that fixes atmospheric dinitrogen. Based on the hypothesis proposed in this work, the Lomagundi event, Great Oxidation Event, and Snow Ball Earth event during the transition period from Archean to Proterozoic can be considered as interconnected events. These events may have led by the expansion of cyanobacteria during the progressive depletion of urea in the Archean ocean, supported by the limited expansion of methanogens due to the proposed depleting Ni concentration in the Archean ocean.